Increasingly Hot Europe Faces More Severe Droughts And Growing Challenges For Water and Land Management

Authors

Sarah Kew, *Royal Netherlands Meteorological Institute (KNMI), De Bilt, The Netherlands*
Mariam Zachariah, *Centre for Environmental Policy, Imperial College, London, UK*
Dominik L. Schumacher, *Institute for Atmospheric and Climate Science, ETH Zurich, Switzerland*
Svenja Seeber, *Institute for Atmospheric and Climate Science, ETH Zurich, Switzerland*
Martin Hirschi, *Institute for Atmospheric and Climate Science, ETH Zurich, Switzerland*
Korbinian Breinl, *Federal Ministry of Agriculture and Forestry, Climate and Environmental Protection, Regions and Water Management (BMLUK), Vienna, Austria*
Klaus Haslinger, *GeoSphere Austria, Vienna, Austria*
Sebastian Lehner, *GeoSphere Austria, Vienna, Austri*a
Vincent Humphrey, *Federal Office of Meteorology and Climatology MeteoSwiss, Zürich, Switzerland*
Hassan Mohammed, *Royal Netherlands Meteorological Institute (KNMI), De Bilt, The Netherlands*
Mónika Lakatos, *HungaroMet Hungarian Meteorological Service, Budapest, Hungary*
Attila Kovács, *HungaroMet Hungarian Meteorological Service, Budapest, Hungary*
Zsófia Erdődiné Molnár, *HungaroMet Hungarian Meteorological Service, Budapest, Hungary*
Sorin Cheval, *National Meteorological Administration, (MeteoRo) Bucharest, Romania*
Alexandru Dumitrescu, *National Meteorological Administration, (MeteoRo) Bucharest, Romania*
Andreja Moderc, *Slovenian Environment Agency (ARSO), Ljubljana, Slovenia*
Živa Vlahović, *Slovenian Environment Agency (ARSO), Ljubljana, Slovenia*
Patricia Blažič, *Slovenian Environment Agency (ARSO), Ljubljana, Slovenia*
Cathleen Frühauf, *Deutscher Wetterdienst (DWD), Braunschweig, Germany*
Andreas Brömser, *Deutscher Wetterdienst (DWD), Offenbach, Germany*
Elke Rustemeier, *Deutscher Wetterdienst (DWD), Offenbach, Germany*
Dace Zandersone, *Latvian Environment, Geology and Meteorology Centre (LEGMC), Riga, Latvia*
Oldrich Rakovec, *Faculty of Environmental Sciences, Czech University of Life Sciences, Prague, Czechia*
Job Dullaart, *Royal Netherlands Meteorological Institute (KNMI), De Bilt, The Netherlands*
Izidine Pinto, *Royal Netherlands Meteorological Institute (KNMI), De Bilt, The Netherlands*
Ben Clarke, *Centre for Environmental Policy, Imperial College, London, UK*
Theodore Keeping, *Centre for Environmental Policy, Imperial College, London, UK*
David García-García, *Department of Applied Mathematics and Aerospace Engineering, University of Alicante, San Vicente del Raspeig, Spain.*
Roop Singh, *Red Cross Red Crescent Climate Centre, The Hague, The Netherlands (based in New Jersey, USA)*
Merel Laauwen, *Wageningen University & Research, Wageningen, The Netherlands*
Friederike Otto, *Centre for Environmental Policy, Imperial College, London, UK*

Review authors

Gerbrand Koren, *Copernicus Institute of Sustainable Development, Utrecht University, Utrecht, The Netherlands*

Sjoukje Philip, *Royal Netherlands Meteorological Institute (KNMI), De Bilt, The Netherlands*

Cite as Kew, S. et al. (2026): Increasingly hot Europe faces more Severe Droughts and Growing Challenges for Water and Land Management (WWA scientific report No. 87) World Weather Attribution. DOI:10.25560/131401

Main findings

- The European drought is a compound crisis, driven by prolonged precipitation deficits and extreme heat, with impacts already evident despite the summer only just beginning. Wildfire activity has also intensified rapidly in western Europe. The drought is placing severe strain on agriculture: historic crop losses, including France's lowest maize harvest in 50 years and the loss of more than one million hectares of maize in Romania, combined with ongoing global conflicts, could drive up food prices and disproportionately affect low-income households. Many countries across Europe are already implementing emergency restrictions or temporary bans on non-essential uses of drinking water. At the household level, water rationing can create increased burden and financial strain, particularly for low-income households. At the same time, low river levels are disrupting cargo transport, while water scarcity is threatening energy production in hydropower-dependent regions.
- Soil moisture integrates the combined effects of anomalous rainfall and evaporation and is a key indicator of agro-ecological drought. In the western region, the April–June conditions are estimated to occur about every 5 years in the present climate. Synthesis of models and observation-based estimates suggests that such a soil drought has become about 5 times more likely than in a climate 1.4 °C cooler. The January-June soil moisture deficits across the eastern region are presently expected roughly every 15 years, and have become about 11 times more probable due to human-induced climate change.
- The low precipitation and high PET conditions were both relatively rare in today's climate. For PET, the western region had an estimated return period of 50 years, and the eastern region of five years. For precipitation, the low rainfall was a 1-in-25 year event in the west, and a 1-in-30 year event in the east.
- Overall, the strong increase in PET based on observed data has shifted drought thresholds, such that rainfall deficits that would not previously have caused drought now result in drought conditions. For both study regions, climate change has increased the severity of the observed drought. The combination of low precipitation and high PET is characteristic of 'extreme' and 'exceptional' drought conditions in the Eastern and Western regions respectively, in today's climate. An event of similar

rarity would have resulted in comparatively milder ‘moderate’ and ‘severe’ conditions in a 1.4°C cooler climate, in the respective regions.

- In the western region, neither observations nor climate models show a long-term change in low April-June precipitation, suggesting that climate change did not play a role in the meteorological drought at the regional scale. However, for PET, both observations and climate models show strong increases over the region, leading to increasingly likely and intense agricultural and ecological drought. The synthesis of these lines of evidence suggests that such highly evaporative conditions as observed in April-June 2026 have become about 80 times more likely, or equivalently about 7% more intense.

- Over the eastern region, observed precipitation changes are sensitive to the timeframe considered. For the April-June period there is a drying trend, there is little long-term change over the 6-month January-June period, and the 12-month totals from July-June show a slight increasing trend. Considering the 6-month accumulations, climate models show an increase stronger than observed, suggesting an overall albeit statistically insignificant drying trend. On the contrary, trends in PET conditions are increasing strongly across all timeframes. For the 6-month totals, the synthesis of observations and climate models suggests that such highly evaporative conditions as observed during January-June 2026 have become about 40 times more likely, or equivalently about 8% more intense.

- With further warming of 1.4°C, in the western domain climate models project a slight decrease in precipitation for April-June, though this is likely not homogeneous across the region. Such intense PET conditions are expected to become around 10 times more likely, and the likelihood of such a soil moisture deficit is projected to double. In the eastern region, models project a further increase in 6-month precipitation, with such low totals becoming only around a third as likely as in today’s climate. However, warming is also expected to cause much higher PET, with a further increase in likelihood of a factor of about 2, and the likelihood of a January-June soil moisture deficit to increase by a factor of about 1.7.

- The results are aggregated across the selected regions and time periods. As a result, they may not capture local variability or shorter periods within individual regions. Consequently, the reported return periods, magnitude changes, and probability ratios apply to the aggregated indices and do not necessarily reflect local conditions.

- Across Europe, drought impacts are increasingly being managed through agricultural insurance, shock-responsive social protection, and emergency financial support. The EU has strengthened resilience by mobilising agricultural reserve funds to support farmers affected by climate-related drought and other extreme weather events.

- Drought response remains uneven across Europe. While the EU Water Framework

Directive promotes sustainable water management, drought management plans are not mandatory, resulting in inconsistent preparedness across EU Member States. At the European level, a unified drought governance policy could help alleviate potential future drought impacts, alongside the Water Resilience Strategy.

CORRECTION: The SPEI maps from Figure 1.3 for the 3-, 6-, and 12-month accumulation periods have been replaced with corrected versions on the website and the scientific report to correct for an error in the plotting routine. These maps are provided to illustrate the 2026 drought event. All analyses were performed using the correct data; therefore, no results, interpretations, or conclusions in the report are affected.

1 Introduction

The European summer of 2026 is already making its mark as being not only exceptionally warm but also exceptionally dry, in Central and Western Europe (Copernicus, 2026a, 2026b). During the last three months (April to June) large swathes of the continent from the southwest in Portugal up to the northeast in southern Finland have seen sub-normal rainfall. Combined with a succession of strong heatwaves, this has led to extreme values in drought indicators (Fig. 1.3, SPEI-3), contributing to wildfires, particularly in France and Spain, where 116,000 and 42,000 hectares have already been burnt, respectively (Reuters, 2026a, EFFIS, 2026). The drought has also led to historically low river levels, where in the Netherlands the government announced water shortage (Reuters, 2026b), while putting pressure on energy production in France (The Guardian, 2026).

Looking back to earlier in the year (Jan-March), the western part of Europe was predominantly wet, whilst in the east conditions were already dry, with the year already beginning with a precipitation deficit from 2025. This results in a split across the main impacted domain in the type of impacts and type of drought experienced.

Drought can be defined in a multitude of ways but there are three main kinds that propagate in severity, starting from meteorological drought - a lack of precipitation, agricultural drought - where the drying soil due to high evapotranspiration influences crop health and growth, and hydrological drought - where water tables drop, river levels fall and water availability becomes an issue due to persistently dry conditions (Wilhite & Glantz, 1985; Van Loon, 2015).

The meteorological drought developed in response to a persistent large-scale circulation anomaly that reduced precipitation across large parts of Europe and was followed by several episodes of extreme heat (Drouard et al., 2019; Liu et al., 2020). The timing of the onset differed between eastern and western Europe. During winter and early spring, high-pressure conditions over northern and central Europe (Fig. 1.1) contributed to a reduced influence of Atlantic weather systems, resulting in below-average precipitation across parts of Germany, Poland, Czechia, Slovakia and the Baltic region where, for example, Latvia experienced its second driest spring on record, with precipitation reaching 50% below seasonal norm and extreme Standardized Precipitation Index (SPI) values (LEGMC, 2026) and the period from September 2025 to May 2026 became the second driest nine-month stretch in recorded history, trailing only behind 1941/1942 (LEGMC, 2026). These deficits accumulated from January onwards, with some areas already affected by dry conditions at the start of the year (GeoSphere, 2026). From April, the circulation pattern expanded westward, with repeated high-pressure conditions over western Europe blocking Atlantic weather systems from reaching the Iberian peninsula, France and northern Italy. The resulting rainfall deficits during April-June rapidly depleted soil moisture across western Europe (Copernicus, 2026). In Spain, for example, June 2026 was the second warmest and the third driest since records began in 1961 (AEMET, 2026).

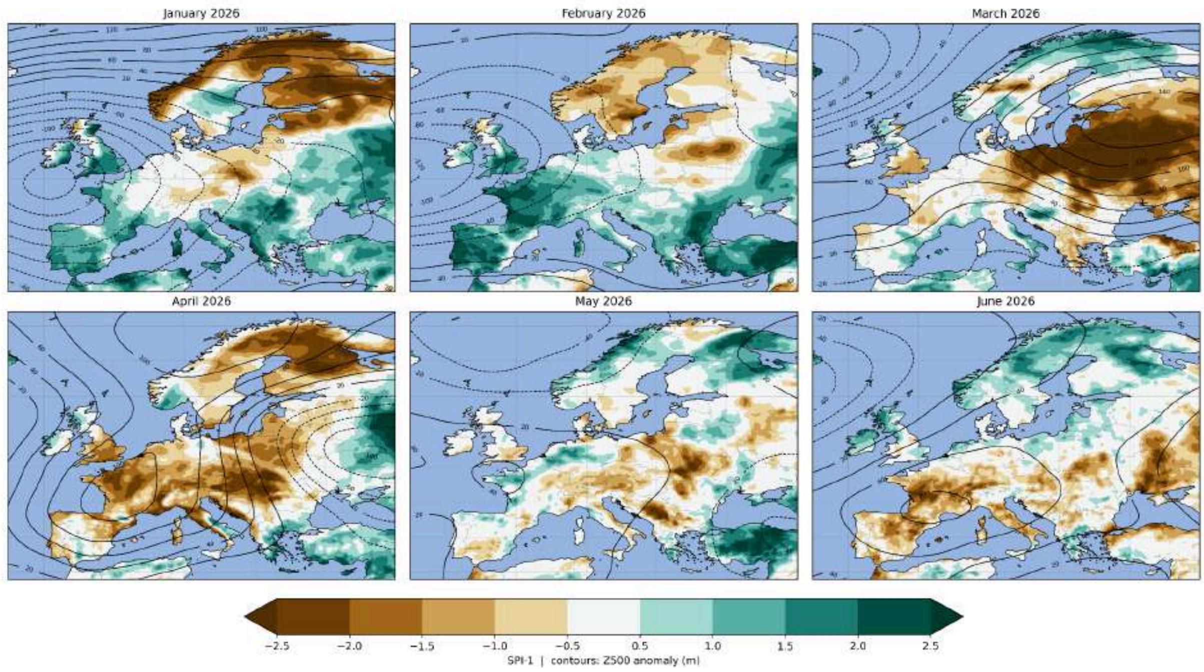

Figure 1.1: 1-month Standardized Precipitation Index (SPI-1) and geopotential height anomalies at the 500 hPa level (Z500) relative to climatology 1991-2020. Data from ERA5 (Hersbach et al., 2020).

The drought was further intensified in June by a series of warm air intrusions from the south, linked to persistent ridging over western and central Europe. These conditions resulted in prolonged periods of clear skies and very high temperatures (Fig. 1.2), including record-breaking temperatures during the late-June heatwave in several countries (DWD, 2026; KNMI, 2026; LEGMC, 2026). A recent study by WWA found that this heatwave was made more likely and intense due to human induced climate change (Keeping et al., 2026). The combination of dry soils and extreme heat increased evaporative demand and reduced evaporative cooling, amplifying surface temperatures and accelerating the transition from meteorological to agricultural and hydrological drought (van Loon, 2015). The unusually sunny conditions due to clear skies over parts of Europe in spring 2026 likely also contributed to soil moisture deficits though enhanced evaporation.

The persistence of the circulation patterns conducive to reduced precipitation, combined with the extreme temperatures during June, contributed to the rapid intensification of drought conditions across much of Europe.

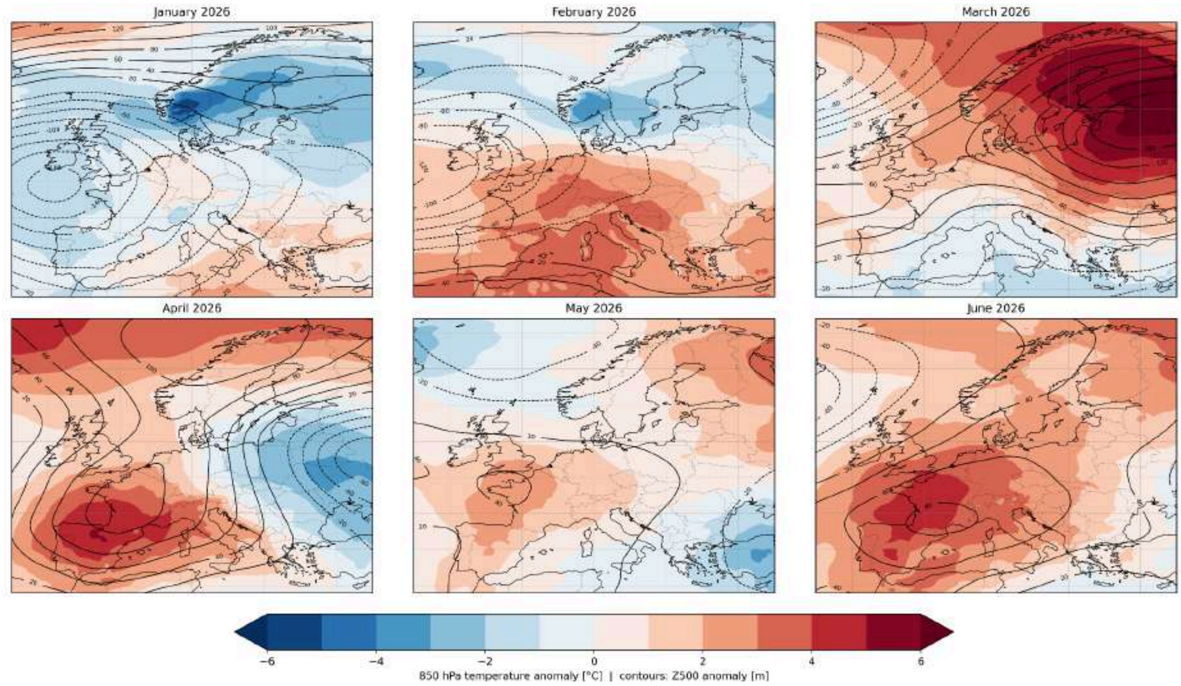

Figure 1.2: Temperature anomalies at the 850 hPa level and geopotential height anomalies at the 500 hPa level (Z500) relative to climatology 1991-2020. Data from ERA5 (Hersbach et al., 2020).

The summer is not over yet and the drought conditions are predicted to remain anomalous (ECHO, 2026), potentially prolonging the already critical conditions. For August–October 2026, the WMO multi-model ensemble indicates rapid development toward strong El Niño conditions with some impacts in Europe. Above-normal temperatures are strongly favoured across southern Europe, with moderate-to-strong model agreement, while precipitation displays a north-south contrast: wetter-than-normal conditions are expected in southern Europe and drier-than-normal conditions in northern Europe, although forecast consistency remains low to moderate across the continent for the season (World Meteorological Organization, 2026; Joint Research Centre, 2026). Under these conditions, drought risk is very likely to intensify across northern Europe, where below-normal precipitation and high temperatures may combine to reduce soil moisture and increase evaporative demand.

1.1 Impacts

In the western Europe, agricultural drought is taking hold, with wildfires being linked to the dry conditions. In a Mediterranean climate, fuel availability for fires can be limited – meaning that a wet winter has a positive effect on available biomass, increasing fire risk in shrublands and grasslands (Batllori et al., 2013). In parts of Spain, Portugal and France, an increasing trend in summer agricultural drought intensity has been attributed to climate change, whilst trends are much weaker earlier in the year (Keeping et al., 2026). Moist spring conditions followed by a hot, dry summer can be linked to the record-breaking Iberian fires of 2025 (Keeping et al., 2026; Parrington and McNorton, 2025), and are also associated with this year's fires. Burned area, the number of fires, and the cumulative seasonal severity rating (GFOI, 2025) are all exceeding or matching current records for France, and burned area is over double average in Spain and Portugal according to European Forest Fire Information System (EFFIS) data at time of publishing (EFFIS, 2026).

Central and Eastern Europe and parts of northern Europe have been heavily impacted by agricultural drought and hydrological drought. Rainfall shortages combined with above average temperatures have reduced soil moisture and stressed vegetation (JRC European Commission, 2026, Toreti et al., 2026). Poland, Czechia and Slovakia have revised down yield forecasts, whereas there is growing concern in parts of France, Hungary, Germany and Italy as the drought continues (Reuters, 2026; Toreti et al., 2026; WSJ, 2026). In Hungary, for example, the harvest of cereals is nearing completion and wheat yields are low, with reported national averages of only 4–4.4 t/ha compared with the typical 5–5.5 t/ha range. The average yield of winter barley is also low, at around 4.3 t/ha. Economists expect food inflation to increase by one percentage point in Europe by next year due to weather uncertainty, current damage to crops and global conflicts (Katanich, 2026; Oxford Economics, 2026).

Major river systems in Italy, France, Poland, England, and the Rhine and Danube region experienced low flow conditions leading to water management challenges, saltwater intrusion, risk to agriculture and freshwater ecosystems and constraints on water availability due to increased demand (Copernicus, 2026).

Discharge levels in the Rhine at Lobith in The Netherlands are very low, with values around 750 m^3/s (on 16 July 2026). At the start of July, the discharge was still around 1000 m^3/s, showing a rapid decline over just two weeks. This value is even lower than the minimum discharge recorded in July 1976, which was around 780 m^3/s. The situation at Lobith illustrates the severity of the drought affecting the wider Rhine basin, including upstream regions in the Alps, Germany, France and the Benelux. The prolonged dry conditions have led to historically low discharges and increasing pressure on available freshwater resources. On 16 July, The Netherlands scaled up to drought level 2, 'actual water shortage' (Rijkswaterstaat, 2026), indicating that additional measures were needed to manage the limited availability of freshwater.

On the 20th of July, the lower Danube water levels in Romania reached their lowest since 1996 after prolonged heat and drought (Reuters, 2026). The decline has triggered irrigation restrictions, disrupted navigation and tourism, and raised concerns for farmers, transport operators, and riverside communities, highlighting growing climate-related pressures on water resources and regional economic activity and resilience.

1.2 Droughts in Europe

In its Sixth Assessment Report (AR6), Working Group 1 (WG1) of the Intergovernmental Panel on Climate Change (IPCC) reported on observed changes in different drought types and the degree to which the observed trend was attributable to anthropogenic influence on the climate (Seneviratne et al., 2021). Table 1.1 shows a summary of findings for the three AR6 regions that partially feature in the event definition regions in this study (Northern Europe, NEU; Western and Central Europe, WCE; Mediterranean, MED), based on evidence available up until 2021. The bulk of both regions studied here are encompassed within the WCE region, though England and Wales are part of NEU and most of Italy and the Iberian Peninsula fall within the MED region.

IPCC AR6 Region	Observed trends by drought type (Confidence in attribution)		
	Agricultural & Ecological	**Meteorological**	**Hydrological**
NEU	Limited evidence	Decrease (Low confidence)	Decrease (Medium confidence)
WCE	Increase (Low confidence)	Limited evidence	Limited evidence
MED	Increase (Medium confidence attr)	Mixed signals	Increase (Medium confidence)

Table 1.1: Summary of findings on observed and attributable trends from IPCC AR6 for different drought types for the three AR6 regions (Northern Europe, NEU; Western & Central Europe, WCE; Mediterranean, MED) at least partially included in the event definition regions in this study.

AR6 reported an observed increase in both agricultural and ecological and hydrological droughts in the Mediterranean, with medium confidence in attributing this to human influence on the climate. However, there were mixed signals in different subregions in changes in meteorological droughts. This indicates a substantial role of increased evapotranspiration due to increased atmospheric evaporative demand in the decreasing moisture availability over the region. Changes were less clear for WCE, with an observed increase in agricultural and ecological droughts, but only low confidence in attribution to human influence, and limited evidence for changes in other drought types. Finally, for NEU, no clear changes were observed in agricultural and ecological droughts, with observed decreases in hydrological and meteorological droughts, albeit also with high subregional variation.

Since AR6, numerous other studies have been conducted including both trend analysis and extreme event attribution for different drought types. In summer 2022, large parts of Europe experienced severe hydrological and soil-moisture drought. Multiple studies have shown that this was made much more likely and intense by human induced climate change; Schumacher et al. (2024) found that such a soil moisture deficit was about 5 times as likely to occur, while Bevacqua et al. (2024) found that human-induced climate change drove about 30% of the soil moisture deficit. This was primarily due to rapid increases in potential evapotranspiration (PET) resulting from rising temperatures and higher available surface radiation. This finding is in line with other studies, which find a consistent and attributable increasing trend in total summer precipitation in many parts of northern Europe and a strong decreasing but not attributable trend in the south (around southern France, Italy and the Iberian Peninsula) (Noto et al., 2023; Vicente-Serrano et al., 2025), with consistent and continent-wide increases in PET (Christidis & Stott, 2021). While plant responses to increasing CO_2 do lead to smaller trends in actual ET compared to PET, resulting in more moderate increases in actual drought severity (Swann et al. 2016, Milly & Dunne 2016), observational datasets show that Central Europe specifically has experienced significant increases in both summer mean ET and extreme ET episodes since the 1980s and that this can be attributed to anthropogenic climate change (Egli et al. 2026, Liu et al. 2021). When these drivers are each accounted for, increases in PET dominate and the net effect is a consistent and continent-wide drying during summer (Christidis & Stott, 2021; Almendra-Martín et al., 2022; An et al., 2023).

1.3 Illustrations of drought development

To illustrate developments and localised impacts of drought, this section describes a few examples for specific countries. Auxiliary material can be found in Appendix A4.

Drought in Hungary

The ongoing drought in Hungary began in the second half of 2025, when severe agricultural drought led to critically dry soils nationwide. The subsequent winter and spring remained drier than average, preventing soil moisture recharge, especially in the Great Plain. As a result, large parts of the country entered the 2026 growing season with a substantial soil moisture deficit, which was further exacerbated by the exceptionally warm and dry conditions in June (HungaroMet, 2026). Soil moisture is below 40% of plant-available water, dropping below 30% in large areas of central Hungary, indicating critically dry conditions. In 2026, sunflower and maize biomass are exceptionally low nationwide, even below the levels observed during the record drought year of 2022.

The situation of Lake Velence has become critical in 2026 (Reuters, 2026). Water levels have fallen below the previous historic minimum recorded during the 2022 drought, reaching approximately 40–50 cm in early July. The extremely low water level threatens aquatic ecosystems, deteriorates water quality, and adversely affects local tourism and recreation. Although the drought has not caused widespread drinking water shortages in Hungary, local water supply systems have come under increased pressure, with temporary restrictions introduced in some areas.

Although droughts are a natural feature of Hungary's climate, recent decades have brought warmer summers and more frequent and intense heatwaves, increasing drought risk (Szentes, 2023). According to the available soil moisture data (*Figure 2.8 (c)*), the current drought ranks among the three most severe drought events observed in Hungary for June, together with the droughts of 2022 and 2025. During dry years, drought conditions are typically most severe and widespread in the Great Plain, as also observed in 2022, when record summer heat further intensified the drought. This highlights the Great Plain as the most drought-prone region of Hungary, with a high risk of persistent and severe droughts.

Drought in Switzerland

Switzerland experienced a rapid transition from an unusually dry spring to widespread drought conditions during the first half of 2026, with the event further intensified by an exceptional early-summer heatwave. Switzerland's drought early warning system (National Drought Platform 2026) released a first warning to regional authorities at the end of May and escalated the warning to its highest level by the end of June.

The development began with spring 2026 being among the warmest and driest since the start of observations, with precipitation deficits beyond 50% affecting large parts of Switzerland, particularly north of the Alps (MeteoSwiss 2026, Figure A4.2.1). This resulted in an earlier onset of vegetation growth and lower than normal soil moisture conditions. Conditions deteriorated further in late June as the drought coincided with an exceptional heatwave, with prolonged periods of very high temperatures enhancing evapotranspiration and accelerating soil drying (MeteoSwiss 2026). Although thunderstorms occurred locally, they were highly heterogeneous and generally insufficient to compensate for the accumulated precipitation deficit (MeteoSwiss 2026).

Low soil moisture evolved into reduced streamflow and lake levels, while several groundwater long-term monitoring stations reached new record seasonal or absolute minima. Elevated water temperatures became widespread, creating stress for aquatic ecosystems and leading to widespread bans on water withdrawals. The agricultural sector suffered a range of impacts ranging from increased irrigation demand and crop water stress to reduced fodder production for cattle (FOEN 2026).

Early warnings and drought impacts in Slovenia

Early warning on worsening spring drought conditions was by the Slovenian Environment Agency first issued in early April when severe drought conditions in the topsoil layer were recorded for northeastern Slovenia (ARSOa, 2026). Early warnings for severe and later extreme drought, as well severe heat stress and severe hydrological drought continued from then on (Figure A4.4.1). Persistent lack of rain and unusually warm and windy weather maintained severe drought conditions throughout April in the north-west, which experienced among the highest surface water balance deficits for this time of year compared to 1991–2020, lacking up to 110 mm of rainfall in 30-day period. At the same time drought intensified into severe and extreme across western half of the country, accompanied by the developing moderate hydrological drought in the groundwater and surface waters. Conditions in topsoil layer and water bodies normalised in the remainder of May and first half of June. Lack of rain, accompanied by an intense heatwave, initiated topsoil drought conditions again in mid-June, which rapidly developed into country-level severe and extreme summer drought by early July and are, as of mid-July, still on-going. Unfavourable weather conditions progressed also into moderate hydrological drought of surface waters and especially groundwaters, where moderate hydrological drought conditions and warnings for severe hydrological drought were present at the country-level in July.

Drought in Latvia

In the Baltic region, the broader atmospheric circulation patterns manifested in severe climatic extremes across Latvia, where the period from September 2025 to May 2026 became the second driest nine-month stretch in meteorological recorded history. This prolonged precipitation deficit culminated in a persistent four-month period of extreme drought (SPI $\leq$ -2) from late January through early May — the longest recorded since 1964 (LEGMC, 2026). Consequently, the severe exacerbation of soil moisture deficits prompted the national meteorological authorities (Latvian Environment, Geology and Meteorology Centre) to issue widespread forest fire danger warnings across the country (LEGMC, 2026). Despite the presence of precipitation in early summer, the deep root zone soil moisture deficit persisted; when warm air masses from the broader European heatwave reached the region in late June, this unrestored baseline further amplified the local thermal response, raising maximum temperature to +33 °C, prompting the issuance of orange level high temperature warning and the occurrence of tropical nights (LEGMC, 2026).

Drought in Germany

Since November 2025, Germany has experienced a precipitation deficit compared to the 1961–1990 period. The exception is February 2026, which was unusually wet but did not alter the overall deficit. In addition, there has been a positive temperature anomaly for several years (with the exception of

January 2026), which has led to higher evaporation. The situation was exacerbated by a heat wave in the second half of June, which was particularly extreme, setting new national all-time records with temperatures exceeding the 40°C mark on multiple occasions (Niemann et al., 2026). So far, July brought precipitation mostly in the form of thunderstorms with local heavy rain which means that precipitation amounts show large variations within a few kilometers.

After the rather dry winter 2025/2026 and dry March soil moisture of the uppermost 60 cm was significantly lower than the 1991 to 2020 average in large parts of the eastern half of Germany. In April regional above-average precipitation in the northeast and very little precipitation in the south shifted the focus of low soil moisture to the south. In May big regional contrasts in soil moisture evolved. While heavy rainfall reached the northern to central regions, in the south the negative deviation of soil moisture increased (Fig. 2.8d) and led to drought stress especially in maize. Despite some precipitation in the first half of June, soil moisture did not recover significantly in southern Germany and plummeted again during an extreme heat wave at the end of June. Thus, soil moisture is now far below the average of July in the southwestern half of Germany. Heatwave and drought effects are ubiquitous across the country, see Section A4.5 for more details.

The forest fire danger index rose to level 3 to 4 during the heatwave, and at level 5 in some areas. Due to high humidity, low forest ignitability and light winds, forest, field, and embankment fires occurred only locally (Niemann et al., 2026). The water availability was affected in both - river discharge and groundwater - becoming extremely low in some areas of Germany. Southern Germany is particularly affected in this regard as well (Fig. A4.5.1, NIWIS July 17, 2026). Navigation restrictions were imposed on inland waterway traffic, for example, on the Rhine between km 334.0 and km 865.515 and on the Danube between km 2201.750 and km 2414.720 (ELWIS July 17, 2026).

1.4 Event Definition

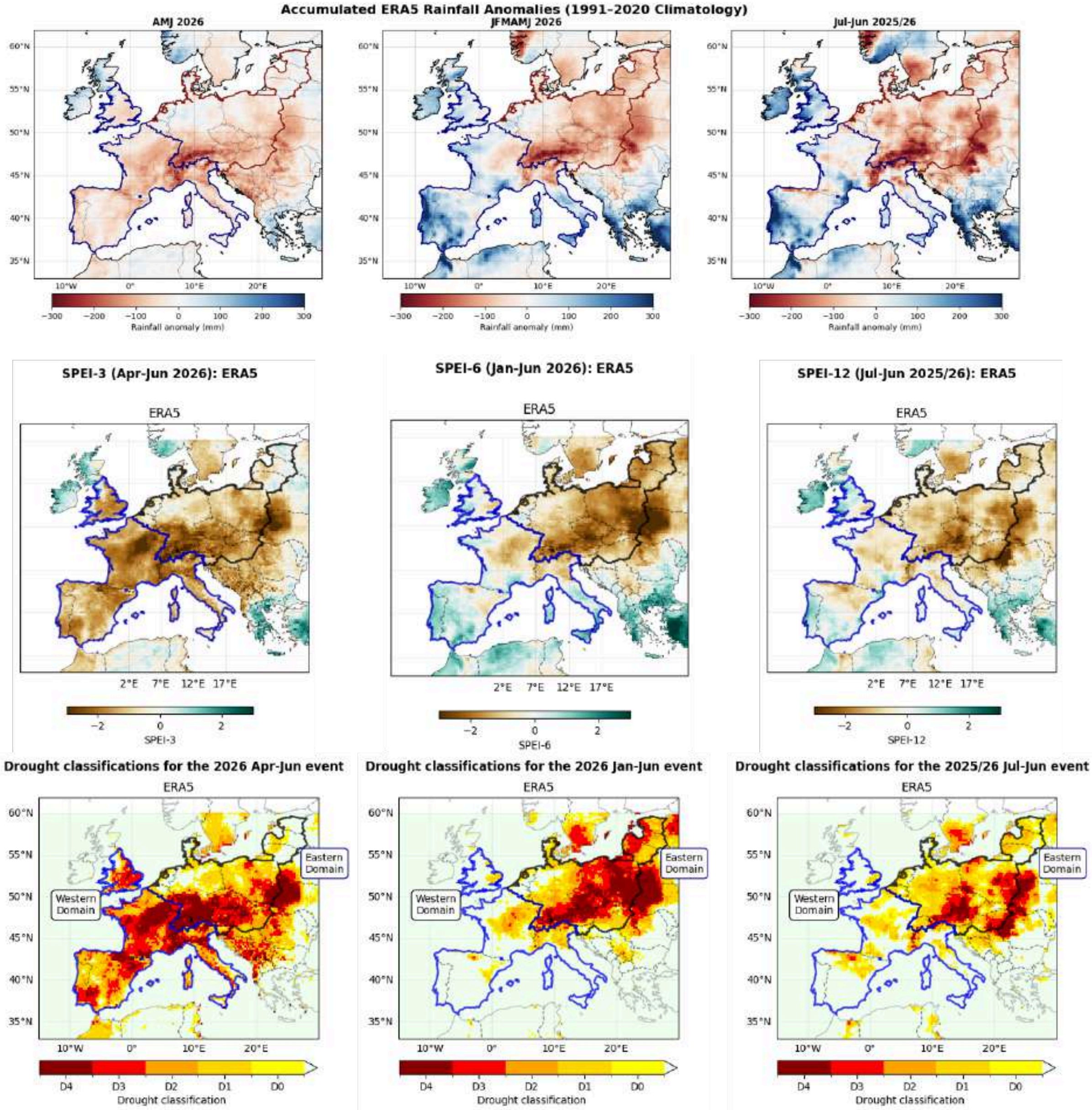

Figure 1.3 Top: Precipitation anomalies wrt 1991-2020 for 3-, 6- and 12-month accumulated precipitation ending in June 2026. Middle: SPEI maps for 3-, 6- and 12- month accumulation periods ending in June 2026 over the region 33-60°N,15°W-30°E. The Western Domain is highlighted in blue and the Eastern Domain is highlighted in black. Bottom: Drought classification maps categorised according to the [US Drought Monitor (USDM)]() system. The categories are based on the n-month SPEI values in June 2026, calculated from ERA5 using the Hargreaves scheme for PET.

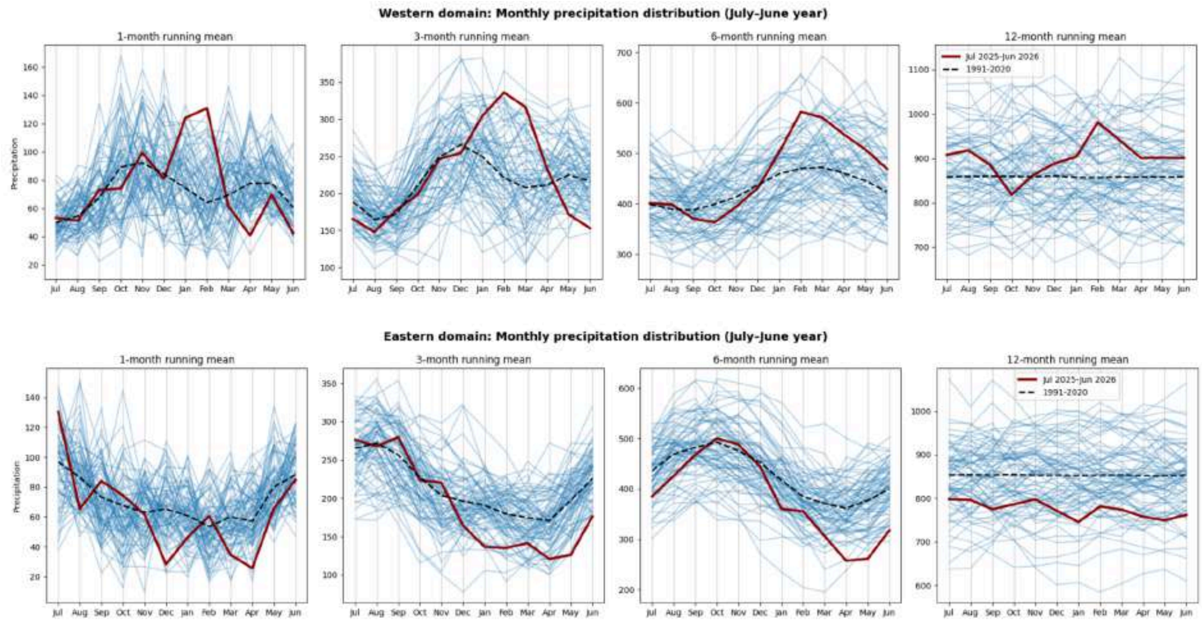

Figure 1.4. Top: n-month running accumulated precipitation area-averaged over the Western Domain- for 1-, 2-, 6- and 12- month accumulations. Bottom: same as (top) for Eastern Domain. The dotted line shows the 1991-2020 climatological average for the n-month rainfall. Blue lines show the n-month running precipitation for all individual years from 1950 -2025.

As noted above, drought can be characterised in several ways. Meteorological drought is defined solely by low rainfall (see top panels in Fig. 1.3 for the precipitation deficits during the 2026 drought wrt to the 1991-2020 climatology), whereas agricultural drought is driven by both rainfall deficits and evapotranspiration. Soil moisture - a measure which combines the effects of these drivers - is the primary measure of agricultural or 'ecological' drought (Seneveratne et al., 2021). Because climate change influences these drivers differently, e.g. increased evapotranspiration driven by regional warming can substantially intensify drought impacts, we assess low rainfall and potential evapotranspiration (PET) separately. It should be noted that actual evapotranspiration (ET) rather than potential evapotranspiration controls the soil moisture budget, and in periods of drought or low soil moisture, actual ET can be substantially lower than PET due to the limited water availability. However, reliable long-term observational records on actual ET are scarce, and actual ET measurements also reflect effects of site management and vegetation development. In addition, analysis on soil moisture directly is complicated by the lack of reliable long-term records, and the fact that soil moisture is a bounded variable. Therefore, we used PET in this analysis to reflect the atmospheric drying capacity, independent of locally varying land surface conditions.

The precipitation anomalies associated with different accumulation periods over the wider region (top panels Fig. 1.3) highlight how the drought is shorter and more recent in the western part of the region and longer-term in the eastern part. The middle panels in Fig. 1.3 shows the SPEI maps for three accumulation periods (3-, 6- and 12-months) ending in June 2026, depicting the on-going drought in Europe. Due to the differences in the climatology and the nature of impacts, we consider two spatial definitions - 1. Over the western part of Europe consisting of England and Wales over the UK, and the countries of Spain, Portugal, France and Italy (hereafter: Western Domain; blue highlighted region in Fig. 1.3), where the impacts are predominantly wildfires that were a result of the on-going dryness and recent hot spells during spring, and 2. The eastern part of the continent consists of Belgium, Hungary, the Netherlands, Germany, Luxembourg, Austria, Czech Republic, Switzerland, Denmark, Poland, Slovenia, Slovakia, Lithuania, Estonia and Latvia (hereafter: Eastern Domain; red highlighted region in Fig. 1.3). As the temporal extent of the drought is quite different in the Western part of Europe compared to the East, we carry out an attribution analysis on three different timescales: the 3-month drought in the western region to reflect the rapidly intensifying drought over the early summer months, and also the 6 and the 12 month drought in the eastern region to reflect a longer period relating to hydrological drought impacts. Figure 1.4 shows the area-averaged running n-month precipitation accumulation series for 1-, 3-, 6- and 12- months for the two study regions. Considering only precipitation, the most recent three month (April to June) of precipitation appears to be most relevant for the drought conditions in the Western domain, while low precipitation during longer periods (6- and 12- months) are important for defining the drought in the Eastern Domain. In addition, soil moisture which has a memory of up to ~6 months, is attributed on the 3-month and 6-month timescale for the western and eastern region respectively. For observed precipitation and PET, all three timescales - 3-month, 6-month and 12-month are analysed in the eastern domain, and the 3-month timescale for the western domain. The Eastern and Western domains are chosen based on SPEI maps for 3-12 month accumulations and are combined regions of individual countries. The regions were originally decided based on countries with a sizable proportion of their land area having SPEI < -1. SPEI maps were retrieved from Global-drought-crops monitoring, Vincente-Serrano et al., (2022), where SPEI is calculated from a Penman-Monteith scheme, however due to the required variables not being available from all climate models, we use an alternative scheme (Hargreaves, see Appendix A1.4) for the study. We acknowledge that there are (parts of) countries also impacted by deteriorating drought conditions that are outside of these domains.

In this report, we study the influence of anthropogenic climate change on events at least as extreme as the current drought by comparing their likelihood and intensity in the current climate and in a 1.4°C cooler climate without human-caused warming (based on Forster et al., 2026). This comparison is performed for each chosen index, i.e. soil moisture, precipitation and PET, separately. We also extend this analysis into the future by assessing the influence of a further 1.4°C of global warming from present. This is in line with the latest Emissions Gap Report from the United Nations Environment Programme, which shows that the world is on track for at least 2.8°C temperature rise given currently implemented policies (UNEP, 2025).

2 Observational analysis

This section first presents the standard observational analysis of gridded precipitation, PET and soil moisture data used in the attribution analysis (Sections 2.1 to 2.2). To assess the return period of the event in the current climate and the trend in this return period and the event's intensity as the climate warms, we follow the method described in Appendix A1.3. Observation-based datasets used are described in Appendix A1.1.

This is followed by an overview of the status and trend of hydrological drought indicators - streamflow and groundwater storage - on the European and regional scale (Sections 2.3 to 2.4).

2.1 Trends in precipitation and PET based on observational data

Figure 2.1 illustrates the annual time series for precipitation and PET for the various accumulation of the different event definitions in the two study regions, based on ERA5 dataset, and Figure 2.2 shows the respective return period curves constructed for the 2026 climate and a 1.4°C cooler climate. The return period estimates in observation-based datasets, where the current event has been included in the trend estimation, are given in Table 2.1 (accumulated precipitation) and Table 2.2 (PET).

For each event definition (domain, temporal aggregation period and variable) a representative return period is chosen for the subsequent observational and model attribution analysis, approximately based on the average return period from the observational datasets. We note that the choice of return period affects the estimated probability ratios but that the estimated changes in intensity are independent of this.

For precipitation (Table 2.1), E-OBS records the lowest domain-averaged precipitation amongst the 3 datasets and paired with that, the highest return periods, whilst ERA5-Land has the lowest return periods. For Apr-Jun precipitation averaged over the Western Domain, return period best estimates range from about 4 to 55 years, and a characteristic event return period of 25 years for Apr-Jun Western Domain is used for the subsequent attribution analysis. For the Eastern Domain, Apr-Jun precipitation return period best estimates ranged from about 8 to 17 years with 15 years chosen for subsequent attribution analysis, Jan-Jun estimates ranged from about 25 to 40 years with 30 years chosen for subsequent attribution analysis, and Jul-Jun estimates ranged from about 11 to 15, with 15 years chosen for subsequent analysis.

For PET (Table 2.2), ERA5 records the highest return periods and E-OBS the lowest return periods amongst the 4 datasets. For Apr-Jun PET averaged over the Western domain, return period best estimates range from about 2 to 90 years, and a characteristic event return period of 50 years for Apr-Jun Western domain is used for the subsequent attribution analysis. For the Eastern domain, Apr-Jun PET return period best estimates range from about 3 to 8 years with 5 years chosen for subsequent attribution analysis, Jan-Jun estimates ranged from about 3 to 6 years with 5 years chosen for subsequent attribution analysis, and Jul-Jun estimates ranged from about 1.7 to 2.2 years, with 2 years chosen for subsequent analysis.

The probability ratio and intensity change results for the observational datasets evaluated at the chosen return periods are shown in Tables 2.3 (accumulated precipitation) and Table 2.4 (PET). In the Western domain, there is no evidence of a trend in Apr-Jun precipitation, with PR best estimates for a similar drought close to unity (no change) and uncertainty ranging from around 4 times less likely to 6 times more likely. There is a very strong trend in PET, with probability ratio best estimates of many orders of magnitude. The lowest lower-bound (E-OBS) in probability ratio is around 900, meaning that the high level of atmospheric drying capacity (PET) reached in 2026 has become, at the very least, at least 900 times more likely than in a 1.4°C cooler climate. The intensity change is around 50 mm - an increase of about 15%.

In the Eastern domain 3-month Apr-Jun precipitation PR best estimates range from around 2 (ERA5-Land) to 4 (E-OBS), meaning that the likelihood of a dry period is now 2-4 times greater than in a 1.4°C cooler climate according to these datasets, while 6-month PRs are straddled around no change and 12-month PRs show that a lack of precipitation such as experienced in the last year may be becoming slightly less likely (1.02 to 2.6 times less likely), albeit with large uncertainties (7 times less likely, up to 6.5 times more likely, depending on the dataset). Likewise, the intensity change varies across the accumulation periods with a change towards less precipitation at the 3-month (Apr-Jun) scale to slightly more precipitation on the annual time scale, yet with uncertainties encompassing no change for each accumulation period. Although precipitation in the Eastern Domain over longer accumulation periods suggests that low precipitation totals are becoming less likely due to climate change, this may in part be due to the incorporation of intense or seasonal rainfall events. While such spells can increase accumulated precipitation totals, they may not be enough for alleviating drought, especially if the rainfall occurs over a short period or when it falls on dry ground and is lost as runoff, reducing potential for soil moisture, groundwater, and reservoir replenishment. For PET, observed trends show a very strong increase, similar to in the western region, with PRs of many orders of magnitude and increases in magnitude averaged across the datasets of about 50 mm (Apr-Jun), 65 mm (Jan-Jun) and 113 mm (Jul-Jun) - increases of order 20%.

*Table 2.1: Magnitudes and estimated return periods of **accumulated precipitation** ending in June 2026 for the West and East domains, based on the three observational datasets that cover the event. The West domain includes only 3-month accumulation periods, whereas estimates for the East domain include 3-, 6- and 12-month accumulation periods.*

Dataset	Western Domain		Eastern Domain					
	Precip-3 (AMJ)		Precip-3 (AMJ)		Precip-6 (Jan-Jun)		Precip-12 (Jul-Jun)	
	Magnitude (mm)	Return period (1 in X-year) (95% C.I.)	Magnitude (mm)	Return period (1 in X-year)(95 % C.I.)	Magnitude (mm)	Return period (1 in X-year) (95% C.I.)	Magnitude (mm)	Return period (95% C.I.)
E-OBS	106	55.6 (19.7 to 302)	134	17.1 (6.78 to 75.8)	233	41.1 (12.8 to 270)	597	14.70 (6.35 to 59.7)
ERA5	153	27.4 (10.2 to 138.24)	176	13.4 (5.56 to 56.9)	318	26.0 (8.64 to 145)	762	11.2 (4.91 to 38.1)
ERA5-Land	191	4.29 (2.26 to 10.6)	186	7.89 (3.56 to 28.5)	323	24.7 (8.17 to 110)	757	11.1 (5.05 to 38.6)

*Table 2.2: Magnitudes and estimated return periods of **accumulated PET** ending in June 2026 for the West and East domains, based on the three observational datasets that cover the event. The West domain includes only 3-month accumulation periods, whereas estimates for the East domain include 3-, 6- and 12-month accumulation periods.*

Dataset	Western Domain		Eastern Domain					
	PET-3 (AMJ)		PET-3 (AMJ)		PET-6 (Jan-Jun)		PET-12 (Jul-Jun)	
	Magnitude (mm)	Return period (1 in X-year) (95% C.I.)	Magnitude (mm)	Return period (1 in X-year) (95% C.I.)	Magnitude (mm)	Return period (1 in X-year) (95% C.I.)	Magnitude (mm)	Return period (1 in X-year) (95% C.I.)
E-OBS	359	2.14 (1.42 to 4.23)	332	2.98 (1.87 to 6.44)	405	3.01 (2.01 to 5.87)	787	1.72 (1.36 to 2.54)
ERA5	364	91.96 (20.1 to 1780)	312	8.13 (3.63 to 34.9)	381	6.39 (3.41 to 17.8)	723	2.20 (1.63 to 3.69)

ERA5-precalc	419	28.0 (8.93 to 223)	353	3.87 (2.26 to 9.54)	423	3.51 (2.11 to 7.47)	779	1.77 (1.39 to 2.63)
ERA5-Land	356	48.8 (13.5 to 553)	303	4.61 (2.48 to 13.8)	371	4.14 (2.48 to 9.35)	708	1.87 (1.46 to 2.90)

Table 2.3: Probability ratio and change in magnitude for ***precipitation indices*** *over the two study regions due to GMST.*

Dataset	Western Domain		Eastern Domain					
	Precip-3 (AMJ)		Precip-3 (AMJ)		Precip-6 (Jan-Jun)		Precip-12 (Jul-Jun)	
	Probability ratio (95% C.I.)	Change in magnitude (%) (95% C.I.)	Probability ratio (95% C.I.)	Change in magnitude (%) (95% C.I.)	Probability ratio (95% C.I.)	Change in magnitude (%) (95% C.I.)	Probability ratio (95% C.I.)	Change in magnitude (%) (95% C.I.)
E-OBS	1.14 (0.25 to 4.77)	-1.59 (-20.4 to 14.7)	4.28 (0.85 to 32.2)	-16.8 (-37.0 to 1.55)	1.13 (0.18 to 6.49)	-2.08 (-34.3 to 24.7)	0.98 (0.14 to 6.46)	0.83 (-62.7 to 65.1)
ERA5	1.43 (0.30 to 6.19)	-5.54 (-30.9 to 15.5)	2.83 (0.56 to 15.5)	-15.2 (-40.3 to 7.40)	0.84 (0.14 to 4.05)	3.72 (-32.5 to 36.8)	0.45 (0.09 to 2.06)	39.04 (-30.1 to 103)
ERA5-Land	1.06 (0.35 to 2.99)	-1.49 (-31.2 to 23.4)	2.07 (0.51 to 9.41)	-12.03 (-37.9 to 10.6)	0.62 (0.12 to 2.82)	10.8 (-25.5 to 40.9)	0.38 (0.08 to 1.57)	46.33 (-19.7 to 114)

Table 2.4: Probability ratio and change in magnitude for ***PET indices*** *over the two study regions due to GMST.*

Dataset	Western Domain		Eastern Domain					
	PET-3 (AMJ)		PET-3 (AMJ)		PET-6 (Jan-Jun)		PET-12 (Jul-Jun)	
	Probability ratio (95% C.I.)	Change in magnitude (mm) (95% C.I.)	Probability ratio (95% C.I.)	Change in magnitude (mm) (95% C.I.)	Probability ratio (95% C.I.)	Change in magnitude (mm) (95% C.I.)	Probability ratio (95% C.I.)	Change in magnitude (mm) (95% C.I.)
E-OBS	12000 (915 to 749000)	49.7 (38.2 to 61.5)	3290 (388 to 92000)	44.4 (33.9 to 54.5)	26200 (1800 to 2100000)	61.6 (49.3 to 72.9)	43200 (4040 to 2600000)	110 (92.5 to 127)
ERA5	1580000 (24000 to 1560000000)	42.6 (29.6 to 54.2)	23200 (1370 to 1420000)	36.2 (26.9 to 45.0)	244000 (9200 to 52000000)	51.0 (39.9 to 60.5)	154000 (10600 to 12300000)	87.5 (73.7 to 101)
ERA5-precalc	310000 (9420 to 71600000)	73.8 (52.7 to 94.0)	264000 (9200 to 105000000)	85.9 (69.0 to 100)	743000 (20800 to 432000000)	99.9 (81.6 to 116)	56400 (4090 to 5170000)	170 (143 to 197)
ERA5-Land	437000 (9700 to 209000000)	40.7 (28.2 to 51.9)	3860 (358 to 118000)	33.9 (25.0 to 42.5)	41100 (2540 to 4070000)	48.5 (37.9 to 58.1)	32800 (3110 to 1590000)	83.4 (70.0 to 96.7)

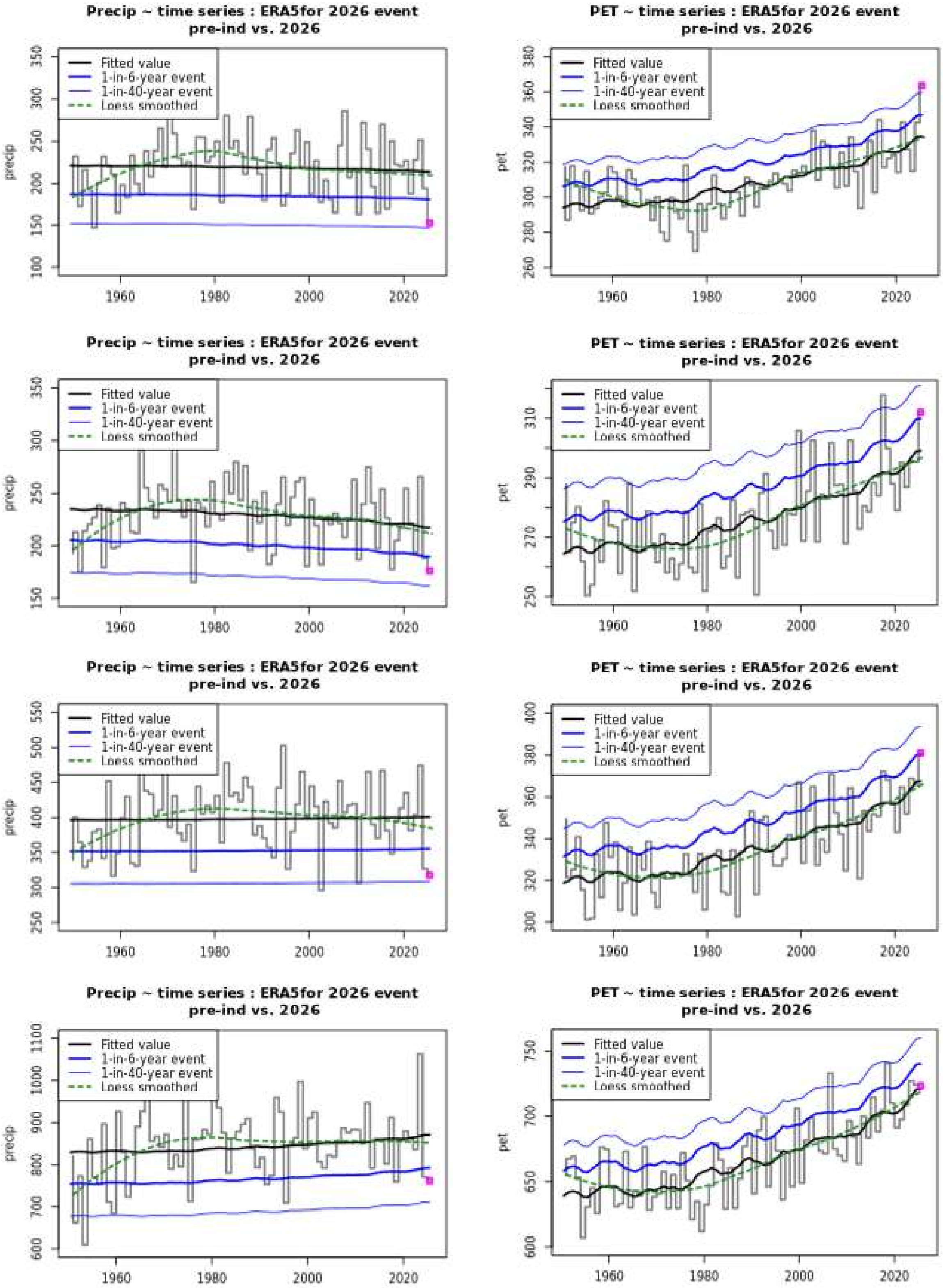

Figure 2.1: Annual time series of Apr-Jun (top 2 rows), Jan-Jun (3rd row) and Jul-Jun (bottom row) for precipitation (left) and PET (right) in ERA5 for the Western Domain (top row) and Eastern Domain (remaining rows). The ERA5 event is shown with the pink box. The loess-smoothed trend is shown with the green dashed line and the fitted statistical model that varies with GMST is shown with the black and blue lines, showing the event (black line), and the 1-in-6 (bold blue) and 1-in-40-year (lighter blue) return period event magnitudes.

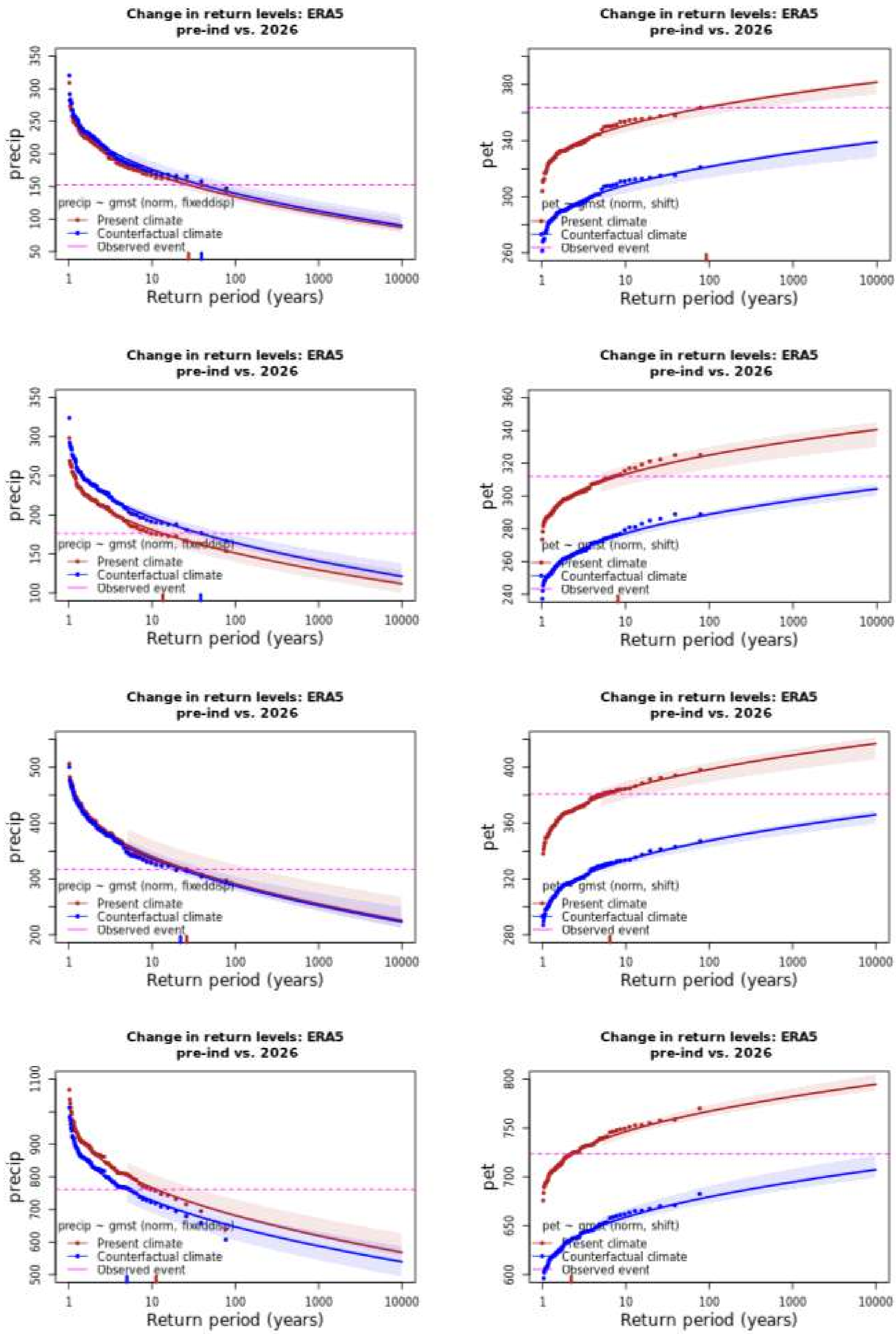

Figure 2.2: Statistical fits to Apr-Jun (top 2 rows), Jan-Jun (3rd row) and Jul-Jun (bottom row) precipitation (left) and PET (right) in ERA5 for the Western Domain (top row) and Eastern Domain (remaining rows). The probability curve for the current climate is shown in red, and for the past 1.4°C

cooler climate in blue, with the shaded band showing the 95% confidence interval. The magnitude of the studied event is highlighted with a horizontal pink line. Red and blue markers on the return-period axis mark the return period for an event of the 2026 magnitude in the current and past climate respectively.

2.1.1. Shift in drought severity

The coloured areas in Fig. 2.3 show the US Drought Monitor drought classifications based on SPEI, standardised with respect to the 1991–2020 climatology, in which SPEI values greater than -0.5 are 'normal or wet conditions'; -0.5 to -0.8 are abnormally dry (D0); -0.8 to -1.3 are moderate drought (D1); -1.3 to -1.6 are severe drought (D2); -1.6 to -2 are extreme drought (D3); and values less than -2 are exceptional drought (D4). For the Western Domain, the classifications are derived from SPEI-3, calculated using accumulated precipitation and potential evapotranspiration (PET) over the three-month period from April to June, using the Hargreaves scheme for PET. For the Eastern Domain, they are based on SPEI-6, calculated from accumulated precipitation and PET over the six months from January to June, and SPEI-12 over the July–June hydrological year.

The solid lines are contours representing combinations of precipitation and PET with equal probability of occurring in the 2026 climate, based on the joint distribution of these variables (see WWA 2023 East Africa Drought for details). The contours are labelled with their corresponding return periods, and the magenta dot marks the precipitation and PET observed in 2026. The dotted lines show the corresponding contours for a climate that is 1.4°C cooler, while the turquoise dot indicates an event in that cooler climate with the same rarity as the 2026 event.

In both regions and for all three instances, the shift in the joint distribution, and hence the increase in drought severity is seen to be driven primarily by the increase in PET. The observed combination of precipitation and PET has an estimated joint return period of approximately 150 years in the Western Domain, implying that these conditions are rare in today's climate. The return period of the observed precip and PET combination during the six month long drought is a relatively less rare 55 year event over the Eastern Domain, and a more common 15 year event considering the precipitation and PET combinations associated with the year-long drought. These conditions are classified as an exceptional drought (D4) in the Western Domain and an extreme drought (D3) in the Eastern Domain relative to the 1991–2020 climatology. By contrast, the precipitation and PET combinations of equivalent rarity in a climate 1.4°C cooler would have resulted in less intense drought conditions, classified as a severe drought (D2) in the Western Domain and a severe (D2) to moderate (D1) drought in the Eastern Domain for the six month- and year-long droughts respectively, following the same 1991-2020 baseline.

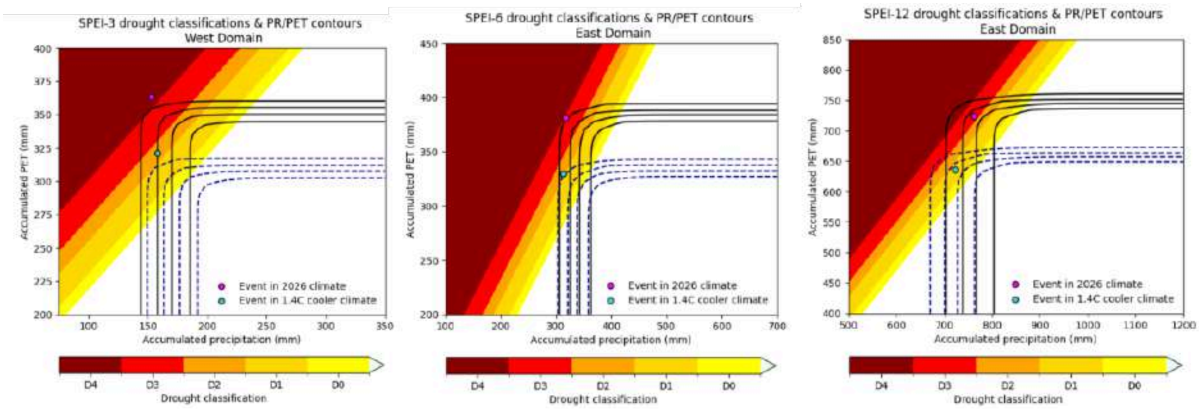

Figure 2.3: US Drought Monitor drought classifications based on SPEI, standardised with respect to the 1991–2020 climatology for the 3- month long (AMJ) drought in Western Domain (left) and the 6-month long (JFMAMJ) (middle) and 12- month long (Jul-Jun) droughts in the Eastern Domain (right). The solid contours indicate return periods under the joint distribution in the current climate, while the dashed contours indicate the same return periods in a 1.4°C cooler climate. The shaded contours represent different levels of drought severity (D0-D4). The magenta point indicates the accumulated precipitation and PET observed in 2026, with this particular combination of precipitation and PET having a joint return period of 84 years; the turquoise point shows an event of equivalent rarity in a 1.4°C cooler climate.

2.2 Trends in root-zone soil moisture based on observational data

2.2.1 ERA5-Land root-zone soil moisture trends

We use ERA5-Land soil water in the top 1 m (Root-zone soil moisture) as an observation-based estimate (Appendix A1.1.1) to compare changes in soil moisture between the past 1.4°C cooler climate and the present climate. Root-zone soil moisture is analysed on the 3-month (April–June) timescale in the western domain, and on the 3-month and 6-month (January–June) timescales in the eastern domain (Section 1.3). Fig. 2.4 shows the 2026 spatial anomaly for the 3-month and 6-month timescales, and Fig. 2.7 shows the seasonal evolution of ERA5-Land monthly root zone soil moisture, revealing that 2026 is one of the driest years in this record in the Eastern Domain, and becoming the driest by June in the Western Domain. Figures 2.5 and 2.6 show the trends and statistical fits for the Western and Eastern Domains respectively.

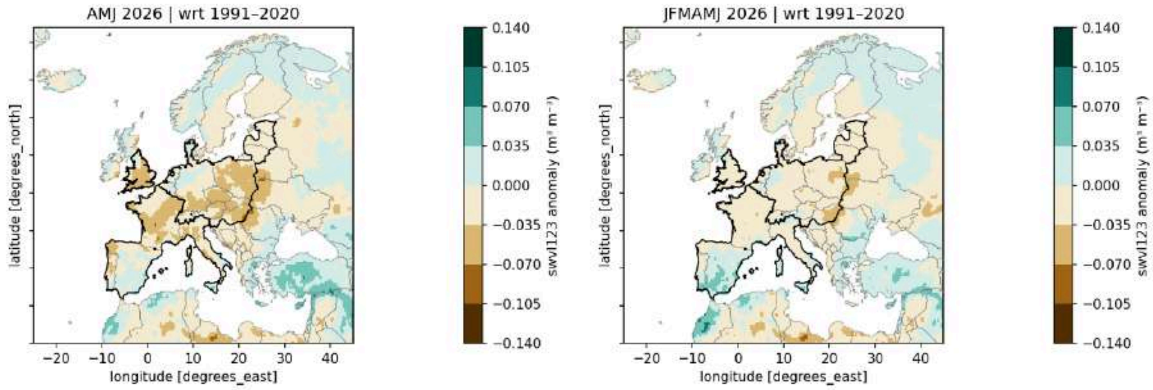

Figure 2.4. ERA5-Land root zone soil moisture anomaly with respect to years 1991-2020 for Apr-Jun 2026 (left) and Jan-Jun 2026 (right).

In the western domain, the 3-month (Apr-Jun) observed deficit has a return period of about 6 (95% CI: 3 to 18) years in the present climate (Table 2.5). A return-period of 6 years is used for the subsequent attribution analysis. There is a significant drying trend observed between the past 1.4°C cooler climate and the current climate, with an intensity change of -6.6% (95% CI: −10.3% to −2.9%) and with conditions as dry as Apr-Jun 2026 having become about 21 (95% CI: 3.5 to 258) times more frequent (Table 2.6).

In the Eastern domain, the 3-month (Apr-Jun) observed deficit also has a return period of about 6 (95% CI: 3 to 19) years in the present climate (Table 2.5) whereas, for the 6-month (Jan-Jun) observed deficit, the return period is about 14 (95% CI: 6 to 86) years in the present climate. Return periods of 6 years and 14 years are used for the subsequent attribution analysis of 3-month and 6-month events respectively.

On both timescales significant drying trends are observed, with a 9.3% (95% CI: 6.0% to 12.2%) decrease in soil moisture and a factor 260 (95% CI: 35 to 4070) increase in likelihood of the observed deficit on the 3-month timescale and a 3.4% (95% CI: 0.8% to 5.5%) decrease in soil moisture and a factor 26 (95% CI: 2.2 to 915) increase in likelihood for the observed deficit on the 6-month timescale (Table 2.6).

Table 2.5: Magnitudes and estimated return periods of root-zone soil moisture in the year 2026 for the West and East domains.

Dataset	Western Domain		Eastern Domain			
	Soil moisture (AMJ)		Soil moisture (AMJ)		Soil moisture (Jan-Jun)	
	Magnitude (m^3/m^3)	Return period (1 in X-year) (95% C.I.)	Magnitude (m^3/m^3)	Return (1 in X-year) period (95% C.I.)	Magnitude (m^3/m^3)	Return (1 in X-year)period (95% C.I.)
ERA5-Land	0.869	6 (3 to 18)	0.887	6 (3 to 19)	1.943	14 (6 to 86)

Table 2.6: Probability ratio and change in magnitude for root-zone soil moisture over the two study regions.

Dataset	Western Domain		Eastern Domain			
	Soil moisture (AMJ)		Soil moisture (AMJ)		Soil moisture (Jan-Jun)	
	Probability ratio (95% C.I.)	Change in magnitude (%) (95% C.I.)	Probability ratio (95% C.I.)	Change in magnitude (%) (95% C.I.)	Probability ratio (95% C.I.)	Change in magnitude (%) (95% C.I.)
ERA5-Land	21 (3.5 to 258)	-6.6 (−10.3 to −2.9)	260 (35 to 4070)	-9.3 (−12.2 to −6.0)	26 (2.2 to 915)	-3.4 (−5.5 to −0.8)

AMJ

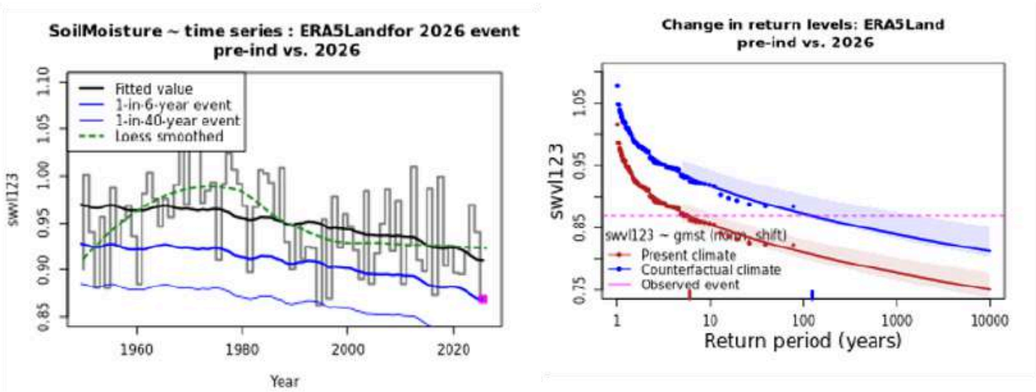

Figure 2.5: Left - Annual time series of Apr-Jun soil moisture in ERA5 for the Western Domain. The ERA5 event is shown with the pink box. The loess-smoothed trend is shown with the green dashed line and the fitted statistical model that varies with GMST is shown with the black and blue lines, showing the event (black line), and the 1-in-6 (bold blue) and 1-in-40-year (lighter blue) return period event magnitudes. Right - Statistical fits to Apr-Jun soil moisture in ERA5-Land for the Western Domain. The probability curve for the current climate is shown in red, and for the past 1.4°C climate in blue, with the shaded band showing the 95% confidence interval. The magnitude of the studied event is highlighted with a horizontal pink line. Red and blue markers on the return-period axis mark the return period for an event of the 2026 magnitude in the current and past climate respectively.

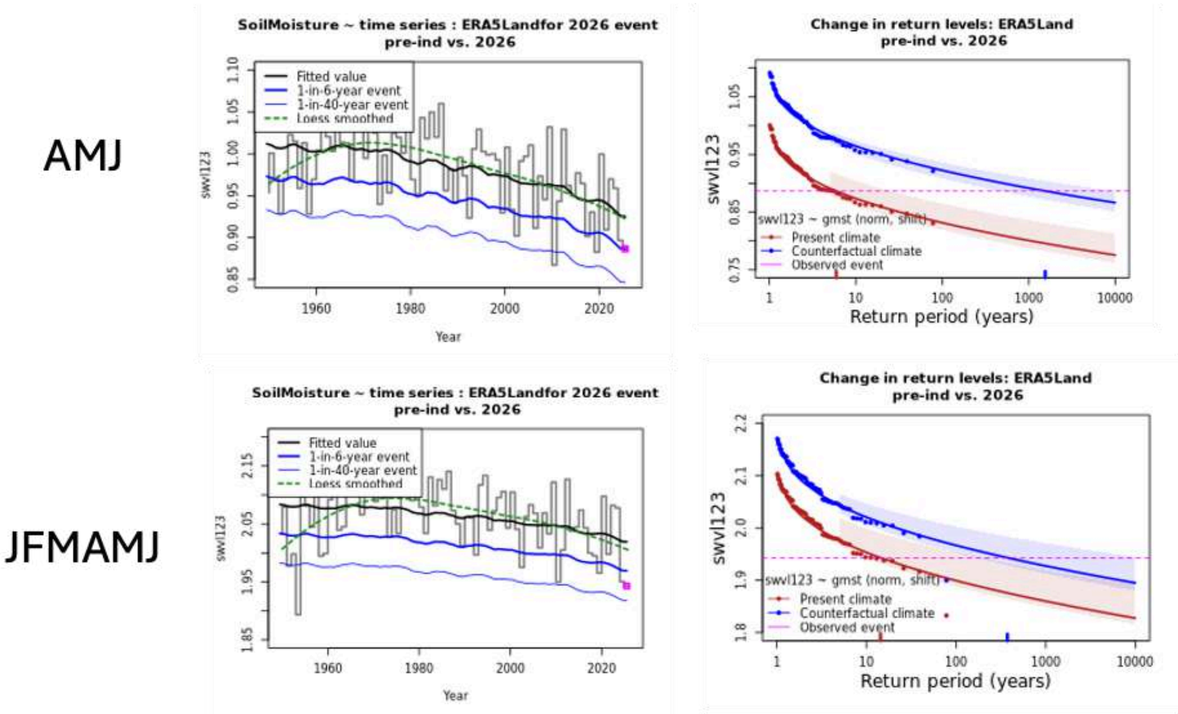

Figure 2.6: Same as for Fig. 2.5 but for the Eastern Domain for AMJ (top row) and JFAMJ seasons (bottom row).

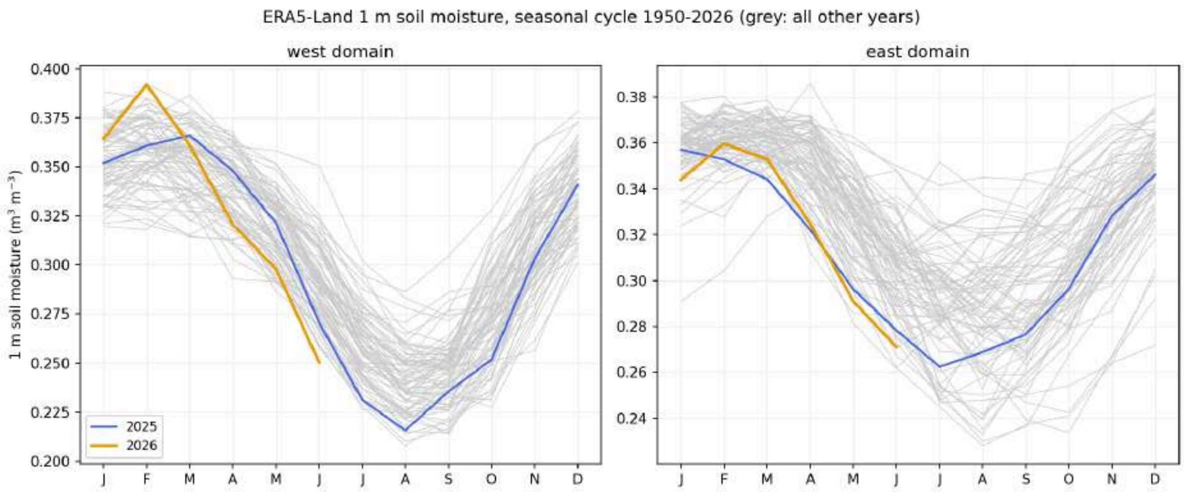

Figure 2.7: Seasonal evolution of ERA5-Land monthly root zone soil moisture for years 1950-2026 for the Western domain (left) and Eastern domain (right).

2.2.2 Local estimates of soil moisture trends

As an illustration of the variability of local soil moisture conditions within the study area we provide soil moisture estimates based on observations / computed soil moisture data for datasets we could obtain (Fig. 2.8). Individual soil moisture sensor measurements are sensitive to local soil condition and sensor limitations, but with careful site-specific calibration they can be appropriately representative of dry condition ([Mittelbach et al., 2011](#)). Averaging over several stations can reduce the uncertainty.

All four data sets come from stations in the Eastern domain (Switzerland, The Netherlands, Hungary and Germany). For the Swiss and German stations, June/July 2026 soil moisture is the lowest on record, whereas for the Dutch and Hungarian data, June/July 2026 soil moisture is one of the lowest in the series, as for the Eastern domain average (Fig. 2.7 above). The second half of 2025 was not particularly dry in Switzerland and Germany, but at some locations and months the early part of 2025 was also dry.

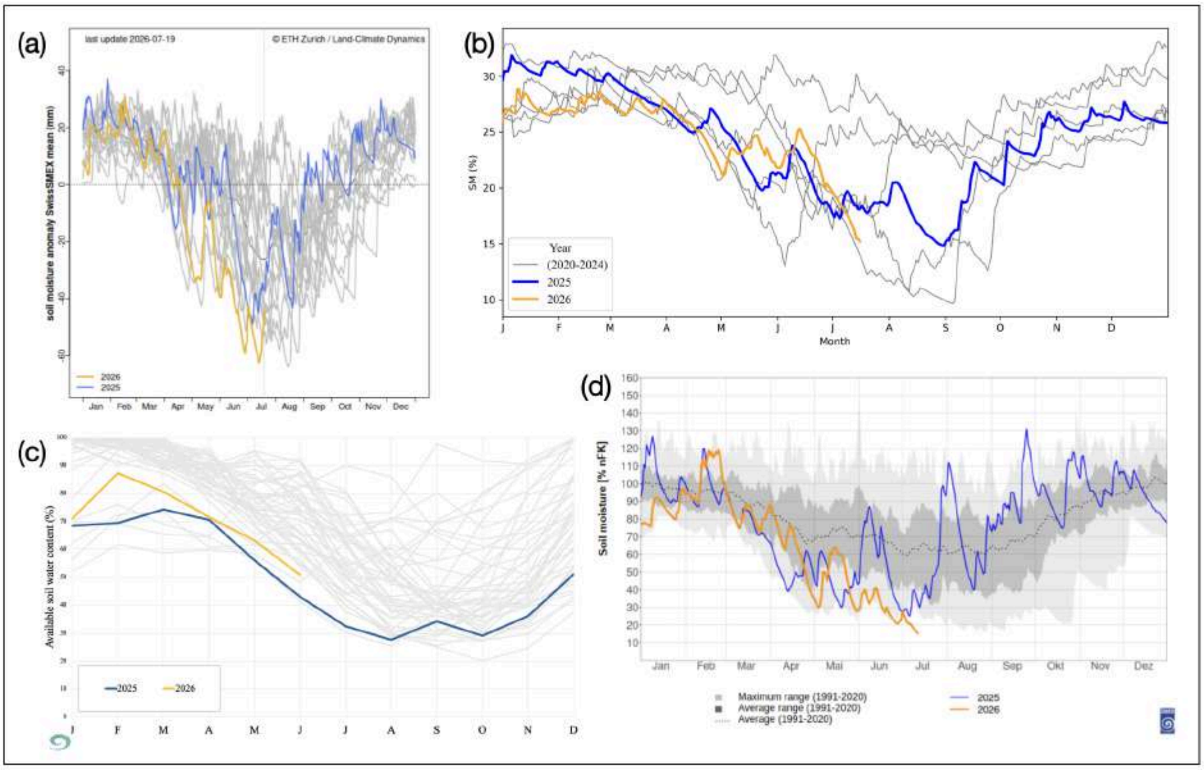

Figure 2.8. Seasonal evolution of root-zone soil moisture in (a) Switzerland SwissSMEX grassland stations (2011–2026) - Averaged soil moisture anomalies (w.r.t. the long-term mean, integrated over the top 50 cm), [ETH, 2026](#), (b) The Netherlands (2020-2026) - Soil moisture is expressed as volumetric water content (%) averaged over two measurement depths (15 and 30 cm) across nine in situ monitoring stations, (c) Békéscsaba meteorological station in the Hungarian Great Plain (1981-2026), the driest region of Hungary - available soil water content expressed as a percentage (0-100cm) based on [computed soil moisture](#) data, (d) German state of Baden-Württemberg in southern Germany - Soil moisture under grass (loamy sand, 0–60 cm depth, station averages), [DWD](#).

2.3 Trends in hydrological variables

To better understand the full extent and consequences of the drought, it is important to investigate the hydrological situation, however an attribution analysis of hydrological variables with respect to climate change was beyond the scope of this rapid analysis. In this section we provide an overview of ground water storage estimates (Sec. 2.3.1) and, as an example of the severe impact of prolonged drought conditions on more localised hydrology, a summary of the intensifying situation in Austria, a subregion of the Eastern Domain (Sec. 2.3.2).

2.3.1 Ground water storage estimates from GRACE-DADM

Ground water storage (GWS) is difficult to measure across large regions or globally, so it is usually studied using hydrological models. Here, we use estimates of groundwater storage from the NASA GRACE/GRACE-FO Data Assimilation for Drought Monitoring (GRACE-DA-DM) Global product (see Appendix A1.1.2 for details).

There are three wetness indicators provided by the product: surface soil moisture (approximately the top 2 cm), root-zone soil moisture (approximately the top 1 m) and shallow groundwater storage (GWS). Each indicator is expressed as a wetness percentile relative to a 1948–2014 climatological reference period, with low percentiles denoting drier-than-normal and high percentiles wetter-than-normal conditions. The three indicators essentially show the same trend, so we will only present the GWS (note that GWS represents model-assimilated groundwater storage rather than in-situ observations).

Figure 2.9 shows the average GWS across the eastern and western domains estimated as follows: for each weekly time step, we selected the grid cells whose centres fall within the west or east domains and computed a latitude-weighted spatial mean of each percentile field to obtain regionally averaged time series over the 2023-2026 study period. The figure shows how the dynamics of the two regions are completely different. On the one hand, the east domain began to lose water reserves from early 2024, reaching the 6th percentile in June 2026. On the other hand, water reserves in the West Domain fluctuate much more rapidly. The data show a severe drought in the second half of 2025, reaching a minimum of the 13th percentile in October. Subsequently, in just six months, the 64th percentile was reached in April, only to fall again to the 21st percentile on 13 July 2026. These trends are not uniform, as can be seen from the linear trends at each grid point for the 3-, 6-, 12- and 30-month periods prior to 13 July 2026 (Fig. 2.10). The large white area in central Europe in the panels of Fig. 2.10 corresponds closely with GWS being very low, less than 2nd percentile (NASA, 2026). As the GWS approaches the lower percentile limit (0), the rate of linear change in percentile/month tends to zero. Over the past 3 months, there is evidence that this area of very low GWS is expanding further to the west in the regions with very negative trends (red area over France in Fig. 2.10 left panel, NASA (2026).

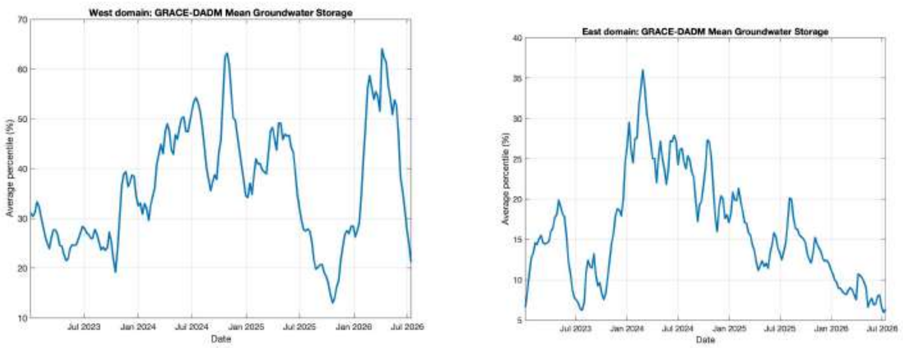

Figure 2.9: Evolution since 2023 of mean ground water storage from GRACE-DA-DM *in the Western domain (left) and the Eastern domain (right).*

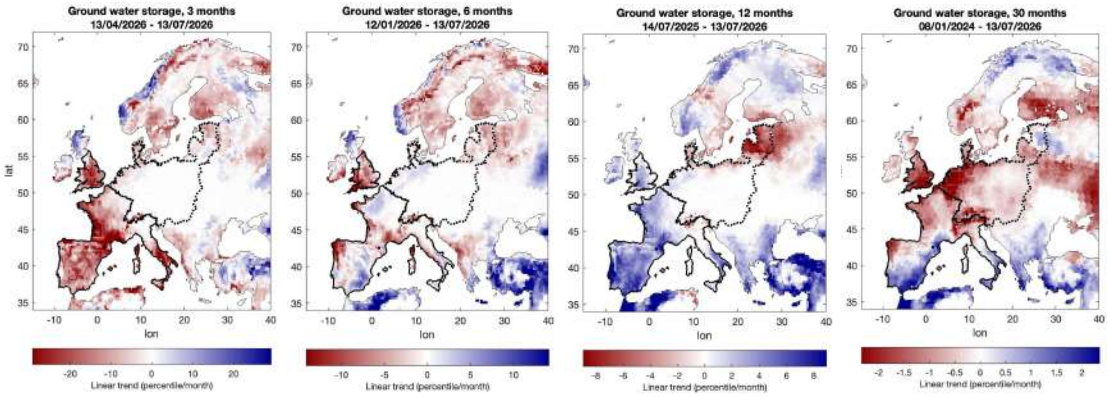

Figure 2.10: Linear trends of GWS from GRACE-DA-DM at each grid point for the 3-, 6-, 12- and 30-month periods prior to 13 July 2026.

2.3.2 Summary of hydrological drought response for Austria

Owing to its strong altitudinal gradients, snow-dominated alpine catchments and diverse hydrogeological settings, Austria exhibits a wide range of hydrological responses to prolonged precipitation deficits. Although severe flooding occurred in September 2024 following exceptionally heavy rainfall, replenishing soil moisture, groundwater and catchment storage across many regions, the subsequent hydrological recovery was only temporary. The winter of 2024/25 was again characterised by below-average precipitation and snow storage, resulting in a prolonged period of below-average recharge that continued throughout 2025 and into 2026.

Hydrological conditions gradually deteriorated during 2025 (Fig. 2.11, Fig. 2.12). Throughout 2025, approximately 55% of Austrian river gauges recorded low or very low monthly streamflow, while around half of the groundwater monitoring stations exhibited low or very low groundwater levels. Although individual rainfall events temporarily improved conditions locally, they did not result in sustained hydrological recovery. The dry autumn and winter of 2025/26 further intensified the situation. By the end of 2025, approximately 60% of both streamflow gauges and groundwater monitoring stations showed low or very low conditions.

Following a short-lived improvement during February 2026, driven by wetter conditions and some snowmelt, hydrological drought intensified during spring. By May 2026, more than 90% of the gauging stations recorded below-average monthly streamflow and around 80% of the groundwater monitoring stations exhibited low or very low groundwater levels.

Rainfall during June resulted in regional improvements, particularly in southern and western Austria. However, these rainfall events were mainly convective and therefore had only a limited effect on groundwater recharge.

As of mid-July 2026, approximately 90% of Austrian groundwater monitoring stations continue to exhibit low or very low groundwater levels, with the most pronounced deficits occurring in Upper Austria, Lower Austria, Burgenland and eastern Styria. Streamflow deficits remain most pronounced in eastern Austria, whereas parts of Tyrol currently show less severe conditions. The prolonged recharge deficit was also reflected in lake levels. By mid-July, Lake Neusiedl was 28 cm below its long-term average, while Lake Constance had reached its lowest level on record for that time of year.

The current hydrological situation reflects the cumulative effects of successive seasons with below-average recharge, including two dry winters, reduced snow storage and an exceptionally dry spring and early summer in 2026. Persistently above-average temperatures since 2024 have further increased evaporative demand, thereby reinforcing the precipitation deficits and limiting groundwater recharge. Short-lived summer rainfall events have so far resulted in only limited hydrological recovery despite locally high precipitation totals.

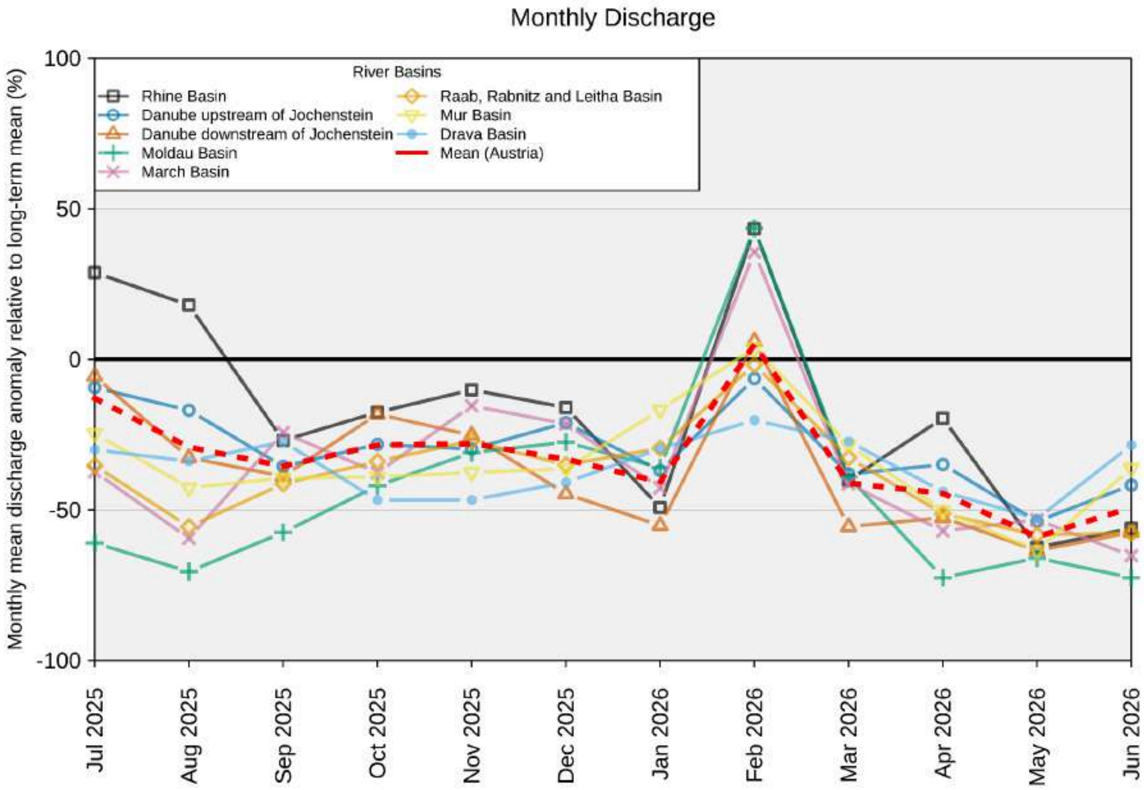

Figure 2.11: Evolution of monthly discharge for Austrian river basins. Discharge anomalies are calculated by comparing the mean flow of the current reporting month against the historical monthly

mean (from the start of the record up to the previous year).

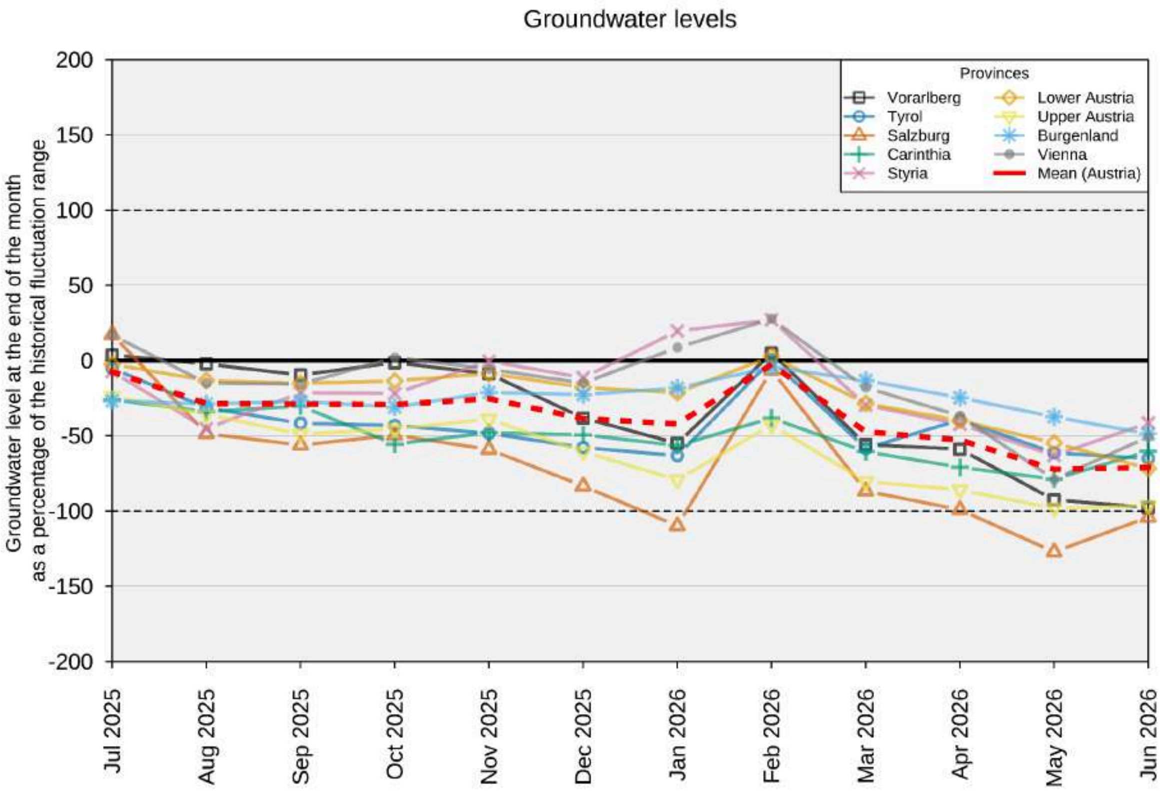

Figure 2.12: Evolution of ground water level for Austrian provinces. Groundwater levels are calculated by comparing the end of month level against the historical fluctuation range (from the start of the record up to the previous year).

2.3.3 Discharge for Elbe River

To provide an illustrative view of the hydrological response within the Central-Eastern Domain, we analysed simulated discharge in the Elbe River at Decin (GRDC station ID: 6140400, upstream area of approximately 51 100 km²), immediately at the Czech/German border. Daily discharge simulated with the mesoscale Hydrologic Model (mHM; Samaniego et al., 2010; Kumar et al., 2013, see Appendix A1.1.2 for details), forced with E-OBS meteorological data, was aggregated to monthly mean values. The 2026 hydrograph was compared with the long-term seasonal flow regime and with selected recent drought years, namely 2018, 2022 and 2025. The mHM–E-OBS modelling framework was previously evaluated against observations of river discharge and terrestrial water storage anomalies and showed good agreement with the observations (Bevacqua et al., 2024, Kettaren et al, 2026).

The simulations (Fig. 2.13) indicate that Elbe discharge decreased substantially below the long-term mean during spring 2026. The mean simulated discharge during April-June 2026 was the lowest for this three-month period in the simulation record beginning in 1950, and was lower than during the selected drought years. This illustrates the propagation of prolonged meteorological and soil-moisture deficits into hydrological drought in the Elbe basin upstream of the Czech-German border. This result is based on a single hydrological model and one river location and should therefore be interpreted as an illustrative assessment rather than a formal attribution of the hydrological drought. A dedicated analysis combining observed discharge records, multiple river basins and hydrological-model ensembles would be required to quantify the contribution of anthropogenic climate change to the low-flow event.

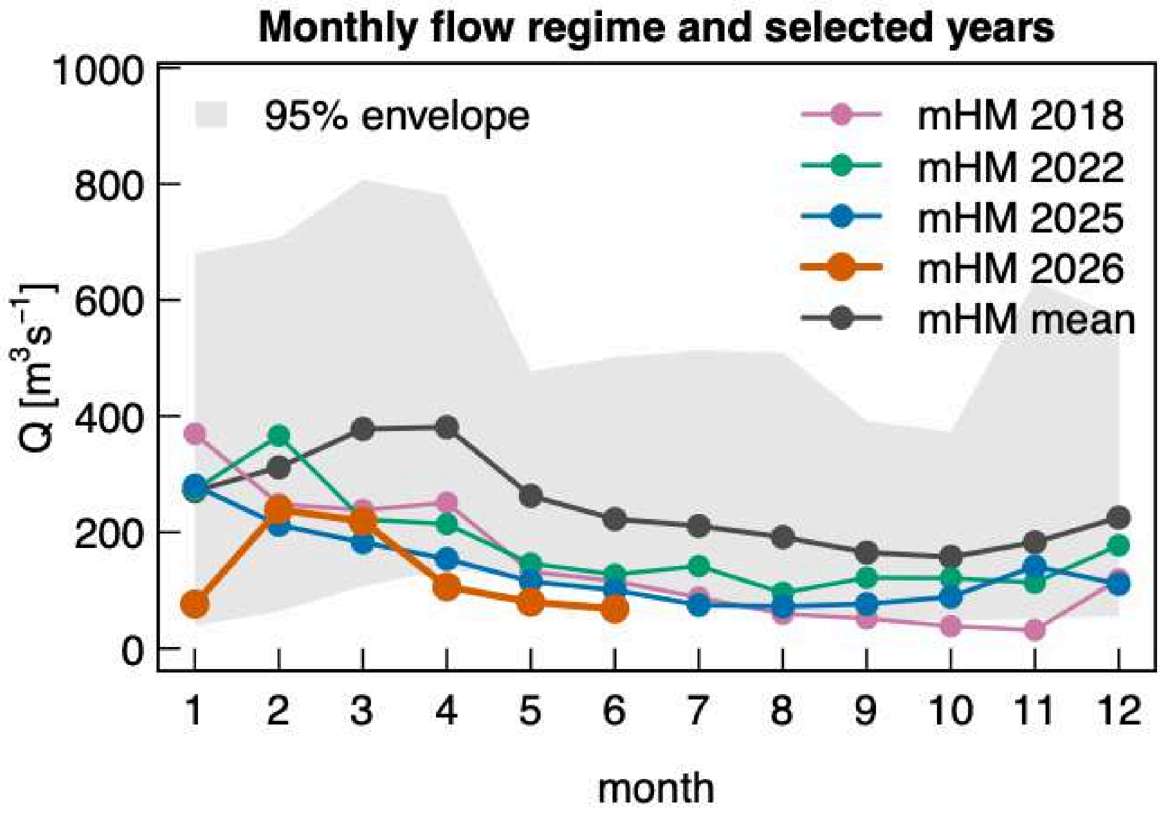

Figure 2.13: Monthly mean discharge of the Elbe River at Decin (GRDC ID: 6140400) near the Czech/German border, simulated by mHM forced with E-OBS meteorological data. Coloured lines show the monthly discharge for 2018, 2022, 2025 and January-June 2026. The dark-grey line shows the 1950-2025 climatological monthly mean, while the grey shading shows the 2.5th-97.5th percentile range for each calendar month over 1950-2025. The mean simulated discharge during April-June 2026 was the lowest for this period in the simulation record beginning in 1950.

2.4 Summary of observed trends

Here we summarise the findings based on observational data.

The current European drought is driven both by anomalously low precipitation and the high evaporative demand linked to anomalously high temperatures. Whilst we find a strong increase in atmospheric evaporative demand (PET) in both study regions and all time scales, we find no significant trend in observed precipitation as the climate warms, although there is an indication that in the Eastern Domain there is a shift from drying to wettening, as the accumulation period lengths from 3 months (AMJ) to 12 months (Jul-Jun). This can be because the longer accumulation periods include wet period interludes, the intensity of which may be increasing as the climate warms due to increased moisture-holding capacity of a warmer atmosphere. Soil moisture, however, which integrates the combined effects of precipitation and evaporation, consistently shows a strong drying signal at both the 3-month (AMJ) time scale and 6-month time scale investigated. In analysing the joint probability distribution of precipitation and PET, it is clearly seen that the increase in drought severity from the past climate 1.4°C cooler climate to present is driven primarily by PET increase.

June 2026 is found to be the driest on record (ERA5-Land, since 1950) in the Western Domain and 2026 is one of the driest Jan-Jun periods in the Eastern Domain. Within the domains it is seen that local conditions can vary but, for soil moisture data available to this study, 2026 is seen to be one of driest years on record so far, especially during April to June.

We carry out no formal attribution of hydrological drought to climate change, but the overview of current situation and trends in terms of hydrological variables (GWS, streamflow) clearly shows the severity of the current drought and a steady decline since 2024 in the Eastern Domain, with the Western Domain also rapidly heading towards hydrological drought. The Eastern decline in GWS and streamflow is clear even at local scales. The Austrian hydrological analysis illustrates that increases in groundwater levels from winter precipitation and short-lived summer convective rain have not been able to retain their hold, with persistently high temperatures since 2024 also reinforcing precipitation deficits and limiting groundwater recharge.

3 Attribution of trends

3.1 Evaluation of climate models

In the subsections below we show the results of the model evaluation for each location. The general procedure is that climate models are evaluated against the observations in their ability to capture:

1. Seasonal cycles: For this, we qualitatively compare the seasonal cycles based on model outputs against observations-based cycles. We discard the models that exhibit ill-defined or poorly timed peaks or troughs in their seasonal cycles with respect to the observations.

2. Spatial patterns: Models that do not match the observations in terms of the large-scale precipitation patterns are excluded.

3. Parameters of the fitted statistical models: We discard the model if the model and observation parameters ranges do not overlap.

The models are labelled as ‘good’,‘reasonable’, or ’bad’ based on their performances in terms of the three criteria discussed above. A model is given an overall rating of ‘good’ if it is rated ‘good’ for all three characteristics. If there is at least one ‘reasonable’, then its overall rating will be ‘reasonable’ and ‘bad’ if there is at least one ‘bad’. For each framing or model setup we also use models that only just pass the evaluation tests if we only have five models or less for that framing that perform well.

In this study, the precipitation, PET and soil moisture metrics were evaluated separately. The study domains incorporated a range of climate zones - ranging from mild temperate to Mediterranean in the western region and ranging from mild temperate to Alpine and continental in the eastern region. Standards for assessing the seasonal cycle in precipitation were slightly softened to account for this. It has been separately verified that the gridded observational precipitation products perform well averaged over the Alpine region (Austria, ERA5 comparison with the high resolution (1 km) daily gridded dataset SPARTACUS based on interpolated station observations and the long-term monthly station-based dataset HISTALP). Overall, 16 models were evaluated for precipitation and PET, and between 9-11 models were retained depending on the event definitions. Tables of the model evaluation results can be found in Appendix A2.

For soil moisture, the CMIP6 ensemble model selection is based on data availability and is therefore similar but not identical to the ensembles used for precipitation and PET. We follow the Schumacher et al. (2024) study of the 2022 European drought for the soil moisture evaluation, i.e. we do not use the fitted statistical parameters of soil moisture itself, but evaluate the models on the soil moisture seasonal cycle and spatial pattern, and additionally based on both temperature and precipitation as auxiliary variables, following the standard procedure above. Each model is evaluated for each relevant event definition and then an overall conclusion is reached for each model. In total, 11 CMIP6 simulations passed the soil moisture evaluation (Appendix A2).

3.2 Synthesis of results

For the event definitions described above we evaluate the influence of anthropogenic climate change on the events by calculating the probability ratio as well as the change in intensity using observations and climate models. Models which do not pass the evaluation described above are excluded from the analysis. The aim is to synthesise results from models that pass the evaluation along with the observations-based products, to give an overarching attribution statement.

Figures in Appendix A3 show the changes in probability and intensity for the observations (blue) and models (red). Before combining them into a synthesised assessment, first, a representation error is added (in quadrature) to the observations, to account for the difference between observations-based datasets that cannot be explained by natural variability. This is shown in these figures as white boxes around the light blue bars. The dark blue bar shows the average over the observation-based products. Next, a term to account for intermodel spread is added (in quadrature) to the natural variability of the models. This is shown in the figures as white boxes around the light red bars. The dark red bar shows the model average, consisting of a weighted mean using the (uncorrelated) uncertainties due to natural variability plus the term representing intermodel spread (i.e., the inverse square of the white bars).

Observation-based products and models are combined into a single result in two ways. Firstly, we neglect common model uncertainties beyond the intermodel spread that is depicted by the model average, and compute the weighted average of models (dark red bar) and observations (dark blue bar): this is indicated by the magenta bar. As, due to common model uncertainties, model uncertainty can be larger than the intermodel spread, secondly, we also show the more conservative estimate of an unweighted, direct average of observations (dark blue bar) and models (dark red bar) contributing 50% each, indicated by the white box around the magenta bar in the synthesis figures.

Over the West Domain, we find no evidence of climate change signal in the AMJ precipitation. The synthesised results from observations and climate models imply no significant change in the likelihood of low precipitation totals due to climate change until now, with PR =1.05 ~1 (uncertainty: 0.26 to 4.24). However, the climate models project a non-significant drying trend under future warming, with a 50% increase in the likelihood of low precipitation such as this one, but not statistically significant (PR=1.46 (uncertainty: 0.6 to 3.55)) and a 4.5% decrease in the amount of precipitation (uncertainty: -14.6 to 6.73).

In contrast, there is a very strong climate change signal in PET. Observations show an exceptionally large increase, with PRs of several hundred thousand, implying that high PET conditions such as the one under study would not have occurred without anthropogenic climate change. This corresponds to an increase in PET of ~16% (uncertainty: 7.09% to 25.32%) in today's climate as compared to an event of similar rarity in a 1.4℃ cooler climate. We note again that PET quantifies the atmospheric evaporative demand and not the actual evaporation, which is limited by available water. Climate models also show increasing response of PET to warming, albeit moderate changes as compared to observations, giving synthesised results that suggesting an overall ~80-fold increase in the likelihood of the observed PET conditions (PR=83.1 (uncertainty: 2.95 to 4330)), and an increase in intensity of 7% (uncertainty: 1.66% to 12.27%). These findings are consistent with previous studies reporting little change in precipitation amounts in both northern and southern Europe (which contains the study region), highlighting that the observed changes in dryness are driven by rising temperatures that lead to higher atmospheric evaporative demand, rather than changes in precipitation.

Over the Eastern Domain, where the impacts of the on-going drought are primarily hydrological in nature, analyses of the six- and twelve- month precipitation show that the low six month and annual precipitation totals such as those observed in 2026 have become less likely. Both observations and climate models indicate that the likelihood of low annual precipitation totals have decreased by a factor of ~2.4 (1/PR=1/0.41), corresponding to a 5% increase in precipitation associated with the event due to 1.4℃ warming since the pre-industrial times. For the six-month precipitation totals, the likelihood of low precipitation totals has decreased by ~2.7 (1/PR=1/0.36) alongside a 7% increase in the precipitation amounts, in today's climate as compared to a 1.4℃ cooler climate. Future projections indicate that this tendency will continue. The likelihood of low annual precipitation totals is projected to halve again relative to the present climate (PR = 0.5; uncertainty: 0.2–1.4), while the precipitation amount associated with the event is projected to increase by 3.5% (uncertainty: −1.5% to +8.5%). For six-month precipitation totals, the likelihood of similarly low values is projected to decrease to around one-third as compared to today, accompanied by an increase of approximately 6% in the associated precipitation amount.

PET in the East Domain shows a strong increase in likelihood and intensity associated with climate change, as with the West Domain. Observations indicate that the observed PET conditions would not have occurred without climate change, as implied by the high Probability Ratio estimates for both six- and twelve- month accumulations (PR =118000 uncertainty: 540 to >4.5M for PET-6 and PR= 59200 uncertainty: 3480 to >1M for PET-12), with best estimated increase in intensity of approximately ~16 to 20%. Climate models show a less pronounced but still strong increase, with a probability ratio of ~8 and an increase in intensity of ~6.4% for both accumulation periods. Combining observational and model evidence gives an overall increase in likelihood of approximately 40- fold for PET-6 and 210-fold for PET-12 and an increase in intensity of about 8%. Looking ahead, future 1.4℃ warming is projected to approximately double the likelihood of 12- month accumulated PET conditions under study, as compared to today (PR= 1.9, uncertainty: 1.8 to 2.1) and increase PET by a further 6.5% (uncertainty: 3.37% to 9.7%). For PET-6, there will be an expected tripling in the likelihood alongside a 5.5% increase in the PET amounts, although this future increase is likely to be conservative for both accumulations, given the stronger signals in observation.

*Table 3.1: Summary of Apr-Jun precipitation and PET results for **western domain**, presented in Figs A3.1.1 and A3.2.1: changes due to GMST include past-present changes and present-future changes. Statistically significant changes at the 95% confidence level are highlighted in **bold text.***

Data	Period	Attributable influence of GMST			
		Precip-3		PET-3	
		Probability ratio (95% CI)	Intensity change (%) (95% CI)	Probability ratio (95% CI)	Intensity change (%) (95% CI)
Observations	Past - Present	1.20 (0.29 to 4.61)	-1.92 (-15.9 to 14.1)	**225000 (1040 to >1m)**	**15.86 (7.09 to 25.32)**
Models		0.92 (0.23 to 3.89)	0.67 (-14.2 to 17.8)	**15.7 (1.04 to 300)**	**4.73 (0.67 to 8.88)**
Synthesis		1.05 (0.26 to 4.24)	-0.69 (-15.1 to 15.9)	**83.1 (2.95 to 4330)**	**6.86 (1.66 to 12.27)**
Models only	Present - Future	1.46 (0.60 to 3.55)	-4.46 (-14.6 to 6.73)	**9.55 (3.95 to 23.2)**	**5.20 (2.83 to 7.62)**

*Table 3.2: Summary of Jan-Jun precipitation and PET results for **eastern domain**, presented in Figs A3.1.2 and A3.2.2: changes due to GMST include past-present changes and present-future changes. Statistically significant changes at the 95% confidence level are highlighted in **bold text.***

Data	Period	Attributable influence of GMST			
		Precip-6		PET-6	
		Probability ratio (95% CI)	Intensity change (%) (95% CI)	Probability ratio (95% CI)	Intensity change (%) (95% CI)
Observations	Past - Present	0.84 (0.13 to 4.66)	1.23 (-10.5 to 14.02)	**118000 (1540 to 48200000)**	**19.66 (5.55 to 35.52)**
Models		0.26 (0.09 to 0.85)	9.56 (0.95 to 18.81)	7.76 (0.80 to 88.2)	**6.06 (1.06 to 11.28)**
Synthesis		0.36 (0.09 to 1.42)	6.89 (-2.95 to 17.49)	**40.3 (2.61 to 1120)**	**7.73 (1.07 to 14.77)**
Models only	Present - Future	0.34 (0.13 to 0.84)	6.14 (1.71 to 10.68)	**3.03 (1.88 to 4.85)**	**5.49 (1.96 to 9.13)**

*Table 3.3: Summary of results for Jul-Jun annual precipitation and PET for the **eastern domain**, presented in Figs A3.1.3 and A3.2.3: changes due to GMST include past-present changes and*

present-future changes. Statistically significant changes at the 95% confidence level are highlighted in ***bold text.***

Data	Period	Attributable influence of GMST			
		Precip-12		PET-12	
		Probability ratio (95% CI)	**Intensity change (%) (95% CI)**	**Probability ratio (95% CI)**	**Intensity change (%) (95% CI)**
Observations	**Past - Present**	0.55 (0.077 to 3.63)	3.98 (-7.22 to 17.4)	**59200 (3480 to >1m)**	**17.68 (4.89 to 32.03)**
Models		0.33 (0.073 to 1.62)	6.40 (-3.69 to 17.5)	8.55 (0.59 to 143)	**6.44 (1.52 to 11.53)**
Synthesis		0.41 (0.073 to 2.24)	5.38 (-5.20 to 17.5)	**214 (13.9 to 7000)**	**7.98 (1.51 to 14.81)**
Models only	**Present - Future**	0.47 (0.15 to 1.39)	3.45 (-1.45 to 8.59)	**1.91 (1.77 to 2.06)**	**6.49 (3.37 to 9.70)**

With regard to the soil moisture results, the synthesized PR indicates that soil-moisture drought of the observed magnitude has become about 5 (uncertainty: 0.93 to 34.8) times more likely in the Western region and about 18 (uncertainty: 2.2 to 210) and 11 (uncertainty: 0.5 to 500) times more likely in the Eastern region for the 3-month and 6-month period respectively. Soil moisture in droughts of similar return period has decreased by about 5.5% (uncertainty: 1% to 10%) in the Western domain, by about 6% (uncertainty: 2.4% to 9%) (Apr-Jun) and 2.6% (uncertainty: -0.3% to 5%) (Jan-Jun) in the Eastern domain between the 1.4°C cooler climate of the past and now, according to the synthesised results. In all three analyses the observations show a stronger drying signal than the models (Figs. A3.3.1-3). The PET results behave in the same way (Figs. A3.2.1-3). The same discrepancy was found for the 2022 European soil-moisture drought (Schumacher et al., 2024a). It is consistent with the observed warming in Europe outpacing climate-model simulations (van Oldenborgh et al., 2009, van Oldenborgh et al., 2022), which has partly been linked to atmospheric-circulation trends that act on top of the thermodynamic warming and are absent or too weak in current models (Vautard et al., 2023; Schumacher et al., 2024b). To the extent that this applies here, the model-based and hence also the synthesized estimates may be conservative. Future (model-based) scenarios suggest further factor increases in soil-drought likelihood (approximately factor 2, 1.7 and 1.7 for the Apr-Jun Western domain, Apr-Jun Eastern domain and Jan-Jun Eastern domain respectively, compared to now) and a further drying (about 2.6%, 1.4% and 0.7%, for the Apr-Jun Western domain, Apr-Jun Eastern domain and Jan-Jun Eastern domain respectively, compared to now) with an additional 1.4°C of warming of the globe.

The soil-moisture results fit together with the precipitation and PET results once the different roles of the two drivers are considered. The increase in evaporative demand is attributable in every accumulation period we analysed, and depletes soil moisture year-round; for the 2022 European summer drought, warming-enhanced evaporation was also identified as the main pathway through which human-induced climate intensified the soil moisture deficit (Bevacqua et al., 2024). The precipitation signal on the other hand depends strongly on the period. As a general tendency, most of western and central Europe is expected to shift towards wetter winters and drier summers, with considerable model spread in both seasons, and spring sits at the transition between the two regimes (Douville et al., 2021; Ranasinghe et al., 2021; Ritzhaupt and Maraun, 2023). The drying tendency in precipitation therefore becomes clearer towards summer. This is also the part of the accumulation window that matters most for soil moisture at the end of June: because of the limited water retention of the soil, precipitation further back in time contributes less and less to the June soil-water content. The accumulated precipitation indices weight all months equally and so dilute this late signal. Over three months the opposing tendencies largely cancel, consistent with the absence of a climate change signal in western AMJ precipitation, and over longer accumulations the winter wetting can dominate, which is what the precipitation analysis in the east shows: the likelihood of low 6- and 12-month precipitation totals has decreased.

None of this contradicts the drying of the soil itself. In terms of intensity, the attributable change is nearly identical across domains at the 3-month scale (about −5.5% in the West and −5.8% in the East; Table 6.3). Over the 6-month period in the East, which includes the winter precipitation increase, this signal is roughly halved, to −2.6%; that the synthesis still points to a soil-moisture decline even at this scale, despite considerable model uncertainty, underlines the strength of the evaporative driver.

Table 3.4: Summary of soil-moisture attribution results for both domains: past–present changes.

Data	**Period**	**West AMJ: PR**	**West AMJ: ΔI (%)**	**East AMJ: PR**	**East AMJ: ΔI (%)**	**East Jan–Jun : PR**	**East Jan–Jun: ΔI (%)**
Observations	Past–Present	**20.6 (3.51 to 258)**	**−6.64 (−10.3 to −2.89)**	**261 (35.1 to 4070)**	**−9.30 (−12.2 to −5.98)**	**26.1 (2.21 to 915)**	**−3.35 (−5.48 to −0.85)**
Models	Past–Present	2.26 (0.46 to 10.8)	−2.48 (−8.40 to 3.43)	2.02 (0.23 to 17.4)	−1.31 (−4.79 to 2.19)	2.24 (0.03 to 146)	−0.42 (−4.37 to 3.53)
Synthesis (weighted)	Past–Present	4.92 (0.93 to 34.8)	**−5.48 (−9.86 to −1.02)**	**18.4 (2.24 to 211)**	**−5.75 (−8.93 to −2.35)**	11.3 (0.48 to 495)	−2.60 (−5.32 to 0.35)
Models only	Present–Future	**1.99 (1.11 to 3.41)**	**−2.64 (−5.01 to −0.29)**	1.67 (0.70 to 3.84)	−1.40 (−3.41 to 0.61)	1.68 (0.32 to 8.60)	−0.70 (−3.07 to 1.67)

3.3 Conclusions hazard

Combining lines of evidence from the synthesis results of the past climate, results from future projections and physical knowledge we communicate that human-induced warming has already increased the likelihood of extreme PET by about 80-fold in the Western Domain and 40-fold (6-month) to 210-fold (12-month) in the Eastern Domain, resulting in soil moisture droughts becoming about 5 times more likely in the Western Domain and 11–18 times more likely in the Eastern Domain than in a 1.4°C cooler climate.

Given current climate policies, in a world 2.8°C warmer than pre-industrial times, as compared to today, extreme PET is projected to become approximately 10 times more likely in the Western Domain, 3 times more likely for 6-month PET, and 2 times more likely for 12-month PET in the Eastern Domain, while the likelihood of comparable soil moisture droughts is projected to increase by about 2-fold in the Western Domain and 1.7-fold in the Eastern Domain.

In the Western Domain, no detectable trend is found in precipitation attributable to warming between now and the pre-industrial climate, although future projections suggest a modest drying trend with around a 50% increase in the likelihood of low precipitation and a 4.5% decrease in the precipitation amounts in a future 1.4℃ warmer world. In contrast the Eastern Domain is projected to become wetter overall, low precipitation such as this year's becoming less likely, and precipitation amounts increasing by approximately 3.5–7%.

Despite these contrasting responses in precipitation, PET has increased many-fold across both regions; this is not surprising because, in a warming climate, atmospheric evaporative demand is expected to increase. This in turn also drives trends in soil moisture droughts. Since observations indicate stronger trends than climate models both in terms of increase in PET and drying in soil moisture, these attribution estimates may be conservative, and therefore under continued warming, even in regions where precipitation is projected to increase, drought risk will continue to amplify.

4 Vulnerability and exposure

In this section we will outline the non-meteorological factors that are worsening or alleviating drought impacts across Europe, looking at key sectors such as energy, agriculture, and drinking water.

4.1 Agriculture

The agriculture sector has been impacted by the drought conditions with France's maize harvest projected to be at its lowest in 50 years, while the Grain Trade Association in Coceral has lowered its forecast for EU maize production by nearly 8 percent to 52.7 million tonnes (Reuters, 2026). In Romania, successive droughts have led to the loss of around one million hectares of maize cultivation since 2019, as farmers increasingly shift to more drought resilient crops (Reuters, 2026). In Slovenia prolonged rainfall deficits led to drying of the topsoil, making soil cultivation more difficult and creating unfavorable conditions for spring sowing and crop root establishment (RTVSLOa, 2026). Moisture shortages on some locations slowed the growth of grasses and cereals, while wheat and barley advanced too rapidly through their developmental stages, resulting in premature ripening and reduced yields (RTVSLOb, RTVSLOc, 2026). Corn growth was also negatively affected, with some areas experiencing more severe impacts depending on soil conditions. Sequential drought events also affected vegetable production which suffered from leaf curling, sunscald, and reduced crop quality (RTVSLOd, 2026). According to Italy's Parmigiano Reggiano Cheese Consortium, heat stress and water constraints have reduced milk production up to 10 percent while also compromising milk quality.

The combination of heat and drought in particular are harmful to crops because the drought limits the amount of water that plants can extract from the soil (e.g., Hao et al., 2025), whereas heat increases vapor pressure deficit and thus the atmospheric demand for moisture (e.g., Grossiord et al., 2020).

Historically, drought has had a significant impact on agriculture in Europe, including reduced crop yields, reduced pasture and forage for livestock, reduced crop quality and knock-on effects on energy costs and supply chains (Olsen et al, 2011). In 2003, for example, the combination of record-breaking heat and drought reduced wheat yields by 11% and maize by 21% on average across Europe (Garcia-Herrara et al., 2010). The hot European summer droughts of 2018 (Beillouin et al., 2020; Hoy et al., 2020; Smith et al., 2020) and 2022 (van der Woude et al., 2023; Feser et al., 2024) also had major impacts on agricultural production. The 2018 drought affected mostly northern-to-central Europe leading to reduced agricultural production (up to 50% reduction for main crops), but this was partly offset due to wetter conditions in southern Europe and associated higher crop yields (up to 34% increase, Toreti et al., 2019). The 2022 heat-drought even led to loss of crop production, which was most severe for maize and sunflower, whereas variability in production of wheat, barley, rapeseed, and rye was mixed (Pinke et al., 2024). Reduced agricultural output can lead to higher food prices, putting relatively more pressure on the most vulnerable people in Europe (Schleypen et al., 2026).

4.2 Critical system and services

Much of Europe's critical infrastructure was designed for historical hydrological conditions where droughts were an infrequent occurrence and is therefore ill equipped to handle drier conditions. Currently 30 percent of Europe's population experiences water stress, with water supply systems unable to meet the region's demand (EEA, 2024). These totals are projected to grow as Europe's water management practices are poorly adapted to the rapid and large-scale changes brought on by climate change (EEA, 2024). A vulnerable water supply also has trickle down effects on several interrelated sectors including agriculture, and freshwater and terrestrial ecosystems (Rossi et al., 2023). Rising temperatures have increased cooling requirements with a 30 percent surge in energy consumption, valued at more than €300 million (Reuters, 2026).

4.2.1 Energy generation

Severe drought in Europe impacts electricity generation from both renewable energy and fossil fuels. For instance during the 2026 period, the French power operator (EDF) had to reduce output (and in some instances shut down reactors) on the Seine and Rhone, to prevent the increased temperature of discharge from harming aquatic ecosystems (Euronews, 2026). During drought years, hydropower utilization rates have been seen to drop by ~5% on average (van Vliet et al., 2016), requiring neighboring countries to step up cross-border energy imports or rely more heavily on fossil-fuel generation (Hu et al. 2026). The extreme heat associated with the current drought conditions further compounds pressures on existing energy systems by reducing the efficiency of solar panels and increasing electricity demand through air conditioning usage.

4.2.2 River transport

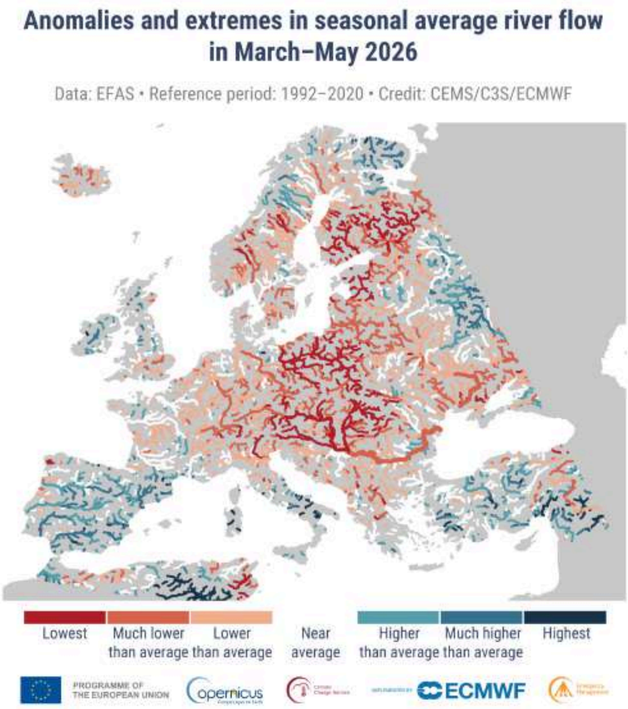

Figure 4.1: River discharge anomalies for March-May 2026 relative to 1992-2020 based on European Flood Awareness System (EFAS).

River flow in major river basins in central and eastern Europe are below normal for this time of year, including the Rhine, Danube, Vistula, Dnieper, and Vuoski (Copernicus, 2026). The Rhine River is reported to have reached about 40cm at Kaub gauge in Germany, and continued low water levels may reduce or eliminate the ability for commercial ships to operate, leading to knock-on effects in industries that rely on shipping for supplies (Freight Perspectives, 2026). During the 2018 drought, reduced water levels in rivers contributed to an estimated 0.2% decline in GDP in the third quarter, which is equivalent to approximately €2.4 billion in economic losses. Prolonged periods of low water could potentially reduce industrial output by 1% per month by disrupting inland waterway transport and supply chains (Global Banking and Finance Review, 2026; Lükerath et al., 2023).

Much of Europe's domestic transportation is conducted through internal waterways. For example, fuel imported through the Netherlands moves inland to refineries, power stations, and consumers via rivers. For instance, Germany's Rhine river alone transports roughly 200 million tons of goods annually (Maguire, 2026). These waterways are particularly vulnerable to drought causing a reduction in barge carrying capacity and ultimately economic damage. In light of these impacts, the EU has taken steps to bolster the resilience of its critical infrastructure by creating the Directive on the Resilience of Critical Entities (European Commission, 2026). This directive aims to create national strategies to identify vulnerable entities that are considered critical or vital for society and the economy.

4.2.3 Water supply and services

Across Europe, water supply comes from groundwater (58-65%), surface water (27-34%), and desalination (~1%) (EEA, 2024). Meanwhile, groundwater is under widespread pressure from pollution and abstraction; about a third of Europe's groundwater lacks sufficient capacity to meet ecosystem or society needs (EEA, 2022). On the demand side, household water conservation is improving; residential consumption per capita decreased by 9% between 2021 and 2026 (EurEau, 2026). However, this progress is challenged by uneven water consumption caused by tourism, especially during summer months, where tourists are not subject to the same water conservation measures as local residents (Florido-Benítez, 2024; Gössling et al., 2012). Furthermore, systemic water loss remains a challenge. Non-revenue water, which encompasses distribution leakages, firefighting, and public cleaning, averages ~22% across Europe, though this has decreased over the last decade (EurEau, 2026). Managing recurrent droughts is made harder by legacy infrastructure. Therefore, improvements such as smart meters, digitalization (e.g. digital twins), and AI (e.g. for managing large datasets) are priority areas of the European Water Resilience Strategy (2025). Finally, circular water practices are unevenly spread throughout Europe (see figure); water reuse is currently not standardized (Lasseur et al., 2026), however, the EU has developed the Water Reuse Regulation to support member states in safely reusing treated urban wastewater for agricultural irrigation (EU, 2024).

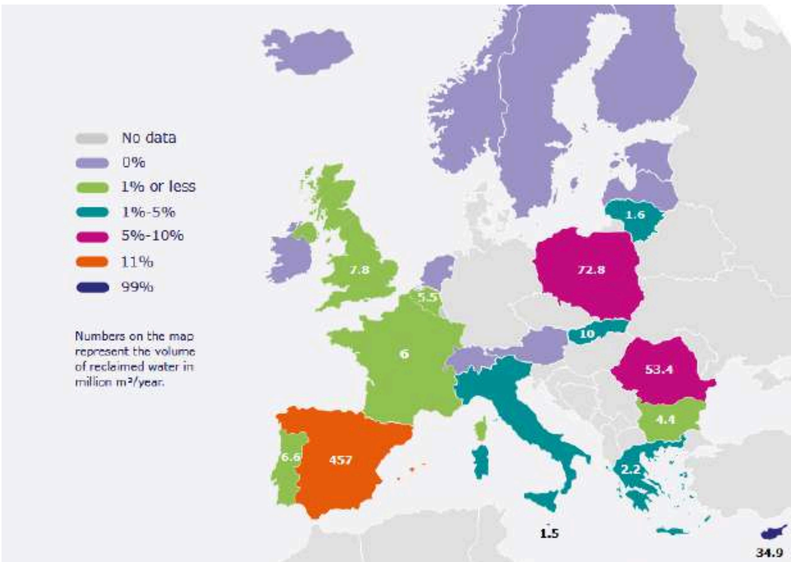

Figure 4.2: Water reuse volume and percentage across Europe (Source: EurEau, 2026)

4.3 Landcover and ecological condition

A drought-stressed ecosystem may have cascading effects from land use and land cover (LULC) change, soil contamination and pollution, invasive alien species (IAS), erosion, and saltwater intrusion. Wildfires and drought contribute to the expansion of IAS and induce changes in land usage (EEA, 2025). Along with the existing climatic conditions, increasing abandonment of cropland, and expansion to forests have increased the risk of droughts in forested areas (natural/ semi-natural), which reduces their ability to sequester carbon (Rossi et al., 2023). Fish mortality, seawater intrusion, eutrophication, algal blooms, and species migration were some cascading impacts reported during early 2000 drought occurrences in Portugal, Finland, Belgium, and the UK (Spinoni, 2016). During 2000 to 2023, drought affected 3% of the EU's cultivated land and 68% of its irrigated lands (EEA, 2025). Between 2019 to 2022, this rose to 5% and 90%, respectively (ibid.). Water security has become a priority as over-exploitation of water worsens the effects of droughts by reducing ground water availability and soil moisture (McCullum, 2024, Rossi et al., 2023).

4.4 Drought risk management

4.4.1 Governance

Drought risk governance in Europe is generally fragmented, with responsibilities shared between individual countries' national ministries, regional environmental agencies, municipal water boards, and water utilities, and currently lacks a unified drought policy (Biella et al., 2026). As such, water is governed in diverse ways across the continent by local governments, publicly owned companies, private operators, or public-private partnerships. Nonetheless, Blauhut et al. (2022) stress an urgent need for the development of a "European macro-level drought governance approach" to adequately deal with future drought impacts.

4.4.2 Policies and plans

At the European Union level, the Water Framework Directive (WFD) aims to promote sustainable water use, prevent further deterioration of water resources, and protect and enhance the status of aquatic ecosystems (EU, 2000). The development of Drought Management Plans (DMPs) is currently not compulsory (EU, 2000). DMPs are in place for 13 member states (Belgium, Cyprus, Germany, Greece, Spain, France, Hungary, Ireland, Italy, Netherlands, Portugal, Romania and Sweden), are being developed for several member states (including Czechia, Finland, Croatia, Luxembourg and Slovenia), while 9 member states have no DMPs in place or in development.

The European Water Resilience Strategy (2025) aims to restore and protect the water cycle, adopt water-smart practices, provide guidance on how to reduce water consumption by 10% by 2030, reduce leaks in pipes, and raise public awareness of water saving practices. One of its key actions of 2026-2027 is to "develop water scarcity indicators and a Technical Guidance on Drought Management Plans" (EU, 2025).

4.4.3 Early warning and early action

To address drought risk, several member states have transitioned from emergency disaster response to proactive tiered-trigger systems that link hydrological indicators (e.g. soil moisture, reservoir levels, groundwater levels) to escalating mandatory actions. For example, the United Kingdom reconvened its National Drought Group on June 18th to monitor risks, preparation, and impacts, and plans to meet monthly throughout the summer (Gov UK, 2026). In the Netherlands, a legally binding water prioritization hierarchy is used by water authorities to distribute surface water; the 4-tiered framework prioritizes vital national safety measures (i.e. dike stability), drinking water, and energy supply, while de-prioritizing shipping and recreation during severe drought (Rijkswaterstaat, n.d.). Poland also has a drought monitoring system which highlights agricultural drought risk for various crops at the commune-level (SMSR, 2026). Hungary introduced a complex agricultural risk management system in 2011 to mitigate production losses caused by adverse weather events, including winter, spring and autumn frost, drought, inland water, heavy precipitation, storms, hail and floods (Hungary Met, 2026). The system provides compensation support for eligible farmers based on the size and type of cultivated land and farmers can access information on weather risks affecting their areas through the free online service.

4.4.4. Emergency response

Several city corporations and local authorities have adopted a combination of demand reduction measures, such as restricting water usage and efficiency improvements and supply augmentation strategies like alternative water sources and increasing storage capacity (OECD, 2025). In Germany, a nationwide water monitoring system has been established to track low water levels in rivers like the Rhine that have disrupted industrial activities (Global Banking and Finance Review, 2026). Cities like Munich introduced strict water conservation measures after prolonged drought pushed daily water consumption to over 360 million litres, well above the usual average usage of around 300 million litres, placing significant pressure on the city's water supply. The city corporation has also imposed water usage restrictions prohibiting excessive water usage for private activities with up to EUR 50,000 fine for violations (AA, 2026). France has placed all 99 inland departments under water restrictions as extreme heatwaves continually intensify drought conditions, this has also resulted in increased monitoring of soil moisture and waterways. Authorities are also expanding heat-response measures by delivering more than 16,500 air conditioning units to hospitals to help manage the impacts of prolonged high temperatures (AA, 2026). Around 100 municipalities in Italy have introduced measures to restrict drinking water use, while some mountainous areas have required water tanker deliveries to address shortage (Swisinfo, 2026). The Piedmont regional government is also seeking additional water supplies from Aosta Valley for agricultural needs, including a request to the Swiss canton of Ticino to increase the volume of water released to the region (Swisinfo, 2026). Due to declining groundwater levels and historically low river flows, several municipalities in Slovenia called for reduced drinking water consumption, while farmers increasingly relied on irrigation systems to mitigate crop losses. As of 11 July 2026, it was recorded that 29 municipalities across the country had introduced bans on the use of drinking water for non-essential purposes, while an additional four municipalities had recommendations for more responsible water use in effect (Žurnal, 2026).

4.4.5 Individual and household coping behaviors

Drought mitigation is made possible, in part, through household coping behavior to reduce water demand. Examples of such measures include temporary water conservation (either voluntary or enforced), emergency water pricing, intermittent water supply (e.g. odd/even day supply), or water reuse (e.g. using greywater for gardens) (Buurman et al., 2017; Laauwen et al. 2026). However, "rebounding" water use, where households and communities increase water use after a sustained period of low demand and/or rationing, remains a common phenomenon (Gonzales & Ajami, 2017). Adaptation to drought conditions is highly unequal; poorer households carry the burden of water rationing, while wealthier households have the capacity to use alternative water sources (e.g. bottled water, private boreholes) (Savelli et al., 2023). Recent research by Schleypen et al. (2026) shows that compound heat and drought events reduce average household income by almost 3% across Europe, and resulting food insecurity is more likely in low-income households than middle-income ones (Kriit et al., 2026).

4.4.6 Insurance and social protection

Across Europe, drought risks are increasingly being addressed through existing agricultural insurance schemes, emergency cash transfer mechanisms and broader social protection measures aimed at supporting vulnerable populations. Given the importance of shock responsive social protection as a key tool for protecting vulnerable populations, using existing beneficiary databases have enabled rapid identification and delivery of assistance and in some cases, scale up of existing social protection programmes. Under the Common Agricultural Policy

2023-2027, the EU maintains an agricultural reserve of at least €450 million annually to respond to market disruptions and exceptional events affecting production (EU, 2026). In response to the increasing climate-related shocks like the current drought situation, Storm Kristin in Portugal, the 2025 drought and heatwaves in Romania and Cyprus as well as freezing temperatures, droughts in Croatia and Slovenia that have severely affected crops, the EU Member States approved the mobilisation of over €56 million from this reserve to support farmers. This funding will benefit producers in Portugal, Romania, Cyprus, Croatia and Slovenia, particularly the fruit, nut, olive, arable crop and mixed livestock farmers. These allocations will be complemented by up to 200% through national funds, further strengthening agricultural resilience to the ongoing droughts (ibid).

5 Conclusions

Overall, the hazard analysis shows that human-induced climate change has increased the likelihood and strength of drought, primarily through increasing atmospheric evaporative demand rather than shifting trends in precipitation deficits itself.

Our vulnerability and exposure analysis shows that the increased severity and frequency of droughts are testing Europe's ability to cope across agricultural, energy, and shipping sectors. While the EU Water Framework Directive promotes sustainable water management, drought management plans are not mandatory, resulting in inconsistent preparedness across EU Member States. At the European level, a unified drought governance policy could help alleviate potential future drought impacts, alongside the Water Resilience Strategy.

Data availability

All time series used in the attribution analysis are available via the Climate Explorer.

Acknowledgements

This work used resources of the Deutsches Klimarechenzentrum (DKRZ), granted by its Scientific Steering Committee (WLA) under project ID bk1088 and datasets provided by ESGF/Copernicus via the DKRZ data pool.

This study benefited from the IPSL computing and data center ESPRI (Ensemble de Services Pour la Recherche à l'IPSL) which is supported by CNRS, Sorbonne Université, CNES, and Ecole Polytechnique.

This work used Imperial College Research Computing Service, DOI: 10.14469/hpc/2232 and the KNMI Climate explorer web tool (https://climexp.knmi.nl/start.cgi).

We acknowledge the E-OBS dataset from the EU-FP6 project UERRA (https://www.uerra.eu) and the Copernicus Climate Change Service, and the data providers in the ECA&D project (https://www.ecad.eu).

References

All references are given as hyperlinks in the text.

Appendices

A1 Data and methods

A1.1 Observational data

A1.1.1 Observational data used for attribution

We first use observational and reanalysis data to estimate the return period of a similar event in the present day and to assess the historical trends with increasing GMST. The datasets used are as follows:

ERA5 - The European Centre for Medium-Range Weather Forecasts's 5th generation reanalysis product, ERA5, is a gridded dataset that combines historical observations into global estimates using advanced modelling and data assimilation systems (Hersbach et al., 2020). For potential evapotranspiration estimates, we use the directly available potential evaporation (pev), which is calculated by the ECMWF Integrated Forecasting System (IFS) as the evaporation from a well-watered surface and assuming no stress from soil moisture. It should be noted that this variable reflects the atmospheric evaporative demand, rather than actual evaporation. In the output tables and synthesis, this data is referred to as ERA5-precalc. Additionally we use the 2m minimum and maximum daily temperature to calculate PET using Hargreave's scheme, and monthly precipitation data from this product at a resolution of 0.25°×0.25°, from the years 1950 to present.

ERA5-Land - This product is a replay of the land component of the ERA5 climate reanalysis (Muñoz-Sabater et al., 2021) produced by the European Centre for Medium-Range Weather Forecasts, with a finer spatial resolution of 0.1° (~9km grid spacing), at hourly time steps from 1950 to 5 days before the current date. The land model used is the tiled ECMWF Scheme for Surface Exchanges over Land incorporating land surface hydrology (H-TESSEL). For an observation-based estimate of soil moisture, we use ERA5-Land soil water in the top 1 m. We additionally use the ERA5-Land 2m minimum and maximum daily temperature to calculate PET using Hargreave's scheme (Appendix A1.4), and monthly precipitation data from this product at a resolution of 0.25°×0.25°, from the years 1950 to present.

E-OBS - This is a gridded land-only observation dataset of Europe, formed from the interpolation of station-derived meteorological observations (Cornes et al., 2018). We use version 33.0e of this dataset, at spatial resolution 0.25° × 0.25° for the 2m minimum and maximum daily temperature to calculate PET using Hargreave's scheme, and monthly precipitation data, from 1920-present.

Covariates
As a measure of anthropogenic climate change we use the (low-pass filtered) global mean surface temperature (GMST), where GMST is taken from the National Aeronautics and Space Administration (NASA) Goddard Institute for Space Science (GISS) surface temperature analysis (GISTEMP, Hansen et al., 2010 and Lenssen et al. 2019). To remove the effect of the El Niño - Southern Oscillation on global mean temperatures, we use a four-year running mean of the GMST, centred on the third year.

A1.1.2 Observational data used for supporting analyses

GRACE-DA-DM

We use estimates of groundwater storage from the NASA GRACE/GRACE-FO Data Assimilation for Drought Monitoring (GRACE-DA-DM) Global product, version 3.0 (GRACEDADM_CLSM025GL_7D), obtained from the NASA Goddard Earth Sciences Data and Information Services Center (GES DISC). The GRACE/GRACE-FO missions measure temporal variations in gravity since 2002, typically on a monthly basis, caused by changes in the water budget. These measurements are aggregated; in other words, they are the result of variations across different layers (soil moisture, canopy, snow, etc.). In this product, terrestrial water storage anomalies derived from GRACE/GRACE-FO are assimilated into the NASA Catchment Land Surface Model (CLSM) within the Land Information System framework using an ensemble Kalman smoother; the assimilation disaggregates the vertically integrated GRACE signal into individual storage components and downscales it in space and time, producing fields at 0.25° resolution with global coverage from February 2003 onward at a weekly (7-day) cadence (Li et al., 2019). Data up to March 2026 are consolidated, while data from 6 April are from the preliminary near-real-time product).

Mesoscale Hydrologic Model (E-OBS driven)

The mesoscale Hydrologic Model (mHM) is a distributed, grid-based hydrological model that simulates snow accumulation and melt, soil-water dynamics, evapotranspiration, runoff generation, subsurface storage and river discharge (Samaniego et al., 2010; Kumar et al., 2013). For this analysis, discharge was obtained from a pan-European mHM simulation at 0.125° spatial resolution and a daily time step. The model was forced with daily E-OBS v33.0e precipitation and minimum, mean and maximum air temperature from 1 January 1950 to 30 June 2026. Potential evapotranspiration was estimated using the Hargreaves-Samani method. Daily discharge was extracted for the Elbe River near Děčín, immediately upstream of the Czech-German border, and aggregated to monthly mean values. The monthly climatological mean and 2.5th to 97.5th percentile range were calculated over 1950-2025.

A1.2 Model and experiment descriptions

We use the CMIP6 ensemble of coupled global circulation models. This consists of simulations from 23 participating models in total (depending on the variable under study) with varying resolutions. For more details on CMIP6, see Eyring et al., (2016). For all simulations, the period 1850 to 2014 is based on historical simulations, while the SSP5-8.5 scenario is used for the remainder of the 21st century.

A1.3 Statistical methods

Methods for observational and model analysis and for model evaluation and synthesis are used according to the World Weather Attribution Protocol, described in Philip et al., (2020), with supporting details found in van Oldenborgh et al., (2021), Ciavarella et al., (2021), Otto et al., (2024) and here. The key steps, presented in sections 3-6, are: (3) trend estimation from observations; (4) model validation; (5) multi-model attribution; and (6) synthesis of the attribution statement.

In this report we analyse time series of soil moisture, precipitation and potential evapotranspiration (PET) for three different time periods - 3 months (April - June), 6 months (January - June) and 12 months (July - June) - for the two study regions western Europe and eastern Europe as defined in Figure 1.3.

A nonstationary Normal distribution is used to model all three indices. For precipitation, the distribution is assumed to scale exponentially with GMST (reflecting the Clausius Clapeyron relation, Trenberth et.al., 2003, O'Gorman and Schneider 2009), with the dispersion (the ratio between the standard deviation and the mean) remaining constant over time; while for the other variables, the distribution is assumed to shift linearly with GMST, while the variance remains constant. The parameters of the statistical model are estimated using maximum likelihood.

For each time series we calculate the return period and intensity of the event under study for the 2026 GMST and for 1.4°C cooler GMST: this allows us to compare the climate of now and of the preindustrial past without human-caused warming (based on Forster et al., 2026), by calculating the probability ratio (PR; the factor-change in the event's probability) and change in intensity of the event. We also calculate the probability ratio and change in intensity of the event under study for a future climate that has warmed by 2.6°C since the pre-industrial period, compared to the climate of now.

A1.4 Estimating PET

The choice of the PET estimation method in calculating SPEI is subjective to and sometimes limited by the availability of meteorological data and the climatic conditions of the region (Trajkovic et al., 2010; Tabari et al., 2013; Zhao et al., 2021). Several studies (Begueria et al., 2014; Van der Schrier et al., 2011; Dai 2011; Sheffield et al., 2012) have compared and evaluated the effect of using different PET equations in the calculation of drought indices. While most of these studies recommend methods that factor radiative and aerodynamic processes (e.g, FAO Penman–Monteith; Allen et al., 1998) in preference to those that consider temperature as the main input (e.g., Thornthwaite; (Thornthwaite (1948), and Hargreaves-Samani; Hargreaves and Samani, 1985), such methods require several climatic parameters and intensive computations. At the same time, there are some temperature based empirical methods: Hargreaves (Hargreaves and Samani, 1982;Hargreaves and Samani, 1985), Baier-Robertson (Baier and Robertson, 1965) and Thornthwaite (Thornthwaite (1948) that serves as good approximations of PET. In this study, we use Hargreaves formula for estimating PET, based on these closely matching the direct PET output available from ERA5 (not shown). The latter is based on surface energy calculations assuming "crops/mixed farming" for the vegetation parameters, that evaporation is not limited by surface water availability, and that the atmosphere is unaffected by this artificial condition (Vicente-Serrano et al., 2022; Copernicus, 2023).

A2 Model evaluation tables

A2.1 Soil moisture

Table A1: *Evaluation results of the climate models considered for attribution analysis of AMJ soil moisture over the Western Domain. For each model, the best estimate of the sigma parameter and the 95% confidence interval obtained via bootstrapping is shown. Furthermore evaluation of the seasonal cycle and spatial pattern are shown.*

	tas_seasonal_cycle	tas_spatial_pattern	tas_sigma	tas_vs_obs	pr_seasonal_cycle	pr_spatial_pattern	pr_dispersion	pr_vs_obs	sm_seasonal_cycle	sm_spatial_pattern	overall
ERA5 (obs; ERA5-Land for SM)			0.7 (0.602 ... 0.829)				0.162 (0.138 ... 0.193)				
ACCESS-CM2 historical-ssp585 (1)	good	good	0.762 (0.655 ... 0.904)	within	reasonable	good	0.132 (0.113 ... 0.156)	overlap	good	good	reasonable
ACCESS-ESM1-5 historical-ssp585 (1)	reasonable	good	0.863 (0.74 ... 1.03)	overlap	reasonable	reasonable	0.154 (0.132 ... 0.184)	within	good	reasonable	bad (pr seasonal cycle east)
BCC-CSM2-MR historical-ssp585 (1)	good	good	0.984 (0.842 ... 1.16)	outside	reasonable	reasonable	0.197 (0.168 ... 0.234)	overlap	bad (much too dry; cycle amplitude too low)	bad (way too dry)	bad (SM cycle+pattern; tas sigma outside obs range)
CESM2 historical-ssp585 (1)	reasonable	good	0.676 (0.579 ... 0.804)	within	reasonable	good	0.172 (0.147 ... 0.205)	within	good	reasonable	reasonable
CESM2-WACCM historical-ssp585 (1)	reasonable	good	0.693 (0.595 ... 0.825)	within	reasonable	good	0.183 (0.156 ... 0.218)	within	good	reasonable	reasonable
CMCC-ESM2 historical-ssp585 (1)	good	good	0.847 (0.724 ... 1)	overlap	reasonable	good	0.195 (0.166 ... 0.233)	overlap	good	good	bad (tas sigma outside obs range in east AMJ)
CanESM5 historical-ssp585 (1)	good	good	0.843 (0.723 ... 1)	overlap	reasonable	reasonable	0.208 (0.177 ... 0.249)	overlap	bad (much too dry; cycle amplitude too low)	bad (way too dry)	bad (SM cycle+pattern; pr dispersion

											outside obs range)
CanESM5-1 historical-ssp585 (1)	good	good	0.824 (0.705 ... 0.976)	within	reasonable	reasonable	0.22 (0.187 ... 0.262)	overlap	bad (much too dry; cycle amplitude too low)	bad (way too dry)	bad (SM cycle+pattern; pr dispersion outside obs range)
EC-Earth3 historical-ssp585 (1)	good	good	0.85 (0.73 ... 1)	overlap	reasonable	good	0.184 (0.157 ... 0.218)	within	good	good	reasonable
EC-Earth3-CC historical-ssp585 (1)	good	good	0.866 (0.74 ... 1.03)	overlap	reasonable	good	0.167 (0.143 ... 0.198)	within	reasonable	reasonable	reasonable
EC-Earth3-Veg historical-ssp585 (1)	good	good	0.945 (0.814 ... 1.13)	overlap	reasonable	good	0.181 (0.154 ... 0.216)	within	good	good	reasonable
EC-Earth3-Veg-LR historical-ssp585 (1)	good	good	0.817 (0.701 ... 0.972)	within	reasonable	good	0.167 (0.142 ... 0.199)	within	good	good	reasonable
MIROC6 historical-ssp585 (1)	bad (summer amplitude overestimated)	bad (Mediterranean too warm)	0.699 (0.597 ... 0.829)	within	good	good	0.162 (0.138 ... 0.193)	within	good	good	bad (tas seasonal cycle + AMJ spatial pattern)
MPI-ESM1-2-HR historical-ssp585 (1)	good	good	0.85 (0.73 ... 1.01)	overlap	good	good	0.168 (0.143 ... 0.202)	within	reasonable	reasonable	reasonable
MPI-ESM1-2-LR historical-s	good	good	0.761 (0.654 ... 0.902)	within	reasonable	reasonable	0.186 (0.159 ... 0.222)	within	reasonable	reasonable	reasonable

sp585 (1)											
MRI-ESM2-0 historical-ssp585 (1)	good	good	0.618 (0.531 ... 0.733)	within	good	reasonable	0.148 (0.127 ... 0.177)	within	good	good	reasonable
NorESM2-LM historical-ssp585 (1)	reasonable	good	0.786 (0.677 ... 0.933)	within	reasonable	reasonable	0.198 (0.169 ... 0.236)	overlap	good	reasonable	reasonable

***Table A2**: Evaluation results of the climate models considered for attribution analysis of AMJ soil moisture over the Eastern Domain. For each model, the best estimate of the dispersion and the 95% confidence interval obtained via bootstrapping. Furthermore evaluation of the seasonal cycle and spatial pattern are shown.*

	tas_seasonal_cycle	**tas_spatial_pattern**	**tas_sigma**	**tas_vs_obs**	**pr_seasonal_cycle**	**pr_spatial_pattern**	**pr_dispersion**	**pr_vs_obs**	**sm_seasonal_cycle**	**sm_spatial_pattern**	**overall**
ERA5 (obs; ERA5-Land for SM)			0.801 (0.686 ... 0.947)				0.131 (0.113 ... 0.156)				
ACCESS-CM2 historical-ssp585 (1)	good	good	0.887 (0.765 ... 1.05)	within	reasonable (1st-half precip ramp-up dampened but present)	good	0.143 (0.122 ... 0.169)	within	good	good	reasonable
ACCESS-ESM1-5 historical-ssp585 (1)	good	good	1.07 (0.918 ... 1.27)	overlap	bad (annual cycle way off, also in Jan-Jun)	reasonable	0.153 (0.13 ... 0.182)	within	good	reasonable	bad (pr seasonal cycle east)
BCC-CSM2-MR historical-ssp585 (1)	good	good	1.24 (1.06 ... 1.47)	outside	reasonable	reasonable	0.179 (0.152 ... 0.213)	overlap	bad (much too dry; cycle amplitude too low)	bad (way too dry)	bad (SM cycle+pattern; tas sigma outside obs range)
CESM2 historical-s	reasonable	good	1.01 (0.865 ... 1.2)	overlap	reasonable	good	0.163 (0.139 ... 0.195)	overlap	good	reasonable	reasonable

sp585 (1)											
CESM2-WACCM historical-ssp585 (1)	reasonable	good	0.883 (0.757 ... 1.05)	within	reasonable	good	0.161 (0.138 ... 0.191)	overlap	good	reasonable	reasonable
CMCC-ESM2 historical-ssp585 (1)	good	good	1.19 (1.02 ... 1.41)	outside	reasonable	good	0.16 (0.137 ... 0.189)	overlap	good	good	bad (tas sigma outside obs range in east AMJ)
CanESM5 historical-ssp585 (1)	good	good	0.892 (0.765 ... 1.06)	within	reasonable	reasonable	0.188 (0.16 ... 0.225)	outside	bad (much too dry; cycle amplitude too low)	bad (way too dry)	bad (SM cycle+pattern; pr dispersion outside obs range)
CanESM5-1 historical-ssp585 (1)	good	good	0.84 (0.721 ... 0.994)	within	reasonable	reasonable	0.189 (0.162 ... 0.225)	outside	bad (much too dry; cycle amplitude too low)	bad (way too dry)	bad (SM cycle+pattern; pr dispersion outside obs range)
EC-Earth3 historical-ssp585 (1)	good	good	1.08 (0.929 ... 1.28)	overlap	reasonable	good	0.157 (0.135 ... 0.186)	overlap	good	good	reasonable
EC-Earth3-CC historical-ssp585 (1)	good	good	1.05 (0.896 ... 1.25)	overlap	reasonable	good	0.161 (0.137 ... 0.191)	overlap	good	reasonable	reasonable
EC-Earth3-Veg historical-ssp585 (1)	good	good	1.02 (0.871 ... 1.2)	overlap	reasonable	good	0.15 (0.128 ... 0.177)	within	good	good	reasonable

EC-Earth3-Veg-LR historical-ssp585 (1)	good	good	0.852 (0.734 ... 1.01)	within	reasonable	good	0.135 (0.115 ... 0.159)	within	good	good	reasonable
MIROC6 historical-ssp585 (1)	bad (summer amplitude overestimated)	bad (Mediterranean too warm)	1 (0.86 ... 1.19)	overlap	reasonable	good	0.131 (0.112 ... 0.156)	within	good	good	bad (tas seasonal cycle + AMJ spatial pattern)
MPI-ESM1-2-HR historical-ssp585 (1)	good	good	0.931 (0.798 ... 1.1)	within	reasonable	good	0.158 (0.135 ... 0.188)	overlap	reasonable	reasonable	reasonable
MPI-ESM1-2-LR historical-ssp585 (1)	good	good	0.826 (0.71 ... 0.98)	within	reasonable	reasonable	0.16 (0.138 ... 0.191)	overlap	reasonable	reasonable	reasonable
MRI-ESM2-0 historical-ssp585 (1)	good	good	0.87 (0.746 ... 1.03)	within	good	reasonable	0.14 (0.12 ... 0.166)	within	good	good	reasonable
NorESM2-LM historical-ssp585 (1)	good	good	0.809 (0.692 ... 0.961)	within	reasonable (late-summer drying overdone)	reasonable	0.145 (0.123 ... 0.173)	within	good	reasonable	reasonable

***Table A3**: Evaluation results of the climate models considered for attribution analysis of JFMAMJ soil moisture over the Eastern Domain. For each model, the best estimate of the dispersion and the 95% confidence interval obtained via bootstrapping. Furthermore evaluation of the seasonal cycle and spatial pattern are shown.*

	tas_seasonal_cycle	**tas_spatial_pattern**	**tas_sigma**	**tas_vs_obs**	**pr_seasonal_cycle**	**pr_spatial_pattern**	**pr_dispersion**	**pr_vs_obs**	**sm_seasonal_cycle**	**sm_spatial_pattern**	**overall**
ERA5 (obs; ERA5-Land for SM)			1.03 (0.886 ... 1.23)				0.118 (0.101 ... 0.141)				
ACCESS-CM2 histor	good	good	0.945 (0.809 ... 1.12)	within	reasonable (1st-half precip ramp-up	good	0.108 (0.0927 ... 0.129)	within	good	good	reasonable

ical-ssp585 (1)					dampened but present)						
ACCESS-ESM1-5 historical-ssp585 (1)	good	good	0.963 (0.827 ... 1.14)	within	bad (annual cycle way off, also in Jan-Jun)	reasonable	0.124 (0.106 ... 0.147)	within	good	reasonable	bad (pr seasonal cycle east)
BCC-CSM2-MR historical-ssp585 (1)	good	good	1.23 (1.05 ... 1.46)	within	reasonable	reasonable	0.121 (0.104 ... 0.143)	within	bad (much too dry; cycle amplitude too low)	bad (way too dry)	bad (SM cycle+pattern; tas sigma outside obs range)
CESM2 historical-ssp585 (1)	reasonable	good	0.947 (0.814 ... 1.13)	within	reasonable	good	0.137 (0.117 ... 0.163)	within	good	reasonable	reasonable
CESM2-WACCM historical-ssp585 (1)	reasonable	good	0.893 (0.766 ... 1.06)	within	reasonable	good	0.112 (0.0956 ... 0.133)	within	good	reasonable	reasonable
CMCC-ESM2 historical-ssp585 (1)	good	good	1.14 (0.979 ... 1.35)	within	reasonable	good	0.133 (0.114 ... 0.158)	within	good	good	bad (tas sigma outside obs range in east AMJ)
CanESM5 historical-ssp585 (1)	good	good	1.17 (1.01 ... 1.38)	within	reasonable	reasonable	0.131 (0.112 ... 0.156)	within	bad (much too dry; cycle amplitude too low)	bad (way too dry)	bad (SM cycle+pattern; pr dispersion outside obs range)
CanESM5-1 historical-ssp585 (1)	good	good	1.01 (0.868 ... 1.21)	within	reasonable	reasonable	0.122 (0.104 ... 0.145)	within	bad (much too dry; cycle amplitude too low)	bad (way too dry)	bad (SM cycle+pattern; pr dispersion outside obs range)

EC-Earth3 historical-ssp585 (1)	good	good	1.23 (1.06 ... 1.46)	overlap	reasonable	good	0.125 (0.107 ... 0.148)	within	good	good	reasonable
EC-Earth3-CC historical-ssp585 (1)	good	good	1.2 (1.02 ... 1.42)	within	reasonable	good	0.112 (0.0964 ... 0.134)	within	good	reasonable	reasonable
EC-Earth3-Veg historical-ssp585 (1)	good	good	1.31 (1.13 ... 1.55)	overlap	reasonable	good	0.112 (0.0963 ... 0.133)	within	good	good	reasonable
EC-Earth3-Veg-LR historical-ssp585 (1)	good	good	1.29 (1.11 ... 1.53)	overlap	reasonable	good	0.116 (0.0994 ... 0.137)	within	good	good	reasonable
MIROC6 historical-ssp585 (1)	bad (summer amplitude overestimated)	reasonable	1.11 (0.955 ... 1.32)	within	reasonable	good	0.0978 (0.0837 ... 0.117)	overlap	good	good	bad (tas seasonal cycle + AMJ spatial pattern)
MPI-ESM1-2-HR historical-ssp585 (1)	good	good	0.954 (0.817 ... 1.14)	within	reasonable	good	0.123 (0.106 ... 0.146)	within	reasonable	reasonable	reasonable
MPI-ESM1-2-LR historical-ssp585 (1)	good	good	1.04 (0.893 ... 1.23)	within	reasonable	reasonable	0.116 (0.0997 ... 0.138)	within	reasonable	reasonable	reasonable
MRI-ESM2-0 historical-ssp585 (1)	good	good	0.909 (0.78 ... 1.08)	within	good	reasonable	0.111 (0.0946 ... 0.132)	within	good	good	reasonable
NorESM2-LM historical-s	good	good	0.878 (0.751 ... 1.05)	overlap	reasonable (late-summer drying overdone)	reasonable	0.118 (0.101 ... 0.14)	within	good	reasonable	reasonable

sp585 (1)											

A2.2 Precipitation

***Table A4**: Evaluation results of the climate models considered for attribution analysis of AMJ precipitation over the Western Domain. For each model, the best estimate of the dispersion and the 95% confidence interval obtained via bootstrapping. Furthermore evaluation of the seasonal cycle and spatial pattern are shown.*

Model / Observations	**Seasonal cycle**	**Spatial pattern**	**Dispersion**	**Conclusion**
EObs			0.180 (0.153 ... 0.200)	
ERA5			0.159 (0.135 ... 0.178)	
ERA5Land			0.156 (0.130 ... 0.175)	
CMIP6				
ACCESS-CM2 - r1i1p1f1 ()	good	reasonable	0.143 (0.110 ... 0.168)	reasonable
ACCESS-ESM1-5 - r1i1p1f1 ()	reasonable	reasonable	0.165 (0.131 ... 0.190)	reasonable
CanESM5 - r1i1p1f1 ()	bad	bad	0.209 (0.164 ... 0.242)	bad (could switch to sp=reas)
CMCC-ESM2 - r1i1p1f1 ()	good	reasonable	0.192 (0.150 ... 0.223)	reasonable
EC-Earth3 - r1i1p1f1 ()	good	reasonable	0.137 (0.102 ... 0.163)	reasonable
EC-Earth3-Veg-LR - r1i1p1f1 ()	good	good	0.156 (0.121 ... 0.179)	good
EC-Earth3-Veg - r1i1p1f1 ()	good	good	0.178 (0.141 ... 0.203)	good
INM-CM4-8 - r1i1p1f1 ()	reasonable	bad	0.249 (0.199 ... 0.282)	bad (could switch to sp=reas)
INM-CM5-0 - r1i1p1f1 ()	good	bad	0.188 (0.147 ... 0.222)	bad (could switch to sp=reas)
IPSL-CM6A-LR - r1i1p1f1 ()	reasonable	good	0.170 (0.134 ... 0.201)	reasonable
MIROC6 - r1i1p1f1 ()	good	reasonable	0.184 (0.145 ... 0.213)	reasonable
MPI-ESM1-2-HR - r1i1p1f1 ()	reasonable	good	0.151 (0.123 ... 0.173)	reasonable
MPI-ESM1-2-LR - r1i1p1f1 ()	good	reasonable	0.177 (0.143 ... 0.202)	reasonable
MRI-ESM2-0 - r1i1p1f1 ()	reasonable	good	0.163 (0.132 ... 0.187)	reasonable
NorESM2-LM - r1i1p1f1 ()	bad	bad	0.172 (0.136 ... 0.200)	bad (could switch to sp=reas)
NorESM2-MM - r1i1p1f1 ()	bad	reasonable	0.178 (0.137 ... 0.210)	bad

Table A5: *Evaluation results of the climate models considered for attribution analysis of JFMAMJ precipitation over the Eastern Domain. For each model, the best estimate of the dispersion and the 95% confidence interval obtained via bootstrapping. Furthermore evaluation of the seasonal cycle and spatial pattern are shown.*

Model / Observations	**Seasonal cycle**	**Spatial pattern**	**Dispersion**	**Conclusion**
EObs			0.131 (0.110 ... 0.146)	
ERA5			0.117 (0.0992 ... 0.131)	
ERA5Land			0.116 (0.0975 ... 0.130)	
CMIP6				
ACCESS-CM2 - r1i1p1f1 ()	reasonable	reasonable	0.111 (0.0859 ... 0.128)	reasonable
ACCESS-ESM1-5 - r1i1p1f1 ()	bad	reasonable	0.122 (0.0944 ... 0.144)	bad
CanESM5 - r1i1p1f1 ()	good	bad	0.140 (0.105 ... 0.164)	bad
CMCC-ESM2 - r1i1p1f1 ()	reasonable	reasonable	0.145 (0.118 ... 0.164)	reasonable
EC-Earth3 - r1i1p1f1 ()	good	reasonable	0.101 (0.0791 ... 0.118)	reasonable
EC-Earth3-Veg-LR - r1i1p1f1 ()	good	good	0.109 (0.0800 ... 0.130)	good
EC-Earth3-Veg - r1i1p1f1 ()	reasonable	good	0.105 (0.0813 ... 0.125)	reasonable
INM-CM4-8 - r1i1p1f1 ()	bad	bad	0.111 (0.0894 ... 0.127)	bad
INM-CM5-0 - r1i1p1f1 ()	bad	bad	0.128 (0.105 ... 0.144)	bad
IPSL-CM6A-LR - r1i1p1f1 ()	reasonable	good	0.0896 (0.0678 ... 0.108)	reasonable
MIROC6 - r1i1p1f1 ()	reasonable	reasonable	0.102 (0.0803 ... 0.121)	reasonable
MPI-ESM1-2-HR - r1i1p1f1 ()	reasonable	good	0.118 (0.0919 ... 0.141)	reasonable
MPI-ESM1-2-LR - r1i1p1f1 ()	reasonable	reasonable	0.116 (0.0831 ... 0.144)	reasonable
MRI-ESM2-0 - r1i1p1f1 ()	good	good	0.110 (0.0862 ... 0.130)	good
NorESM2-LM - r1i1p1f1 ()	bad	bad	0.125 (0.0947 ... 0.145)	bad
NorESM2-MM - r1i1p1f1 ()	bad	reasonable	0.0801 (0.0611 ... 0.0941)	bad

Table A6: *Evaluation results of the climate models considered for attribution analysis of annual (Jul-Jun) precipitation over the Eastern Domain. For each model, the best estimate of the dispersion and the 95% confidence interval obtained via bootstrapping. Furthermore evaluation of the seasonal cycle and spatial pattern are shown.*

Model / Observations	Seasonal cycle	Spatial pattern	Dispersion	Conclusion
EObs			0.102 (0.0842 ... 0.116)	
ERA5			0.0934 (0.0759 ... 0.108)	
ERA5Land			0.0926 (0.0750 ... 0.107)	
CMIP6				
ACCESS-CM2 - r1i1p1f1 ()	reasonable	reasonable	0.0962 (0.0764 ... 0.111)	reasonable
ACCESS-ESM1-5 - r1i1p1f1 ()	bad	reasonable	0.0900 (0.0661 ... 0.110)	bad
CanESM5 - r1i1p1f1 ()	good	bad	0.0851 (0.0709 ... 0.0954)	bad (could switch to sp=reas)
CMCC-ESM2 - r1i1p1f1 ()	reasonable	reasonable	0.109 (0.0886 ... 0.126)	reasonable
EC-Earth3 - r1i1p1f1 ()	good	reasonable	0.0746 (0.0552 ... 0.0899)	reasonable
EC-Earth3-Veg-LR - r1i1p1f1 ()	good	good	0.0898 (0.0672 ... 0.112)	good
EC-Earth3-Veg - r1i1p1f1 ()	reasonable	good	0.0871 (0.0649 ... 0.107)	reasonable
INM-CM4-8 - r1i1p1f1 ()	bad	bad	0.0920 (0.0719 ... 0.109)	bad (could switch to sp=reas)
INM-CM5-0 - r1i1p1f1 ()	bad	bad	0.0750 (0.0590 ... 0.0867)	bad (could switch to sp=reas)
IPSL-CM6A-LR - r1i1p1f1 ()	reasonable	good	0.0605 (0.0457 ... 0.0718)	bad
MIROC6 - r1i1p1f1 ()	reasonable	reasonable	0.0789 (0.0622 ... 0.0917)	reasonable
MPI-ESM1-2-HR - r1i1p1f1 ()	reasonable	good	0.0818 (0.0652 ... 0.0954)	reasonable
MPI-ESM1-2-LR - r1i1p1f1 ()	reasonable	reasonable	0.105 (0.0803 ... 0.128)	reasonable
MRI-ESM2-0 - r1i1p1f1 ()	good	good	0.0770 (0.0614 ... 0.0888)	good
NorESM2-LM - r1i1p1f1 ()	bad	bad	0.0884 (0.0652 ... 0.106)	bad (could switch to sp=reas)
NorESM2-MM - r1i1p1f1 ()	bad	reasonable	0.0646 (0.0492 ... 0.0770)	bad

A2.3 PET

Table A7*: Evaluation results of the climate models considered for attribution analysis of AMJ PET over the Western Domain. For each model, the best estimate of the sigma parameter and the 95% confidence interval obtained via bootstrapping. Furthermore evaluation of the seasonal cycle and spatial pattern are shown.*

Model / Observations	Seasonal cycle	Spatial pattern	Sigma	Conclusion

EObs			12.8 (10.9 ... 14.5)	
ERA5			12.6 (10.7 ... 14.1)	
ERA5-precalc			21.9 (18.6 ... 24.7)	
ERA5Land			12.4 (10.5 ... 13.8)	
CMIP6			(...)	
ACCESS-CM2-r1i1p1f1 ()	good	good	13.9 (10.5 ... 16.5)	good
ACCESS-ESM1-5-r1i1p1f1 ()	good	good	18.9 (14.8 ... 21.9)	good
CanESM5-r1i1p1f1 ()	good	good	15.7 (12.6 ... 17.9)	good
CMCC-ESM2-r1i1p1f1 ()	good	good	18.4 (14.2 ... 21.1)	good
EC-Earth3-r1i1p1f1 ()	good	good	14.4 (11.1 ... 17.0)	good
EC-Earth3-Veg-LR-r1i1p1f1 ()	good	good	12.9 (9.96 ... 15.1)	good
EC-Earth3-Veg-r1i1p1f1 ()	good	good	17.2 (13.0 ... 20.5)	good
INM-CM4-8-r1i1p1f1 ()	bad	reasonable	26.9 (21.7 ... 30.5)	bad
INM-CM5-0-r1i1p1f1 ()	reasonable	reasonable	22.9 (18.0 ... 27.0)	reasonable
IPSL-CM6A-LR-r1i1p1f1 ()	good	good	12.7 (10.4 ... 14.4)	good
MIROC6-r1i1p1f1 ()	reasonable	reasonable	18.6 (14.0 ... 22.3)	reasonable
MPI-ESM1-2-HR-r1i1p1f1 ()	good	good	14.9 (11.8 ... 17.2)	good
MPI-ESM1-2-LR-r1i1p1f1 ()	good	reasonable	16.1 (12.9 ... 18.6)	reasonable
MRI-ESM2-0-r1i1p1f1 ()	good	good	12.5 (9.08 ... 15.4)	good
NorESM2-LM-r1i1p1f1 ()	good	reasonable	13.4 (10.8 ... 15.2)	reasonable
NorESM2-MM-r1i1p1f1 ()	good	good	13.4 (10.7 ... 15.3)	good

Table A8: *Evaluation results of the climate models considered for attribution analysis of JFMAMJ PET over the Eastern Domain. For each model, the best estimate of the sigma parameter and the 95% confidence interval obtained via bootstrapping. Furthermore evaluation of the seasonal cycle and spatial pattern are shown.*

Model / Observations	**Seasonal cycle**	**Spatial pattern**	**Sigma**	**Conclusion**
EObs			16.3 (13.8 ... 18.4)	
ERA5			13.3 (11.3 ... 14.8)	
ERA5-precalc			22.8 (19.2 ... 25.7)	
ERA5Land			13.2 (11.2 ... 14.7)	
CMIP6				

ACCESS-CM2 historical-rcp85 (1)	good	good	15.5 (11.7 ... 18.9)	good
ACCESS-ESM1-5 historical-rcp85 (1)	reasonable	good	26.5 (18.1 ... 33.2)	reasonable
CanESM5 ()	good	good	15.5 (12.0 ... 18.2)	good
CMCC-ESM2 ()	good	good	23.8 (20.0 ... 26.2)	good
EC-Earth3 ()	good	good	14.4 (11.1 ... 16.8)	good
EC-Earth3-Veg-LR ()	good	good	14.3 (11.8 ... 15.9)	good
EC-Earth3-Veg-LR ()	good	good	20.2 (16.2 ... 22.8)	good
INM-CM4-8 ()	reasonable	reasonable	19.9 (15.5 ... 23.8)	reasonable
INM-CM5-0 ()	reasonable	reasonable	18.9 (15.6 ... 21.2)	reasonable
IPSL-CM6A-LR ()	good	good	18.0 (14.1 ... 20.9)	good
MIROC6 ()	good	reasonable	20.6 (16.0 ... 24.2)	reasonable
MPI-ESM1-2-HR ()	good	good	15.0 (11.4 ... 17.6)	good
MPI-ESM1-2-LR ()	good	reasonable	13.6 (10.7 ... 15.8)	reasonable
MRI-ESM2-0 ()	good	good	14.0 (10.8 ... 16.3)	good
NorESM2-LM ()	good	reasonable	16.4 (12.9 ... 18.9)	reasonable
NorESM2-MM ()	good	good	14.8 (11.1 ... 17.8)	good

Table A9*: Evaluation results of the climate models considered for attribution analysis of annual (Jul-Jun) PET over the Eastern Domain. For each model, the best estimate of the sigma parameter and the 95% confidence interval obtained via bootstrapping. Furthermore evaluation of the seasonal cycle and spatial pattern are shown.*

Model / Observations	**Seasonal cycle**	**Spatial pattern**	**Sigma**	**Conclusion**
EObs			25.0 (21.3 ... 28.2)	
ERA5			19.8 (17.0 ... 22.3)	
ERA5-precalc			38.4 (32.7 ... 43.0)	
ERA5Land			19.7 (16.9 ... 22.1)	
CMIP6				
ACCESS-CM2 historical-rcp85 (1)	good	good	19.6 (16.0 ... 22.7)	good
ACCESS-ESM1-5 historical-rcp85 (1)	reasonable	good	36.5 (27.2 ... 43.7)	reasonable
CanESM5 (1)	good	good	23.1 (18.8 ... 26.5)	good
CMCC-ESM2 (1)	good	good	34.2 (27.7 ... 39.8)	good
EC-Earth3 (1)	good	good	22.5 (18.5 ... 25.3)	good
EC-Earth3-Veg-LR (1)	good	good	23.1 (17.3 ... 27.6)	good
EC-Earth3-Veg-LR (1)	good	good	27.6 (21.7 ... 31.6)	good
INM-CM4-8 (1)	reasonable	reasonable	28.5 (21.2 ... 34.2)	reasonable
INM-CM5-0 (1)	reasonable	reasonable	27.8 (21.5 ... 32.3)	reasonable
IPSL-CM6A-LR (1)	good	good	25.4 (19.7 ... 29.3)	good

MIROC6 (1)	good	reasonable	29.8 (23.5 ... 34.8)	reasonable
MPI-ESM1-2-HR (1)	good	good	24.9 (18.5 ... 29.1)	good
MPI-ESM1-2-LR (1)	good	reasonable	24.8 (19.4 ... 29.1)	reasonable
MRI-ESM2-0 (1)	good	good	17.7 (14.0 ... 20.3)	good
NorESM2-LM (1)	good	reasonable	26.6 (21.1 ... 30.3)	reasonable
NorESM2-MM (1)	good	good	21.2 (16.2 ... 25.0)	good

A3 Synthesis Figures

A3.1 Precipitation synthesis plots

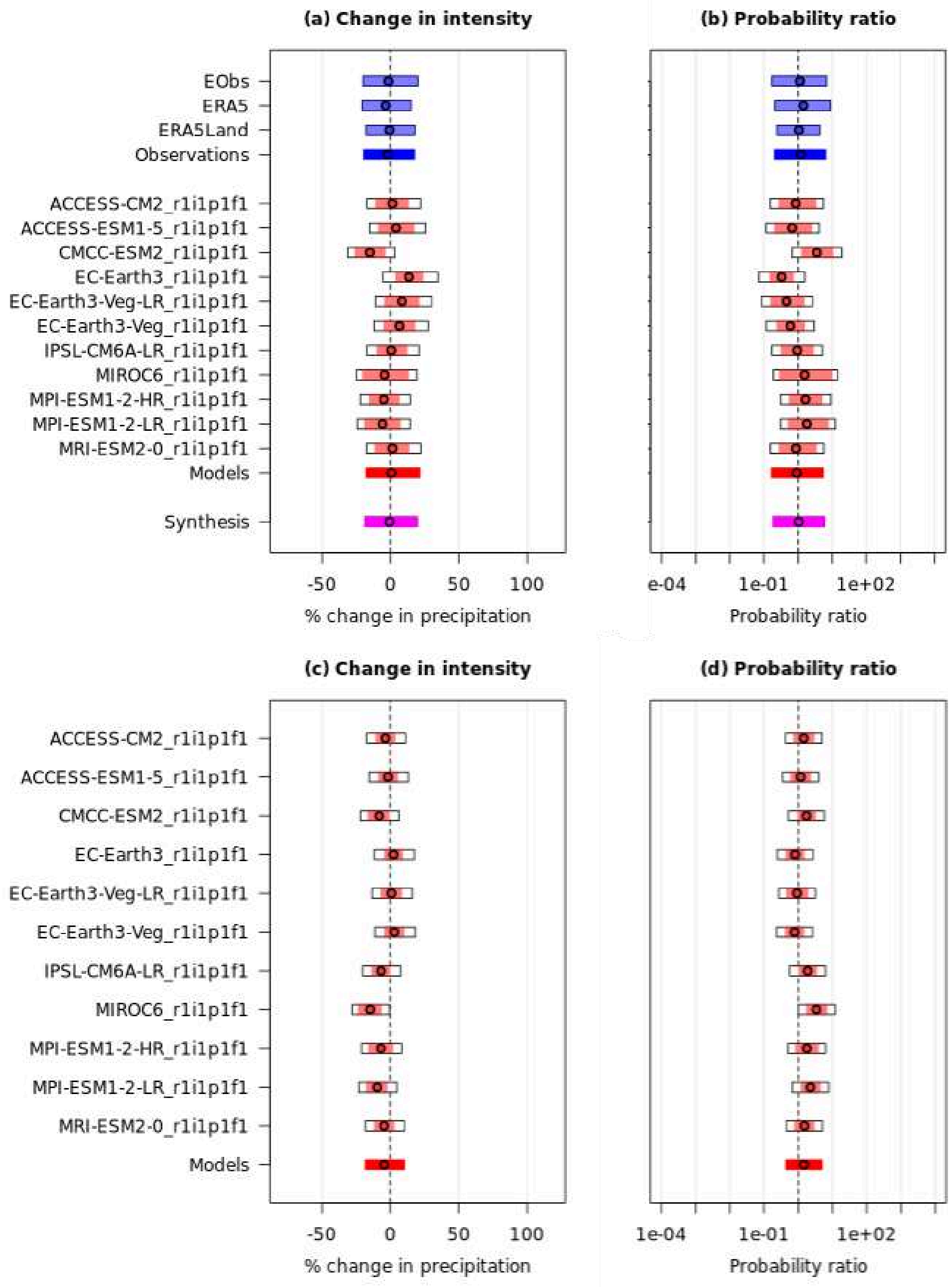

Figure A3.1.1 *(a) Change in intensity for precip AMJ (%) and (b) Probability Ratio for the Western Domain from past to present. (c) same as (a) and same as (b) from present to future.*

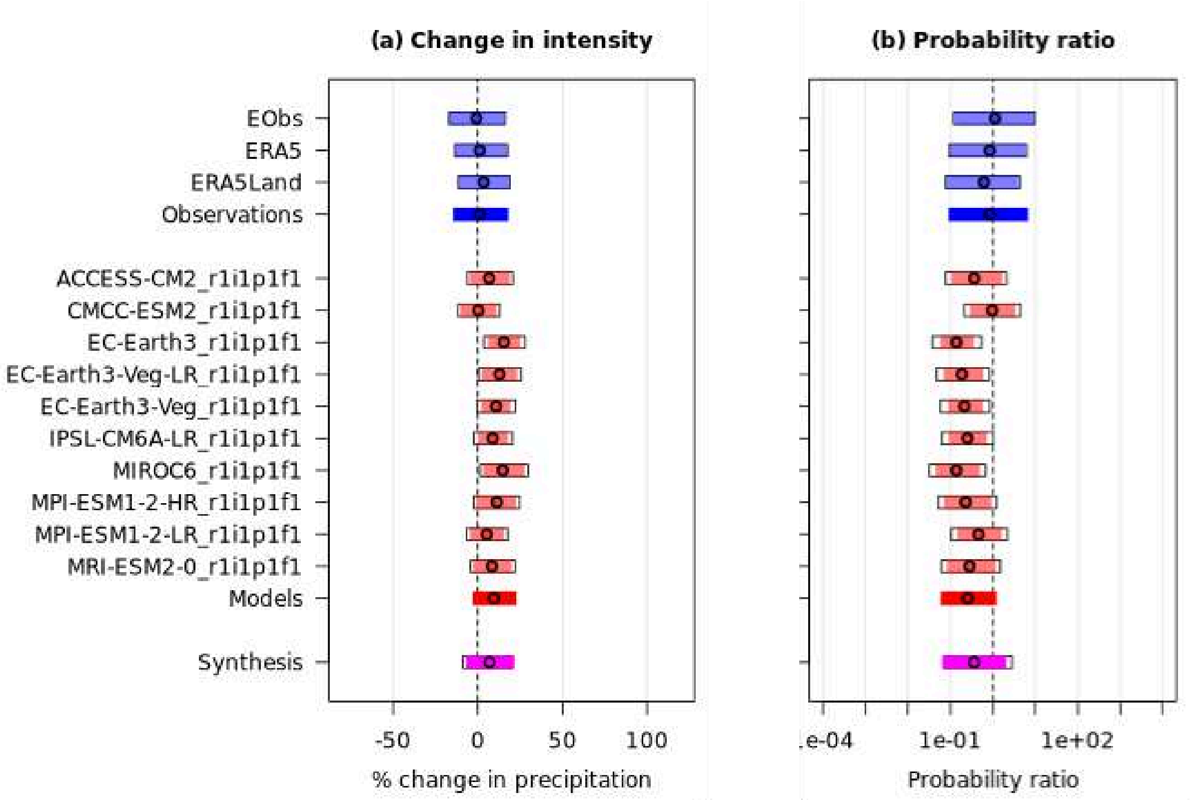

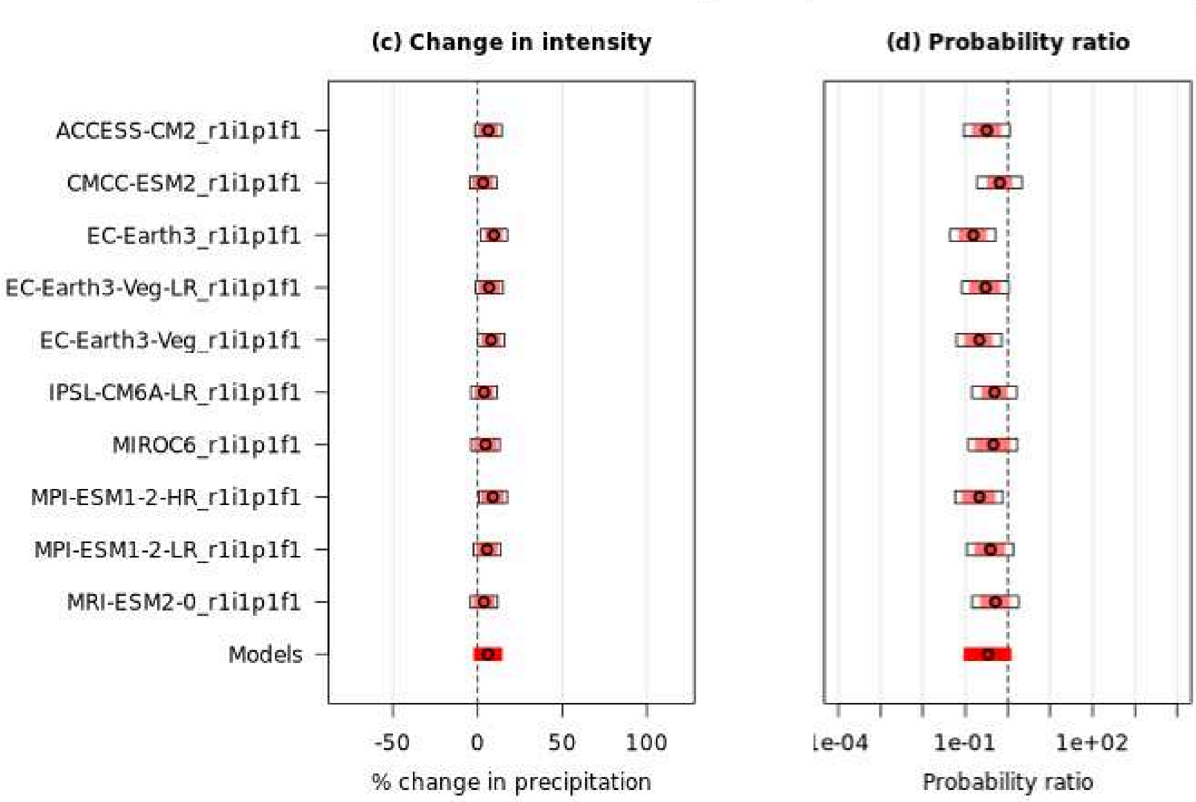

Figure A3.1.2 *(a) Change in intensity for precip during Jan to June (%) and (b) Probability Ratio for the Eastern Domain from past to present. (c) same as (a) and same as (b) from present to future.*

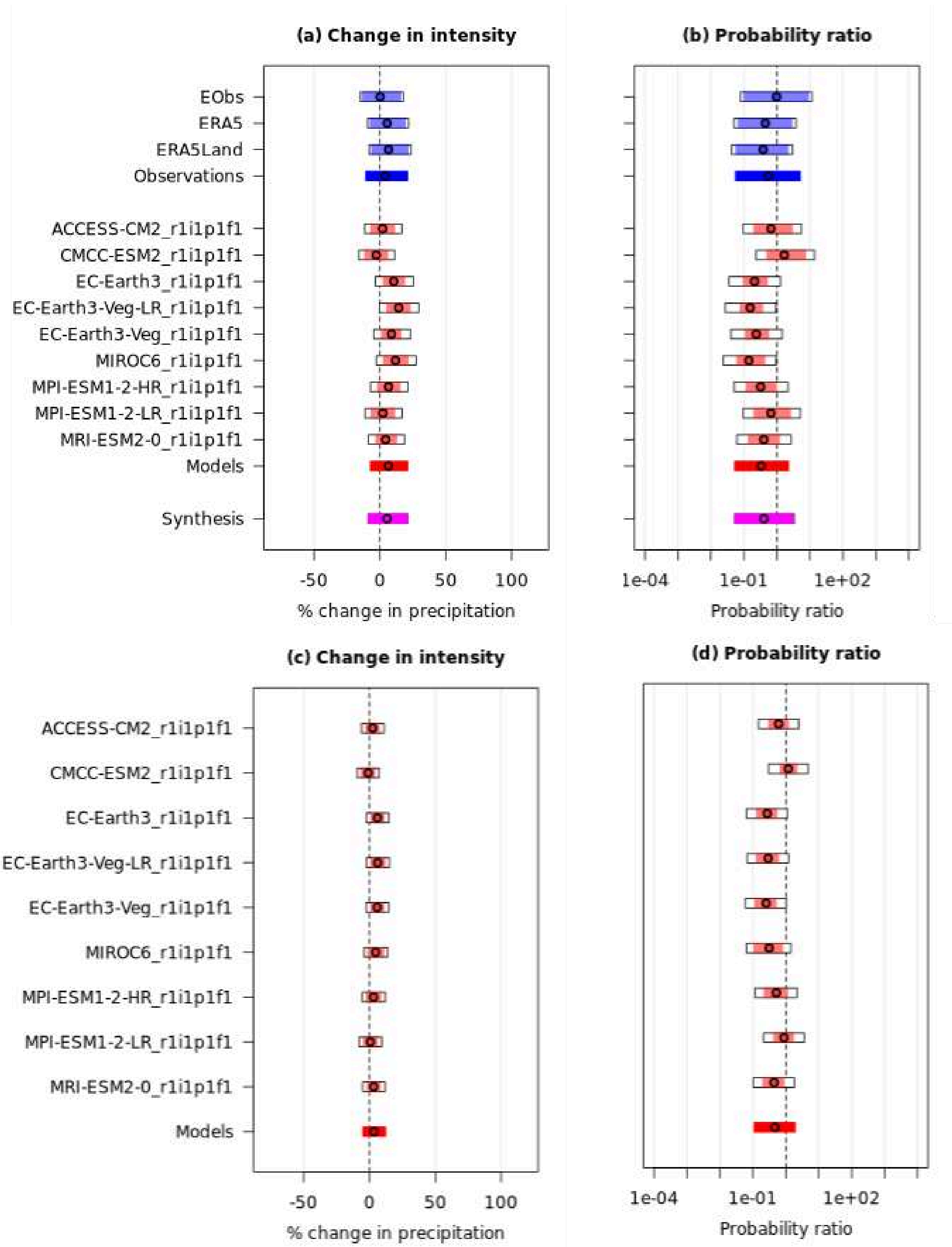

Figure A3.1.3 *(a) Change in intensity for precip during July to June (%) and (b) Probability Ratio for the Eastern Domain from past to present. (c) same as (a) and same as (b) from present to future.*

A3.2 PET synthesis plots

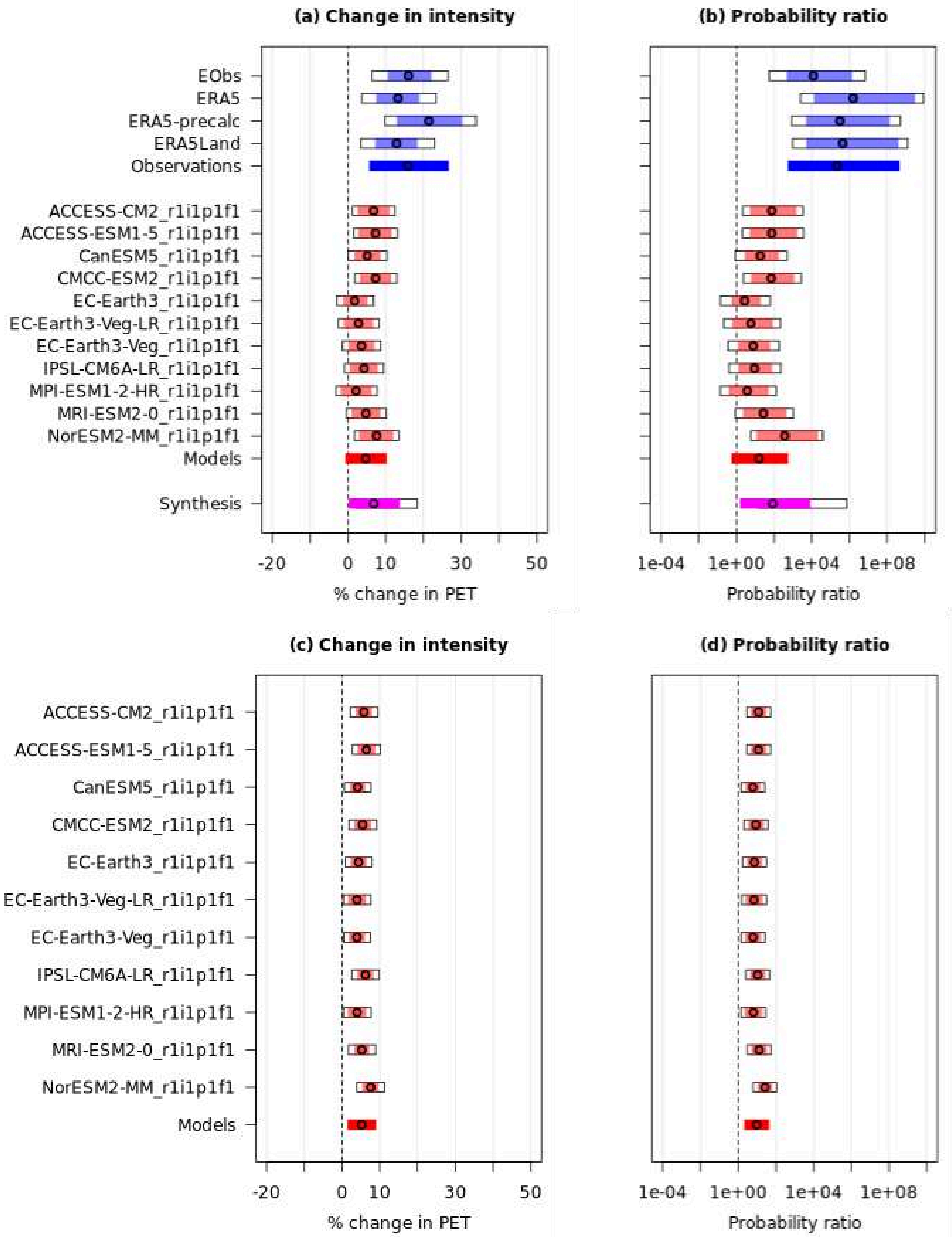

Figure A3.2.1 *(a) Change in intensity for PET AMJ (%) and (b) Probability Ratio for the Western Domain from past to present. (c) same as (a) and same as (b) from present to future.*

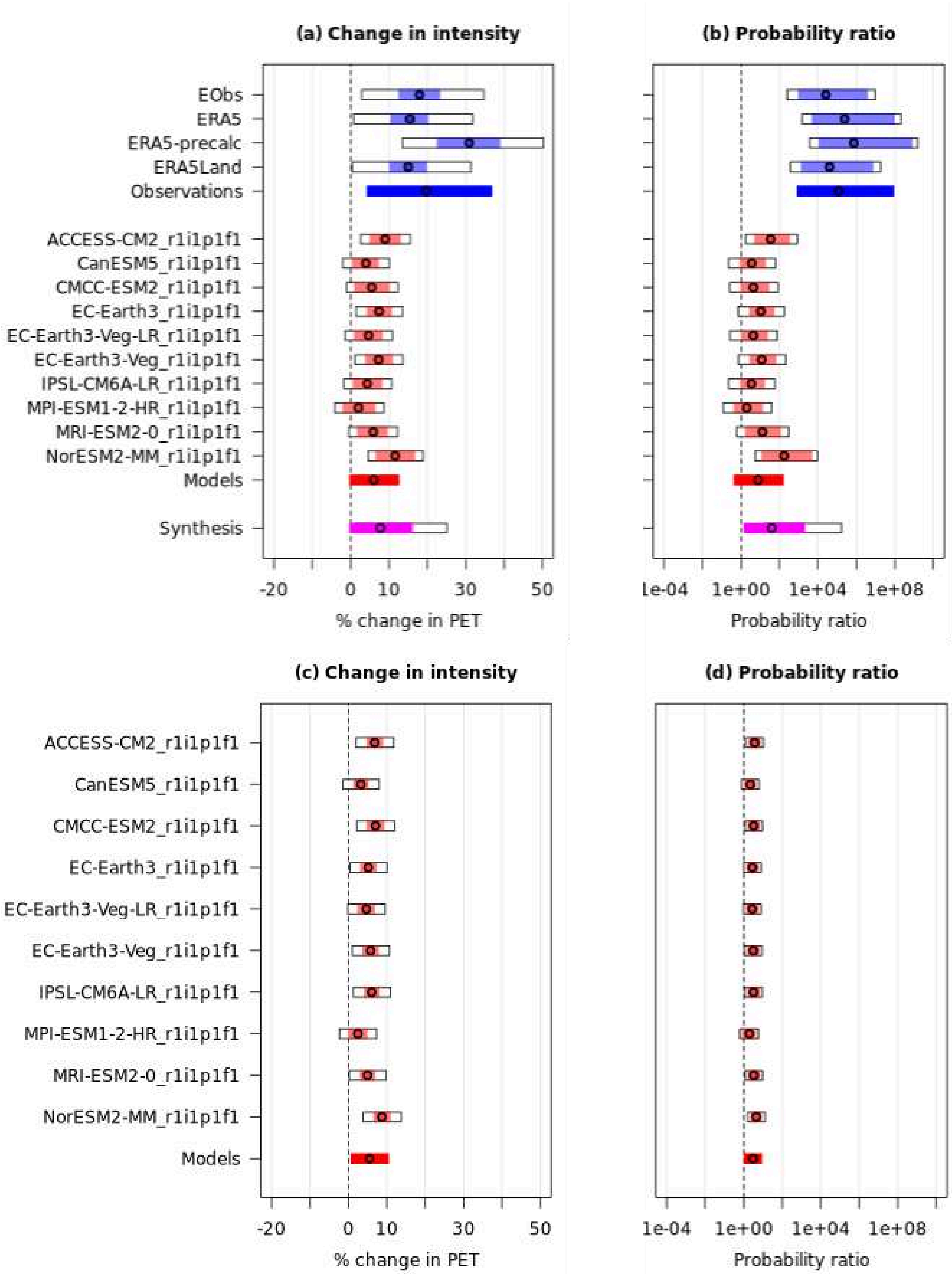

__Figure A3.2.2__ (a) Change in intensity for PET during Jan to June (%) and (b) Probability Ratio for the Eastern Domain from past to present. (c) same as (a) and same as (b) from present to future.

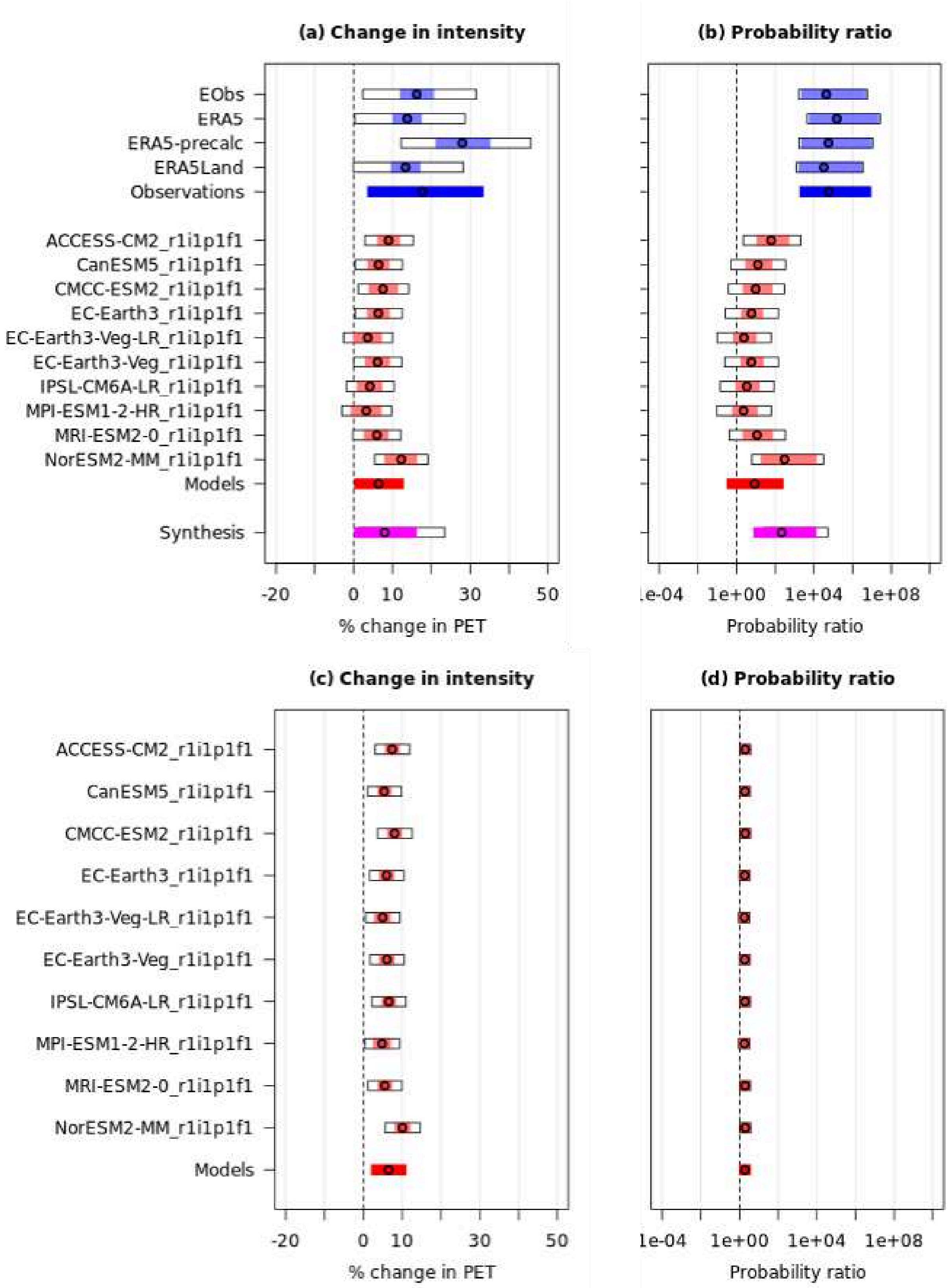

Figure A3.2.3 *(a) Change in intensity for PET during July to June (%) and (b) Probability Ratio for the Eastern Domain from past to present. (c) same as (a) and same as (b) from present to future.*

A3.3 Soil moisture synthesis plots

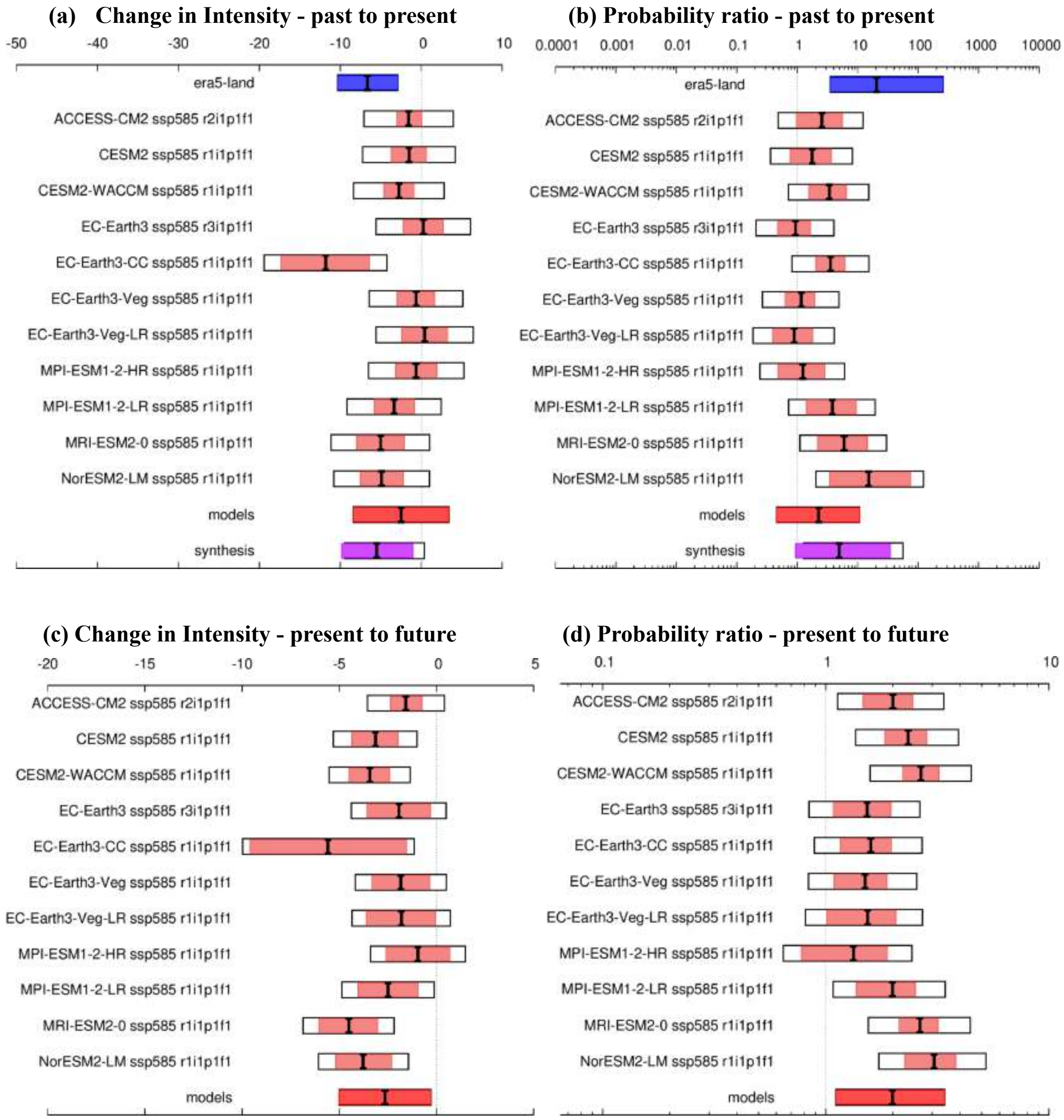

Figure A.3.3.1*: (a) Change in intensity for soil moisture AMJ (%) and (b) Probability Ratio for the Western Domain from past to present. (c) same as (a) and same as (b) from present to future.*

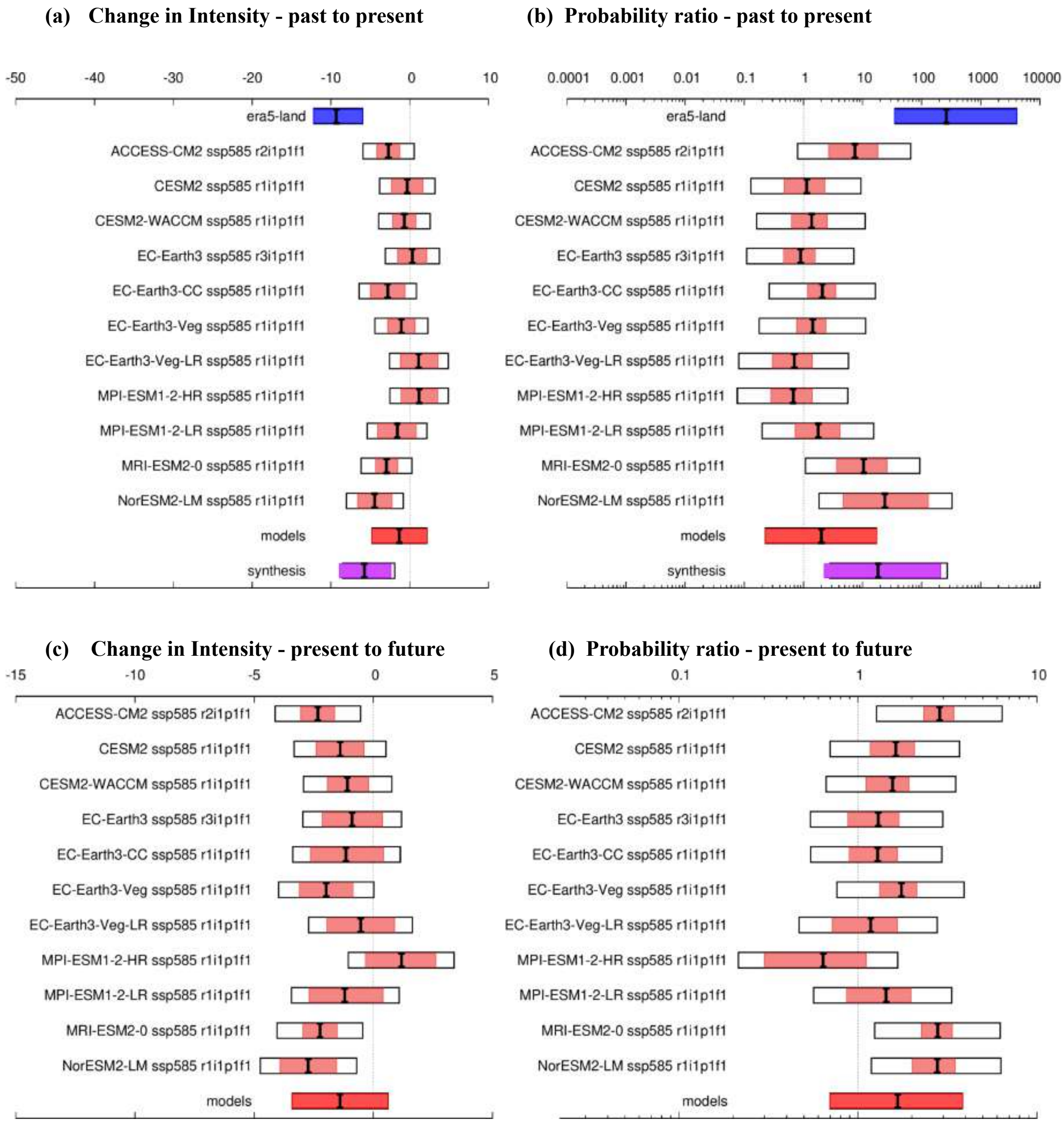

Figure A.3.3.2*: (a) Change in intensity for soil moisture AMJ (%) and (b) Probability Ratio for the Eastern Domain from past to present. (c) same as (a) and same as (b) from present to future.*

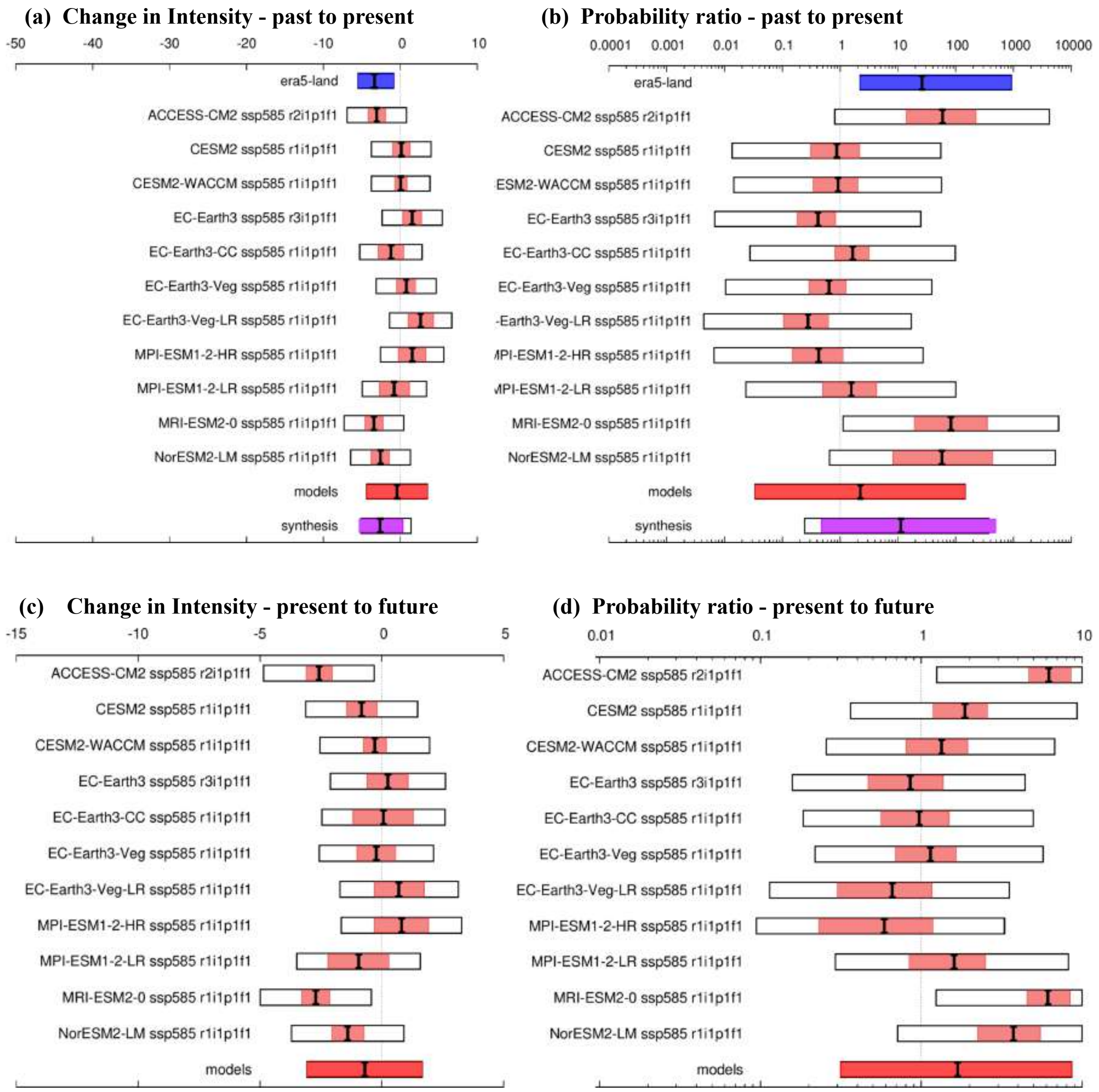

Figure A3.3.3 *(a) Change in intensity for soil moisture during Jan to June (%) and (b) Probability Ratio for the Eastern Domain from past to present. (c) same as (a) and same as (b) from present to future.*

A4 Country specific conditions

A4.1 Hungary

The ongoing drought in Hungary began in late 2025. Dry winter and spring conditions prevented soil moisture recharge, especially in the Great Plain, while the exceptionally warm and dry June further intensified the drought in 2026. Soil moisture is below 40% of plant-available water, dropping below 30% in large areas of central Hungary, indicating critically dry conditions Figure A4.1.1.

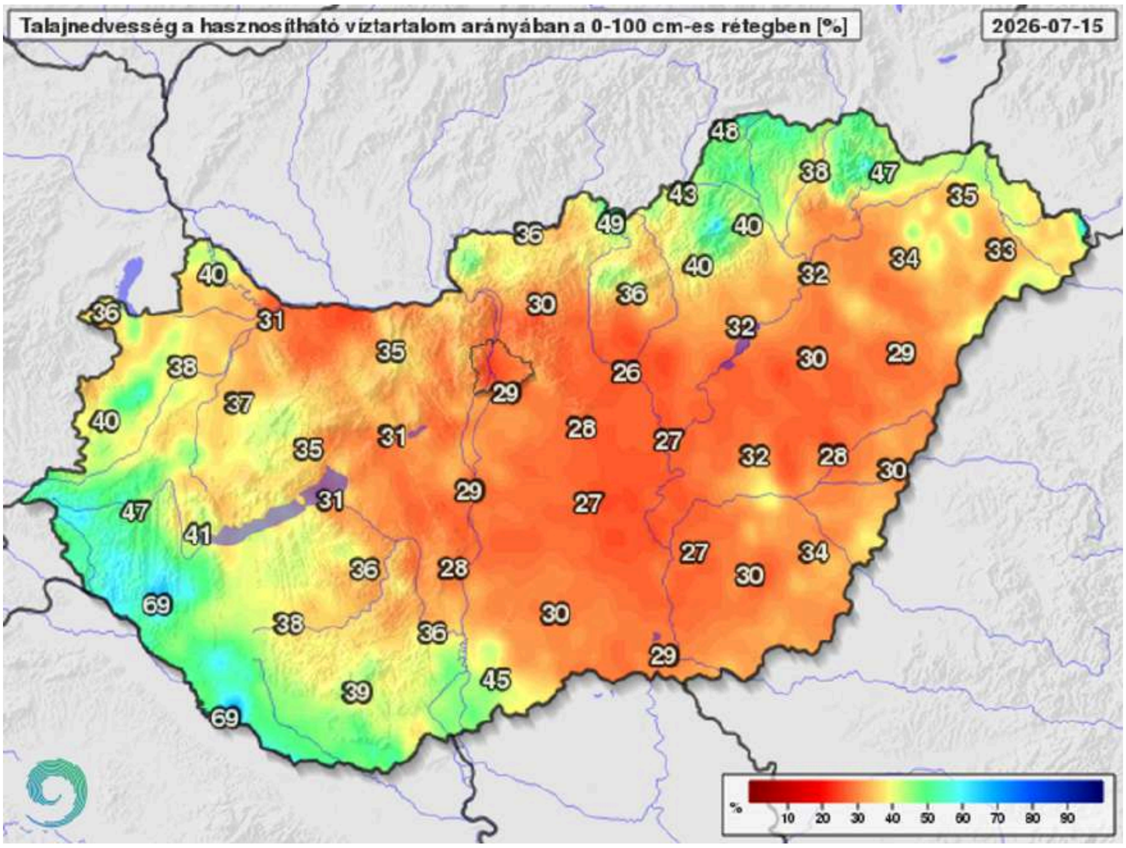

Figure A4.1.1. Soil moisture deficit in the root zone (0-100 cm), 15 July 2026. Source: HungaroMet

The HungaroMet agricultural drought monitoring system is based on soil moisture. Daily soil moisture is calculated on a 5×5 km grid for three soil layers (0–20, 20–50 and 50–100 cm), weighted according to crop root-zone distribution, and classified into drought categories. Assessments are provided separately for winter crops (cereals and winter rapeseed) and summer crops. The proportion of Hungary affected by moderate or server drought currently exceeds four-fifths of the country.

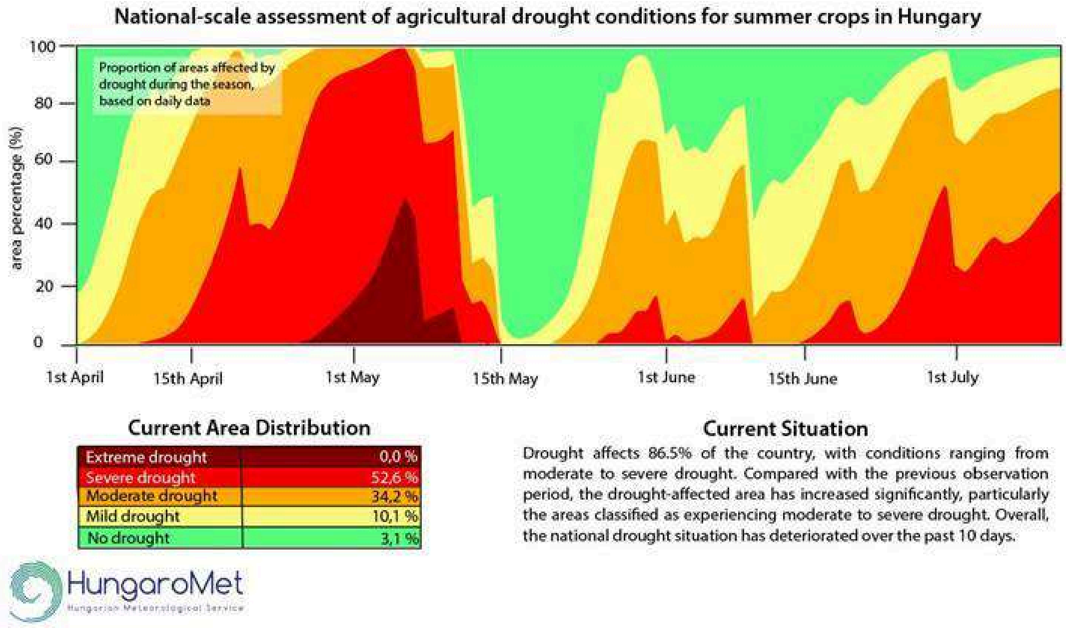

Figure A4.1.2. Agricultural Drought Conditions for Summer Crops in Hungary, 12 July 2026. Source: HungaroMet Hungarian Meteorological Service

Satellite-based monitoring of summer crop drought impacts in Hungary

Arable crops are monitored using satellite-based NDVI observations across four major agricultural regions of Hungary. For each crop, eight randomly selected non-irrigated fields are tracked in each region and compared with reference years representing low and high yields.

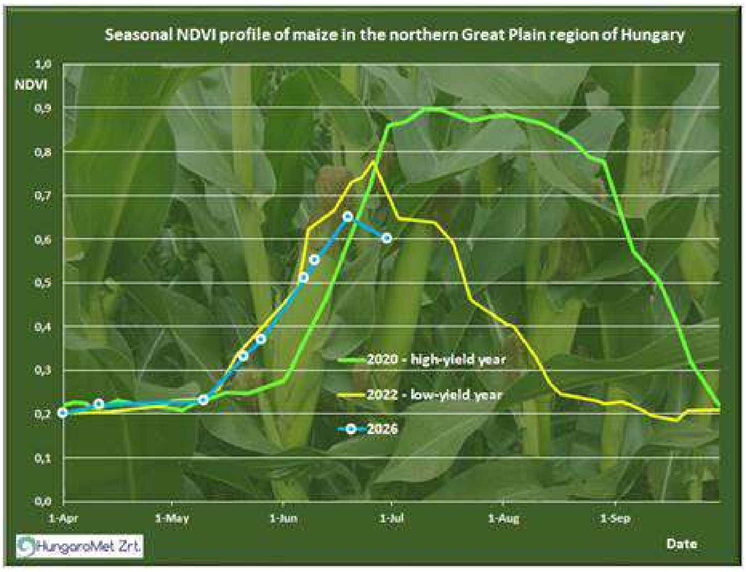

Figure A4.1.3. Seasonal NDVI profile of sunflower fields in the Great Plain region based on Sentinel-2 data, compared with high- and low-yield years. Source: HungaroMet

Agricultural Risk Management System in Hungary

Since 2011, Hungary's agricultural risk management system has supported farmers affected by weather-related losses, including drought. The Hungarian Meteorological Service provides operational drought information based on station observations and radar data, available through the free agro.met.hu service.

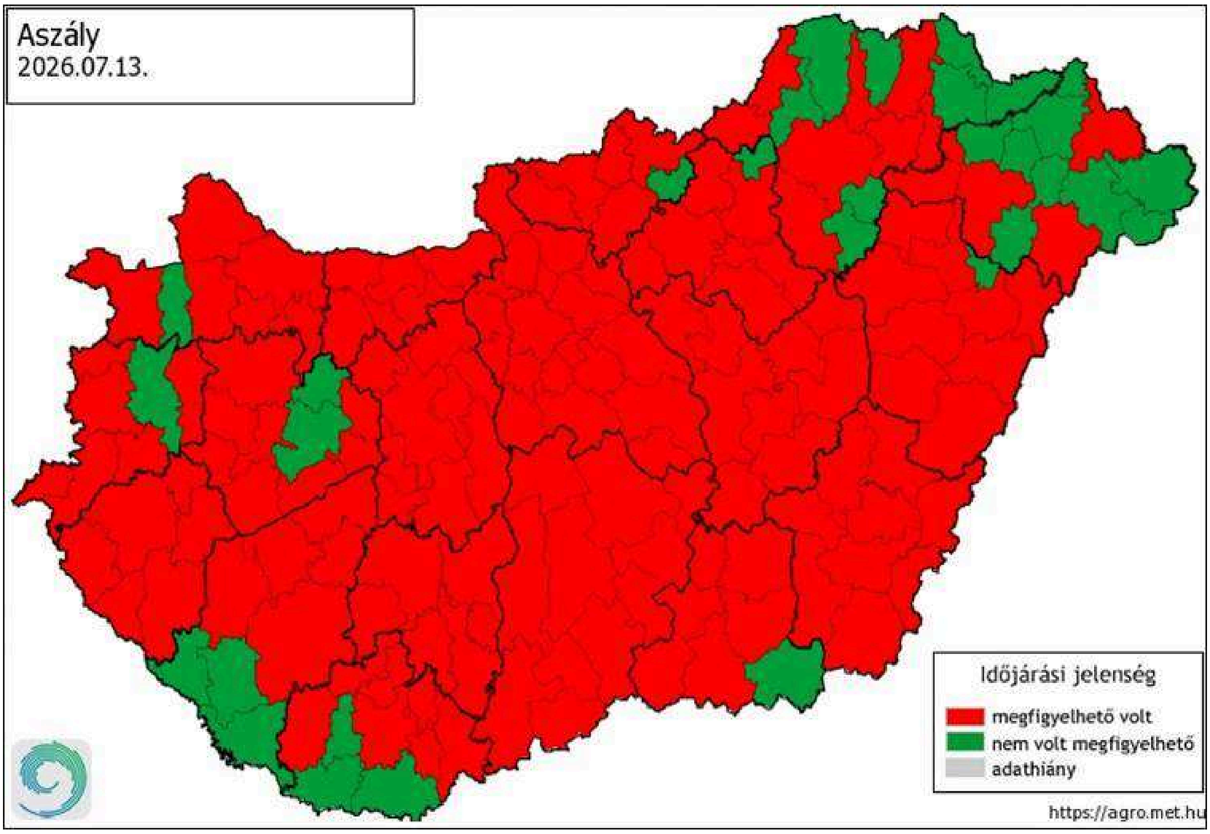

Figure A4.1.4. Drought conditions in Hungary at NUTS3 level (orange: drought, green: no drought, grey: missing data) on 13 July 2026. In the agricultural risk management system, drought is defined as follows: within a period of thirty consecutive days, the total precipitation does not exceed 10 mm, or the total precipitation does not exceed 25 mm and the maximum daily temperature exceeds 31 °C on at least fifteen days. Souce: https://agro.met.hu/

A4.2 Switzerland

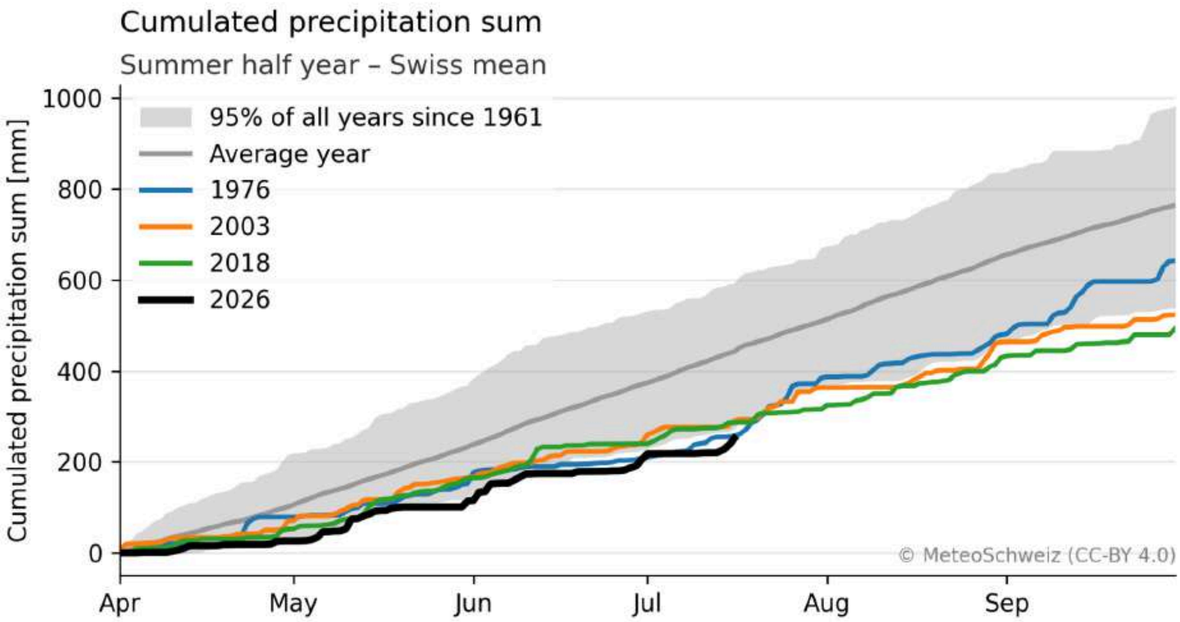

Figure A4.2.1. Cumulative precipitation sums from April to September (national means statistically derived from raingauge measurements). A lower curve indicates a drier year.

A4.3 Austria

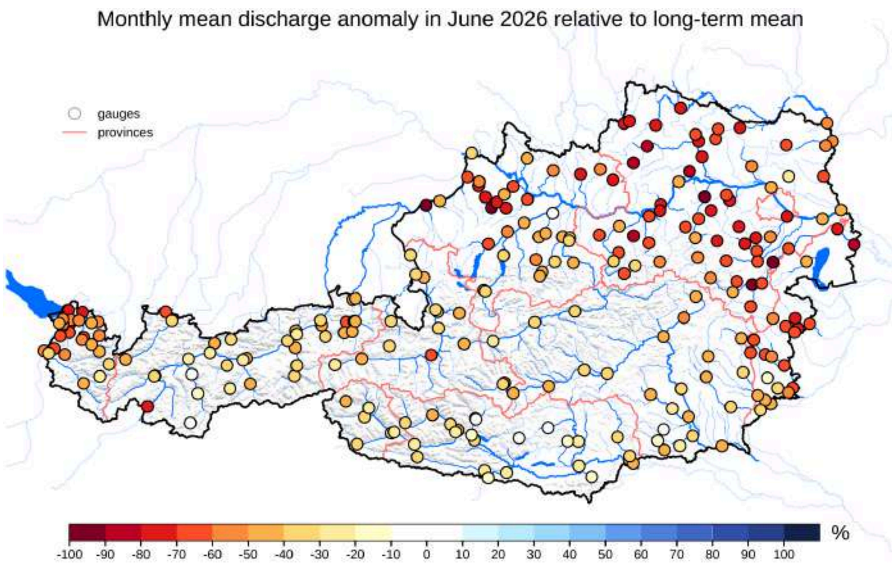

Fig. A4.3.1 Mean monthly discharge anomaly in June 2026 relative to the long-term mean for Austrian discharge gauges.

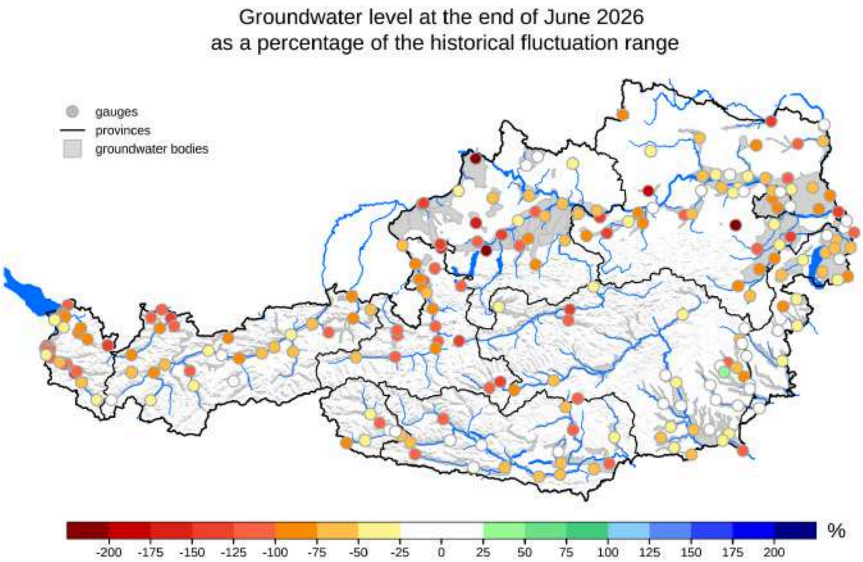

Figure A4.3.2: Groundwater level at the end of June 2026, as a percentage of the historical fluctuation range, measured at Austrian discharge gauges.

A4.4 Slovenia

Early warnings for Slovenia are shown in Figure A4.4.a. Early warnings for drought continued every week into early May (ARSOb, ARSOc, ARSOd, ARSOe, 2026). First early warning on severe heat stress was issued by Slovenian Environment agency on 19 June 2026 (ARSOf, 2026) and continued throughout second half of June as heatwave intensified. Early warning on severe and extreme drought conditions in the topsoil layer was issued by the Slovenian Environment Agency weekly since the beginning of July 2026. Some of the groundwater bodies in wider central Slovenia had not had water level replenished since the onset of spring drought, entering mid-July with early warning of severe hydrological drought (ARSOg, ARSOh, 2026).

Figure A4.4.1: Timeline of weekly published early warnings for drought in the topsoil layer between January and mid-July 2026 (ARSO, 2026).

The consequences of insufficient rainfall were evident in the reduced yields of winter crops and grass–clover mixtures. The first cut of permanent grassland was below average, and significantly lower yields were also expected on more extensive grasslands at higher elevations (Gorenjski glas, 2026. RTVSLOe, 2026). As a result, a larger proportion of vegetables failed to meet market quality standards and had to be discarded. Reduced grass growth also led to lower forage production. Intense and lasting heatwave was possibly the main reason behind impacts detected in livestock farming, since decrease in average milk yield, milk fat content, and milk protein content all coincide with the heatwave during the third decade of June and early July (KGZS, 2026).

A4.5 Germany

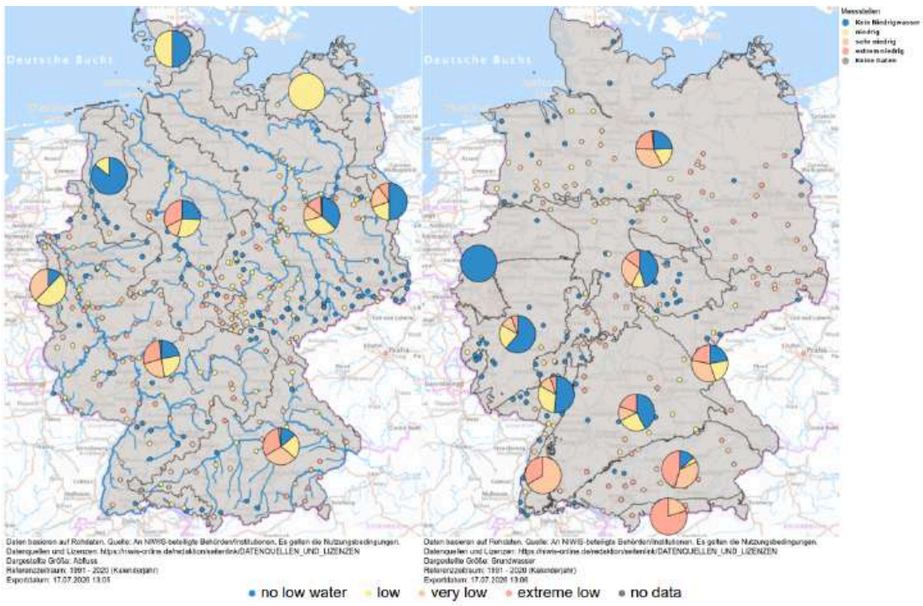

Figure A4.5.1: a) river discharge and b) ground water situation 17.7.2026 in Germany according to NIWIS.

Heat wave effects on agriculture

In many regions in the Southwest half of Germany, drought stress affects maize, sugar beet and grassland, while grain harvest occurred widespread significantly earlier than usual. In the northeastern half of Germany drought effects are visible in places but generally the situation is not extraordinarily severe. The heatwave had little further impact on winter barley and winter rapeseed, as both crops were already ripening. An impact on yield is to be expected for winter wheat, however, as it was still in the grain-filling phase in some regions; the high temperatures may have led to premature ripening and, consequently, a lower thousand-grain weight (TGW). No discernible effects from the heat are expected for sugar beet and maize. In fruit and wine growing, the combination of heat and high levels of global radiation has caused - in some cases - severe sunburn damage. Especially in the western parts precipitation was mostly sparse.